
Project Report

March 2005

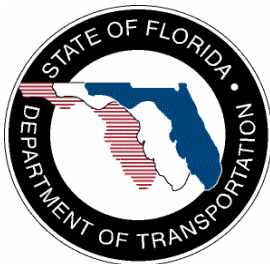
UF Project No. 455404712
Contract No. BD545, RPWO# 21

SELF-CONSOLIDATING CONCRETE (SCC) STRUCTURAL INVESTIGATION

Principal Investigator:	H. R. (Trey) Hamilton, P.E., Ph.D.
Graduate Research Assistant:	Ted Labonte
Project Manager:	Marcus Ansley, P.E.

Department of Civil & Coastal Engineering
College of Engineering
University of Florida
Gainesville, Florida 32611

Engineering and Industrial Experiment Station



Technical Report Documentation Page

1. Report No. BD545, RPWO# 21	2. Government Accession No.	3. Recipient's Catalog No.	
4. Title and Subtitle SELF-CONSOLIDATING CONCRETE (SCC) STRUCTURAL INVESTIGATION		5. Report Date March 2005	
		6. Performing Organization Code	
7. Author(s) T. Labonte and H. R. Hamilton III		8. Performing Organization Report No. 4910 45 04 047	
9. Performing Organization Name and Address University of Florida Department of Civil & Coastal Engineering P.O. Box 116580 Gainesville, FL 32611-6580		10. Work Unit No. (TRAIS)	
		11. Contract or Grant No.	
12. Sponsoring Agency Name and Address Florida Department of Transportation Research Management Center 605 Suwannee Street, MS 30 Tallahassee, FL 32301-8064		13. Type of Report and Period Covered Final Report	
		14. Sponsoring Agency Code	
15. Supplementary Notes			
16. Abstract <p>Self-consolidating concrete (SCC) is a relatively new approach to making concrete and is characterized by its high flowability and resistance to aggregate segregation in the plastic state. SCC has become a popular alternative for commercial precast elements in Florida. In response to producer's requests to use SCC, Florida Department of Transportation (FDOT) initiated a study in which full-scale precast, pretensioned AASHTO Type II beams were constructed and tested. SCC trial mix designs were developed in conjunction with the participating precast producer. These trial mixes included extensive plastic property testing of the SCC trial mixes. Three beams were constructed using SCC, and three using a conventional FDOT approved mix. The major tasks included performing plastic and hardened property tests, constructing SCC beams without vibrating, determining the prestress transfer length, monitoring the camber, and finally testing the beams in such a manner as to produce flexure and shear dominated failure modes.</p> <p>No notable differences were found in prestress transfer length, mean camber growth, flexural capacity, shear capacity, or observed web cracking (during load testing) between the SCC and standard beams. One exception was the fully bonded strand slip in shear-slip test two, which resulted in a 15% lower ultimate capacity for SCC. It is believed that, based on the transfer length measurements, the abrupt prestress transfer conditions may have contributed to the early slip. Total deflections measured during the load tests indicated that the standard mix had slightly better ductility than SCC with the standard beams reaching an average of 17.1% more deflection than the SCC beams at the ultimate load.</p>			
17. Key Word Self-compacting concrete, prestressed, precast, flexure, shear		18. Distribution Statement No restrictions. This document is available to the public through the National Technical Information Service, Springfield, VA, 22161	
19. Security Classif. (of this report) Unclassified	20. Security Classif. (of this page) Unclassified	21. No. of Pages 117	22. Price

ACKNOWLEDGMENTS AND DISCLAIMER

The authors would like to acknowledge and thank the Florida Department of Transportation for providing the funding for this research project. This project was a collaborative effort among the University of Florida, FDOT Structures Research Laboratory (Tallahassee) and the FDOT State Materials Office (Gainesville). Mix development and materials testing was conducted by Charles Ishee, Mario Paredes, Richard Delorenzo and Charlotte Kasper at FDOT State Materials Office. Structural testing was conducted by the FDOT Structures Research Laboratory (Marc Ansley, David Allen, Frank Cobb, Steve Eudy, Tony Johnston, Paul Tighe). The authors would also like to thank Gate Concrete Products Company Jacksonville, FL and Jim Kunberger and Bruce Hunter for constructing the specimens and Eckart Buehler with Master Builders for technical assistance with the mix designs. Finally, the authors would like to thank Ghulam Mujtaba for his input and technical expertise in developing and conducting this research.

The opinions, findings, and conclusions expressed in this publication are those of the authors and not necessarily those of the State of Florida Department of Transportation.

Table of Contents

<u>INTRODUCTION.....</u>	<u>6</u>
1.1 BACKGROUND	6
1.2 RESEARCH APPROACH	6
<u>EXPERIMENTAL PROGRAM.....</u>	<u>8</u>
2.1 INTRODUCTION.....	8
2.2 MATERIAL TESTING	8
2.3 BEAM DESIGN AND CONSTRUCTION	8
2.4 PRESTRESS TRANSFER LENGTH AND STRAND SLIP	11
2.5 CAMBER MONITORING.....	12
2.6 STRUCTURAL TESTING	13
<u>TEST RESULTS AND DISCUSSION</u>	<u>16</u>
3.1 TRIAL MIX TESTS.....	16
3.2 VERIFICATION MIX TESTING.....	17
3.3 BEAM CONSTRUCTION	18
3.4 CASTING MIX MATERIAL TESTS	18
3.5 PRESTRESS TRANSFER LENGTH AND STRAND SLIP	21
3.6 CAMBER MONITORING.....	24
3.7 SHEAR TEST	25
3.8 SHEAR-FLEXURE TEST	30
3.9 SHEAR-SLIP TEST	34
<u>CONCLUSIONS.....</u>	<u>40</u>
<u>RECOMMENDATIONS</u>	<u>42</u>
<u>REFERENCES.....</u>	<u>43</u>
<u>APPENDIX A - MIX DESIGN AND TRIAL MIXES.....</u>	<u>44</u>
<u>APPENDIX B - BEAM DESIGN AND CONSTRUCTION.....</u>	<u>47</u>
<u>APPENDIX C - CAMBER MONITORING.....</u>	<u>55</u>
<u>APPENDIX D - SHEAR TEST</u>	<u>56</u>
<u>APPENDIX E - SHEAR- FLEXURE TEST.....</u>	<u>74</u>
<u>APPENDIX F - SHEAR-SLIP TEST.....</u>	<u>100</u>

Executive Summary

This report presents the results of a comprehensive testing program comparing the structural performance of AASHTO Type II bridge girders constructed with self-consolidating concrete to those constructed with the standard mix currently in use. Self-consolidating concrete (SCC) is a new material, and it is characterized by its high flowability and resistance to aggregate segregation in the plastic state. In response to requests by the Florida precast industry for the approval of SCC use in bridge girders, the Florida Department of Transportation and the University of Florida jointly conducted the research described in this report. The objectives of the research were to compare the construction, material properties (fresh and hardened), transfer length, camber, and structural behavior with shear and flexural failure modes.

After trial mixes were used to determine the optimum mix design, six 42 ft prestressed AASHTO Type II girders were constructed. Three beams were cast with SCC, and three beams were cast with a standard FDOT approved mix. Material tests using samples from the casting batch were conducted. An analysis and comparison of the transfer lengths and strand slip during the prestress transfer was conducted. The camber growth of all beams was measured for 188 days, and a comparison of the SCC camber growth versus the control camber growth was included. The structural performance of the SCC beams was measured and compared to the control beams using a full set of instrumentation with shear and flexural failure modes.

In summary, there was little notable difference in performance between the SCC beams and standard mix beams. The process of mix development and beam fabrication, however, did highlight the importance of quality control when using SCC.

1 INTRODUCTION

1.1 BACKGROUND

Self-consolidating concrete (SCC) is a highly workable, non-segregating concrete that does not require mechanical vibration during placement. SCC evolved out of underwater concrete admixture technology in Japan in the 1980's and the desire to make the casting process more efficient due to a low skilled labor supply (Okamura 1996). Several European countries adopted the use of SCC starting in the early 1990's, and have successfully constructed many bridges, buildings, and other concrete structures using this material. In the United States, SCC is currently being used mainly in the precast industry for the construction of non-critical structural components and other products that are not highly stressed elements of major concrete structures. Several pedestrian bridges have been constructed with SCC in the US, and there have been successful applications of SCC in building construction.

SCC can flow to fill areas around dense reinforcement and through thin openings under its own weight with minimal formation of voids, segregation or bleed (PCI 2003). Additional advantages include eliminating mechanical vibration, improving formed surface finishes, reducing finishing time, improving labor force efficiency, improving working conditions, and safety. The workability of SCC is better than the highest class of workability associated with normal high-performance concrete typically used in precast concrete fabrication plants (PCI 2003). Standards currently being developed define a concrete mix as being SCC when the mix meets quantifiable workability criteria based on its confined flowability, passing ability, and resistance to segregation. The highly flowable properties have stimulated the development of several new plastic property tests that are applicable only to SCC.

In general, the available research suggests that the mechanical properties of SCC are comparable to those of typical concrete mixes. Khayat, Manai, and Trudel (2001) reported on the in-place mechanical properties of walls cast with SCC. It was found that the difference between compressive strengths of cores from the top and bottom of the SCC walls was approximately 8 percent.

Sonebi, Tamimi, and Bartos (2001) tested the structural performance of 8-in. by 12-in. by 12.5-ft beams. The variations of the concrete properties along the SCC beams were found to be small. The SCC performed slightly better than typical concrete in terms of the in-place compressive strengths as a percentage of the 28-day cylinder strengths, with the SCC being in the range of 80% to 100%, and the typical concrete being in the range of 75% to 80%. The SCC beams also performed slightly better in terms of cracking. The typical concrete beams had more cracks that were wider than that of the SCC beams. The researchers partially attributed this to the SCC concrete having a 10% higher compressive strength than that of the typical concrete mix. Also, the ultimate moment capacities of the SCC beams and typical concrete beams were comparable.

1.2 RESEARCH APPROACH

This project had several phases. Initially the FDOT State Materials Office conducted mix designs in cooperation with the precast supplier. Plastic and hardened properties of the SCC were tested in both the laboratory and field trial mixes. Once the mix design had been

completed, the precast supplier fabricated the girders using the design mix. FDOT Structures Research Center and University of Florida personnel instrumented the girders to determine prestress transfer length. The girders were then shipped to the FDOT Structures Research Center where they were monitored for camber growth for several months. At the conclusion of the camber monitoring period, the beams were tested in shear or flexure to determine the structural capacity and behavior.

2 EXPERIMENTAL PROGRAM

2.1 INTRODUCTION

Trial mixes were used to obtain mix designs with the targeted fresh properties. Six 42-foot AASHTO Type II beams were constructed and samples were taken from the casting mix to be used for material testing. Three of the six beams were constructed with SCC, and three beams were constructed with a typical approved mix. Instrumentation was installed on the beams before the transfer of prestress to measure the transfer lengths. Camber monitoring started immediately after the transfer of prestress and continued for approximately 200 days from casting. All beams were finally tested to destruction in states of high shear and flexure with adequate strand development length, and the beams were tested in a state of high shear with the possibility of an inadequate available strand development length.

2.2 MATERIAL TESTING

An FDOT class VI mix with a target concrete compressive strength of 8,500 psi was used as a template for the development of two pairs of *standard* concrete mixes and SCC mixes, respectively. This work was conducted by the FDOT State Materials Research Office. The trial mixes were batched and tested to determine the optimum mix design and to determine if any adjustments to the relative constituent quantities were necessary. The relative quantities of cement, fly ash, and water were the same for each pair of mix designs.

SCC plastic properties can vary significantly depending on the mixing method. Consequently, a verification mix was conducted at the plant to ensure that the plastic properties remained unchanged when mixing was performed with a production mixer. Additionally, samples were taken from the actual casting mix for material testing. The material property comparisons from the casting mix included in this report are cylinder compressive and tensile strength, shrinkage, and surface resistivity.

2.3 BEAM DESIGN AND CONSTRUCTION

The objectives of the beam testing were to compare the strand transfer length, camber growth, and structural properties of the beams. A total of six beams were constructed for this testing. Four of the beams (two SCC and two standard) were designed to be tested in flexure and shear with a composite cap to simulate the composite action of the bridge deck. Two (one SCC and one standard) were designed to be tested in shear without the benefit of the composite action from the deck. These specimens also had light shear reinforcement at the ends to determine the effect (if any) on the shear behavior.

The AASHTO Type II beam tendon size and configuration were designed to meet the requirements of AASHTO LRFD Bridge Design Specification for a fictitious bridge in which the beams were assumed to be spaced at 6 ft with a 40-ft span. The tendon was composed of 12 0.5-in. diameter ASTM A416 Gr 270 prestressing strands. Two strands were debonded for a length of 6 ft. The deck thickness was assumed to be 10 inches. Florida Department of Transportation

(FDOT) software (LRFD P Beam Version 1.85) was used to design the beam. The beam details are shown in Figure 1 through Figure 6

The flexural beams were tested with a composite concrete top flange (Figure 4) to model the compression area provided by the bridge deck in actual service conditions. The top flange was constructed by FDOT Structures Laboratory personnel prior to testing using a Class II (Bridge Deck) ready-mix concrete ($f'_c = 4,500$ psi).

The stirrup spacing away from the end region of the non-capped beams was set at four feet. A typical FDOT prescribed arrangement of mild steel reinforcement was included in the end region of the non-capped beams to force the failure location to the area of minimal shear reinforcement (Figure 2 and Figure 5). The first five stirrups were double leg with the remaining stirrups single leg.

The stirrup spacing away from the end region of the capped beams was set at 12 in. to ensure a flexural failure mode. The first five stirrups in the capped beam were double leg with the remaining stirrups single leg.

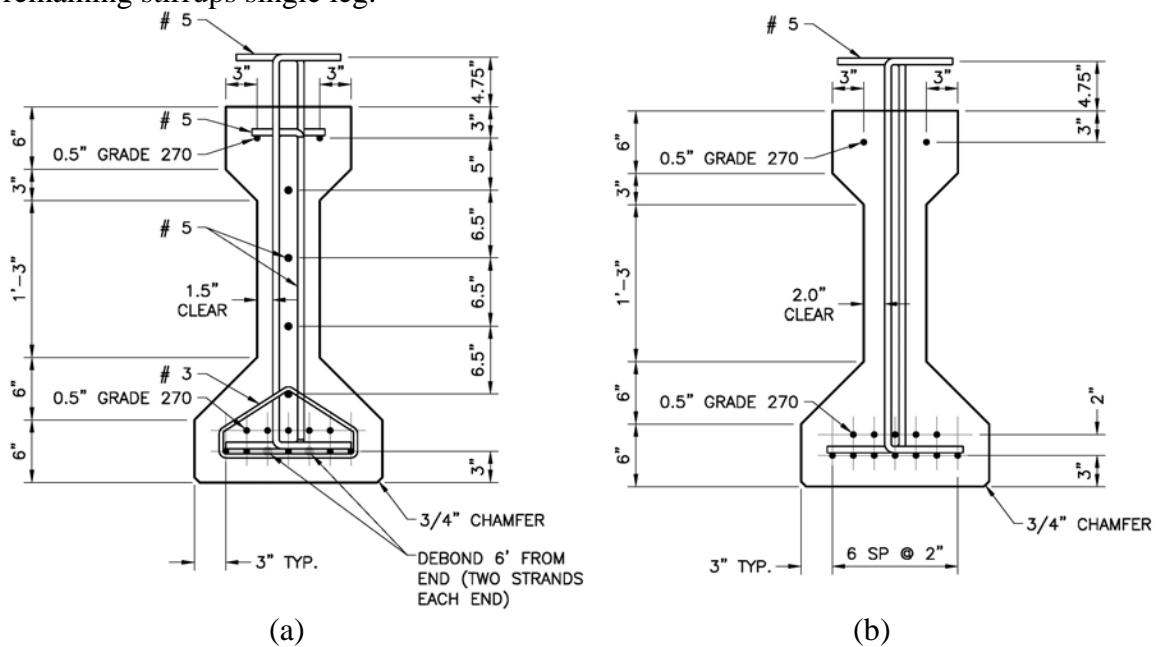


Figure 1. Prestressed beam design detail (a) end section (b) middle section

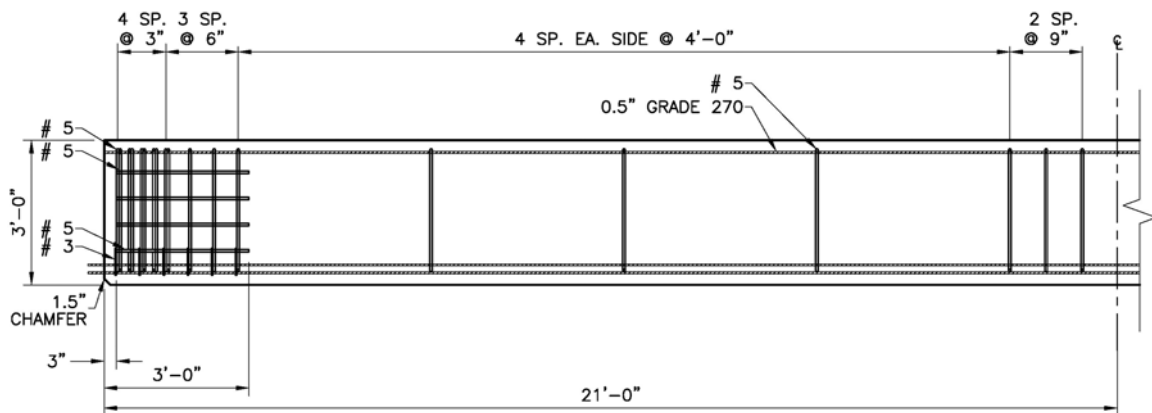


Figure 2. Non-capped beam elevation detail

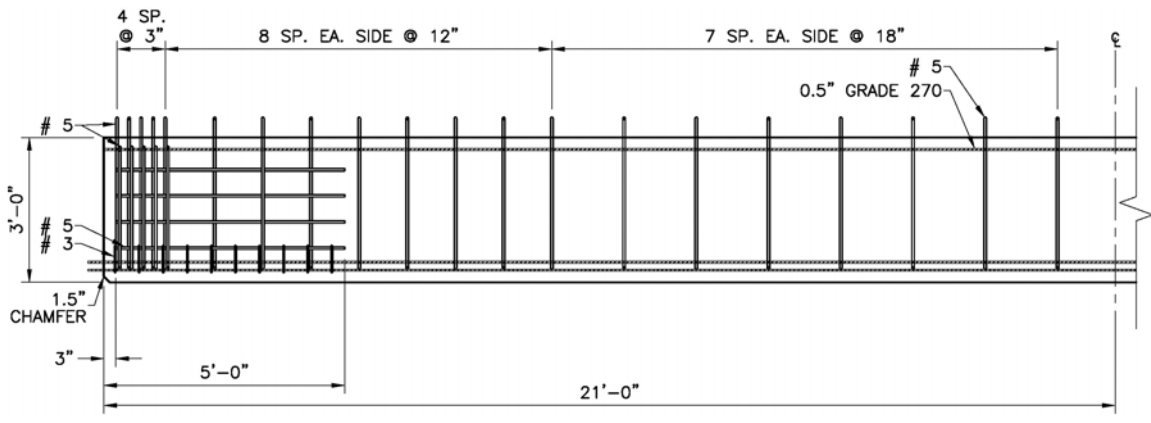


Figure 3. Capped beam elevation detail

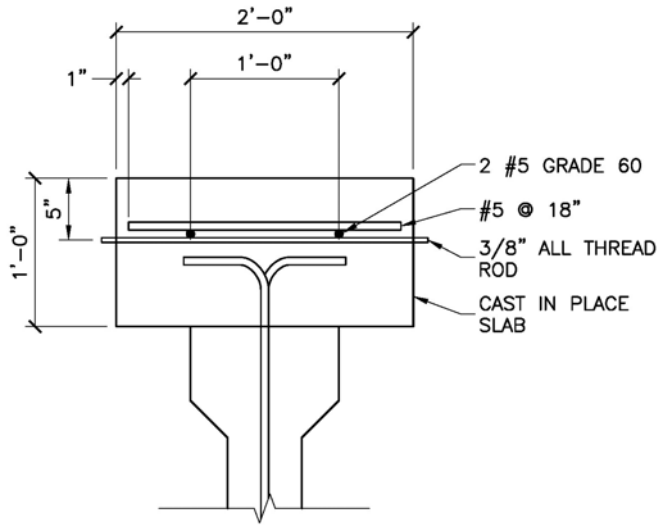


Figure 4. Composite Cap Detail



Figure 5. Stirrup and confinement reinforcement at end of non-capped shear beam



Figure 6. Stirrup and confinement reinforcement at end of capped flexure beam

The six 42-foot long AASHTO Type II beams were cast in a single day at a prestressed concrete plant in Jacksonville, FL. FDOT quality assurance personnel were present to ensure the beams were cast using correct procedures and met specified tolerances. To eliminate a vibration carry-over effect from the consolidation of the standard concrete due to the continuously connected forms, all standard concrete beams were cast and consolidated before the SCC beams were poured. No consolidation was utilized on the SCC beams (Figure 7).

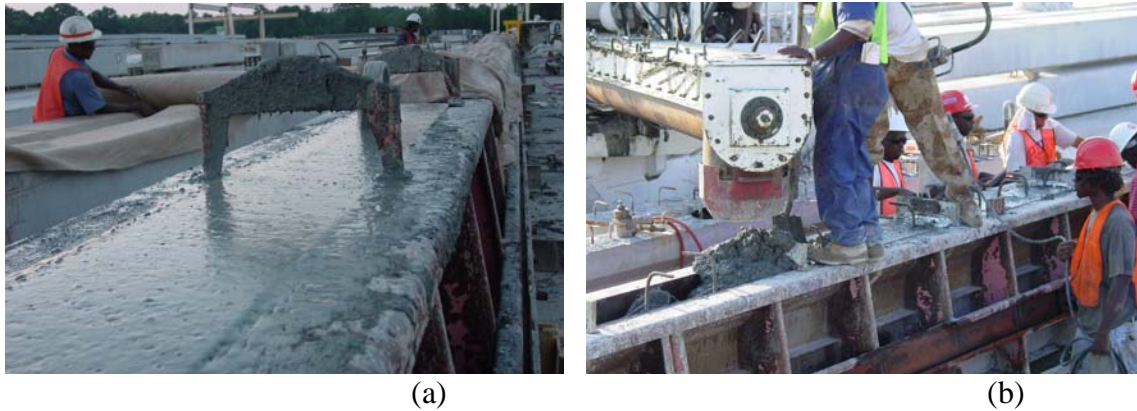


Figure 7. Concrete placement (a) SCC beam immediately after concrete placement (b) standard concrete mix during placement.

2.4 PRESTRESS TRANSFER LENGTH AND STRAND SLIP

The beams were cast in a single line on a single casting bed. The transfer of prestress was accomplished by torch-cutting single strands simultaneously between alternate pairs of beam ends as shown in Figure 8. Cuts were also made at each end of the casting bed, resulting in each beam having one end in which the strands were released suddenly. This method of release is quite abrupt and has been shown to result in longer transfer lengths than a gradual release (Russell and Burns 1997).

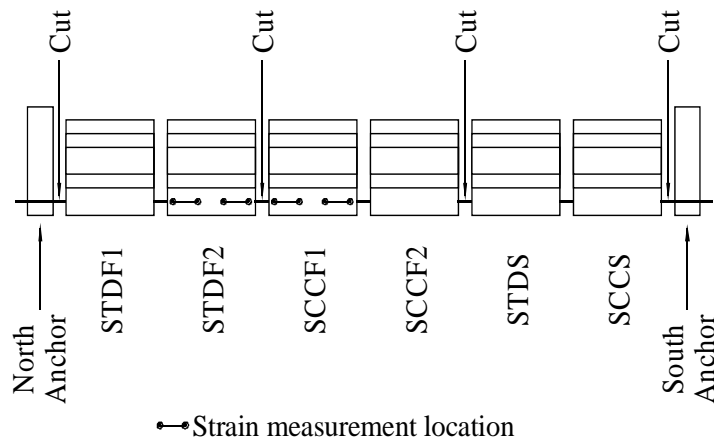


Figure 8. Specimen configuration in prestressing bed.

Due to low early concrete strengths in both the SCC and standard beams and scheduling conflicts, the prestress transfer was delayed until fifteen days after casting. The five-day cylinder compressive strengths from the precasting plant were 3170 psi for the standard concrete and 3810 psi for the SCC. It is not known why the early strengths were low. One possibility is thought to be a change in the cement used to produce the concrete, which occurred after the verification mix but before the beam mix.

Before the transfer of prestress, strain gauges were installed on the bottom flange of each end one standard beam and one SCC beam (Figure 9). The data gathered from these strain gauges before and after release were used to calculate the transfer lengths of the strands.

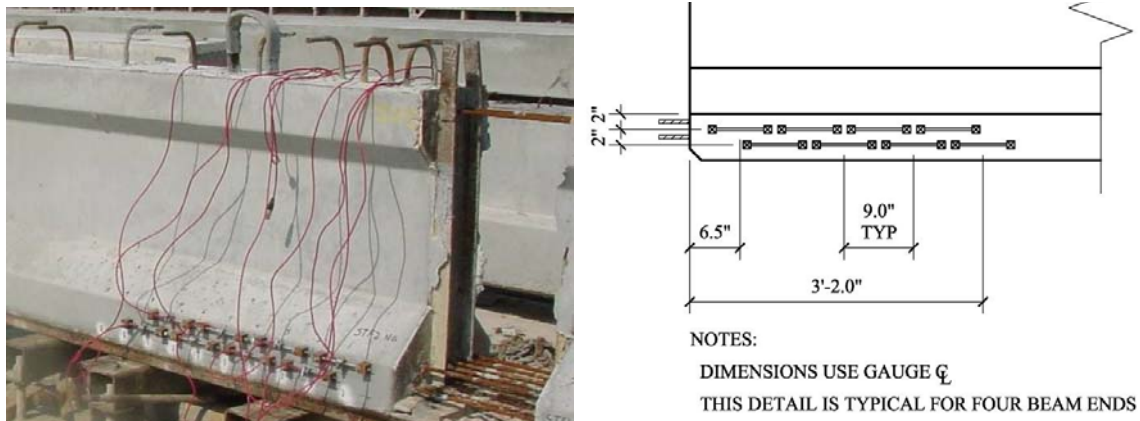


Figure 9. Transfer length instrumentation setup

2.5 CAMBER MONITORING

The camber on each beam was monitored from transfer of prestress to approximately 200 days after casting. The camber monitoring setup consisted of piano wire strung over pulleys on the vertical face of the top flange at each end of all beams (Figure 10). A scale was affixed to

each beam behind the wire at the beam midspan, and a mirror was installed behind each scale to eliminate parallax errors. Measurements were taken at sunrise to eliminate heating effect errors.



Figure 10. Camber monitoring of beams

2.6 STRUCTURAL TESTING

All beams were tested in three-point loading as shown in Figure 11 with the distances specified in Table 1. Both ends of each beam were tested by placing the middle loading point close to the respective end. The testing program was designed to compare the structural behavior of SCC beams with standard beams, including ultimate load, deflection at the ultimate load, measured to theoretical capacity ratio, strand slip, and web cracking load. The focus of the testing was on the flexural and shear failure modes. The shear span (A/d) was varied among the test configurations to force either a flexural or shear failure mode, as indicated in Table 1. Furthermore, the distance from the end of the beam to the center of the support was reduced to enhance the chance of strand debonding and slip. In subsequent discussions, each test will be referred to by the designation given in Table 1. For instance S1-SCCS is the shear test conducted on the north end of beam SCCS.

Table 1. Test setup geometry

Test-Beam	Target Failure mode	Location*	A	B	C	A/d
S1-SCCS	Shear	North	6'-0"	28'-6"	1'-6"	2.25
S2-SCCS		South	5'-0"	28'-6"	1'-0"	1.88
S1-STDS		North	6'-0"	28'-6"	1'-6"	2.25
S2-STDS		South	5'-0"	28'-6"	1'-0"	1.88
F1-SCCF1	Flexure	North	9'-2"	21'-2"	1'-0"	2.50
F2-SCCF1		South	10'-0"	20'-0"	1'-0"	2.73
F1-STDF2		North	9'-2"	21'-2"	1'-0"	2.50
F2-STDF2		South	10'-0"	20'-0"	1'-0"	2.73
SS1-SCCF2	Strand Slip	North	6'-6"	28'-6"	6"	1.76
SS2-SCCF2		South	6'-0"	29'-0"	6"	1.63
SS1-STDF1		North	6'-6"	28'-6"	6"	1.76
SS2-STDF1		South	6'-0"	29'-0"	6"	1.63

* Location of beam end in casting bed.

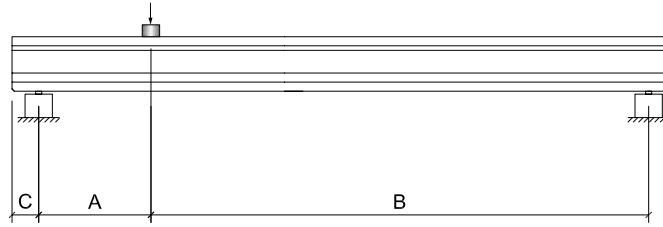


Figure 11. Three point loading test geometry

Two of the six beams were constructed and tested to investigate the shear behavior of the SCC beam as compared to the standard beam (*Shear* in Table 1). It was intended that the shear test geometry would create a concrete strut or node crushing failure mode, along with the possibility of some bonded strand movement. Two beams were constructed and tested to investigate the structural behavior of the SCC beam as compared to the standard beam in a condition of combined shear and flexure (*Flexural* in Table 1). The intent was that the geometry of the shear-flexure tests would cause a flexural failure mode with considerable shear cracking. Finally, two of the beams were tested in a condition of high shear with a short available development length (*Strand-slip* in Table 1). The beam was positioned on the support such that there was a six-inch overhang at the bearing. This bearing placement was used to promote a strand slip failure mode. The wide stirrup spacing previously discussed in SCCS and STDS used to minimize the influence of the transverse steel on the performance of the beams. The other four beams included a standard arrangement of steel reinforcing, which meet the requirements of the AASHTO LRFD Bridge Design Specification for a fictitious bridge as detailed previously.

The test setup and instrumentation for each test is shown in Figure 12 through Figure 14. Linear variable displacement transducers (LVDTs) were used to monitor beam deflection and strand movement at the beam end. Additionally, crack gauges were installed on the vertical face of the beam web and oriented to measure diagonal tension. The crack gauges were type PI-5-200 manufactured by TML. Also, crack gauges were installed on top of the beam and oriented to measure strain in the transverse direction. For the shear-flexure tests, crack gauges were installed in a line on the vertical faces of the beam under the position of the load cell to monitor the strain due to flexure. The strand pattern and instrumented strands are shown in Figure 15. The load was increased at a rate of approximately 0.15 kips per second until a peak capacity was identified.

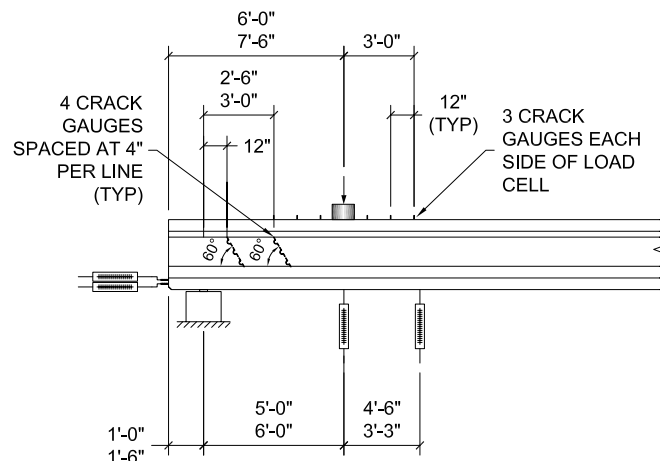


Figure 12. Shear test setup and instrumentation

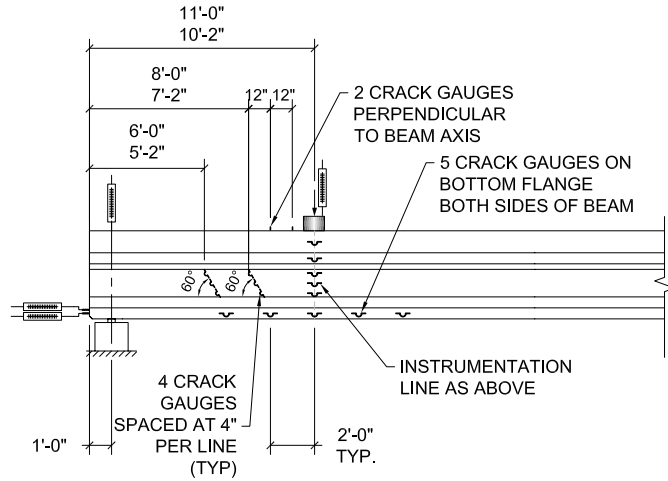


Figure 13. Shear-flexure test setup and instrumentation

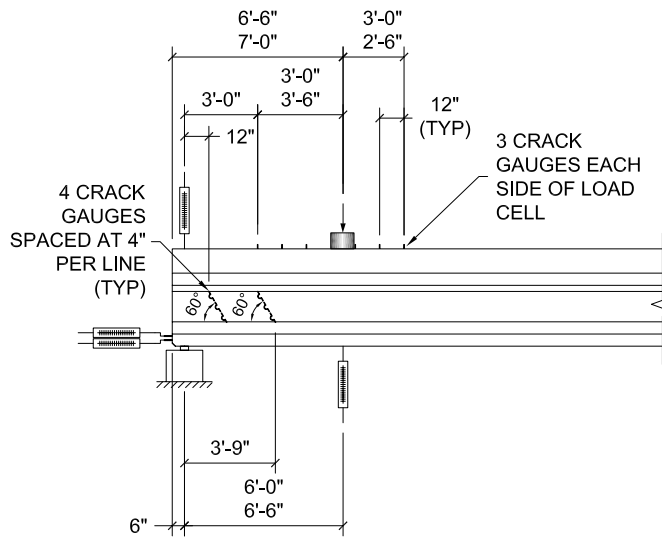


Figure 14. Shear-slip test and instrumentation

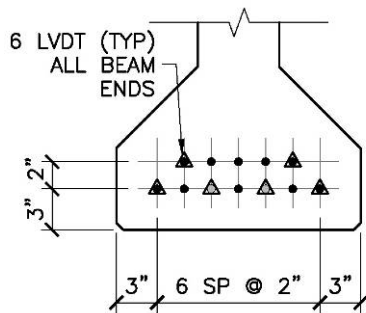


Figure 15. Strand instrumentation

3 TEST RESULTS AND DISCUSSION

3.1 TRIAL MIX TESTS

Trial mixes were prepared using the designs shown in Table 2. Table 3 shows the plastic property testing for the trial batches including unit weight, slump, spread, J-Ring, and L-Box tests. The hardened property testing included compressive (Figure 16) and tensile strength (Table 4) tests at varying ages. To achieve the targeted plastic properties for the mixes, it was necessary to add multiple dosages of HRWR to the Pair A SCC mix and the Pair B control mix with the total dosage equal to that indicated in Table 2. The admixture supplier indicated that a smaller quantity added in a single dose would have the same effect. After conducting the plastic and hardened property tests, it was determined that mix design Pair B would be used for the verification batch. The mix was modified slightly so that a smaller dosage of high-range water reducing (HRWR) admixture was added to the control mix and a larger HRWR dosage was used to create the SCC properties with little change in other constituent volumes.

Table 2. Trial mix designs

Constituents*	Description	Pair A		Pair B*	
		Control (lbs/cy)	SCC (lbs/cy)	Control (lbs/cy)	SCC (lbs/cy)
Cement	Lehigh Type I/II	686	686	752	752
Fly ash	ISG Class F	154	154	168	168
Coarse aggregate	Tarmac #67	1725	1400	1307	1307
Fine aggregate	Florida Rock silica sand	1047	1400	1414	1414
Water	Local	252	252	258	258
Admixtures		(oz/cy)	(oz/cy)	(oz/cy)	(oz/cy)
Air entraining agent	MBVR-S	5.0	1.7	1.8	1.8
Set retarding water reducer	Pozzolith 100 XR	25.2	12.6	13.8	13.8
High range water reducer	Glenium 3200 HES	25.2	73.5	62.1**	64.4

*Mix design selected for verification mix and to construct beam

**Final mix used 27.6 oz/cy in a single dose

Table 3. Trial mix fresh properties

Plastic properties	Pair A		Pair B	
	control	SCC	control	SCC
Unit weight	138.5 pcf	142.5 pcf	145.8 pcf	146.6 pcf
Air content	5.50%	4.25%	2.50%	2.25%
Temperature	73°F	74°F	74°F*	73°F
Slump	5.3-in.	n/a	5.0-in.	n/a
Slump flow	n/a	26.8-in.	n/a	27.5-in.
Slump flow T-20	n/a	3.7 sec	n/a	13.2 sec
J-ring spread	n/a	21.5"	n/a	23.5"
J-ring T-20	n/a	15.2 sec	n/a	40.3 sec
J-ring H1/H2	n/a	5.8 in./4.3 in.	n/a	6.0 in./4.3 in.
L-box T-200	n/a	2.4 sec	n/a	6.0 sec
L-box T-400	n/a	5.8 sec	n/a	14.1 sec
L-box H1/H2	n/a	5.3 in./3.5 in.	n/a	5.3 in./3.3 in.

*Approximate value

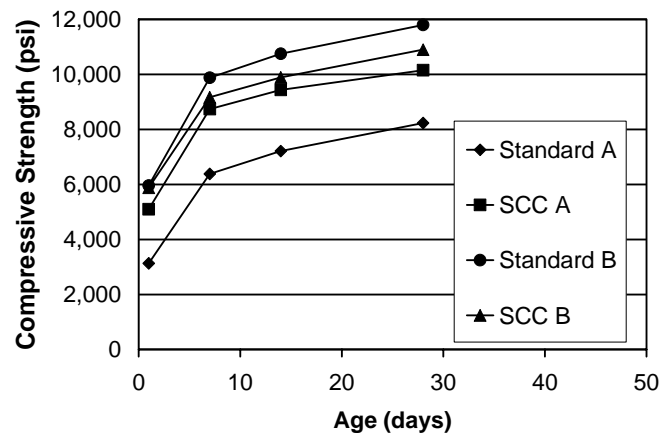


Figure 16. Trial mix average compressive strength gain

Table 4. Trial mix 28-day tensile strength using split cylinder (psi)

Pair A		Pair B	
Control	SCC	Control	SCC
705	835	860	815

3.2 VERIFICATION MIX TESTING

The mix design for pair B from Table 2 was used to create full-size batches at the plant. This mix was also used for constructing the beams. The plastic property testing included slump,

spread, J-ring, L-box, and V-funnel tests. A summary of the test results is shown in Table 5. The plastic properties were found to be comparable or better than the small mixes prepared initially.

Table 5. Verification mix plastic properties

Test	Standard	SCC
Slump	7.2-in.	n/a
Slump flow	n/a	27.2 in.
Slump flow T-20	n/a	1.3 sec
J-ring spread	n/a	28.0 in.
J-ring T-20	n/a	1.3 sec
J-ring H1/H2	n/a	5.75 in./5.5 in.
L-box H1/H2	n/a	4.0 in./4.0 in.
L-box T-200	n/a	0.5 sec
L-box T-400	n/a	1.0 sec
U-box H1/H2	n/a	13.75 in./14.0 in.
V-funnel flow	n/a	2.0 sec

3.3 BEAM CONSTRUCTION

It is estimated based on observations made by one of the authors during beam construction that the SCC beams were poured in approximately 40% less time, and they required approximately 50% fewer workers than the standard beams due to the increased flow rate of the concrete and the elimination of side mounted and internal vibrators. Eliminating use of vibrators also reduced the noise level of the casting process, resulting in a more pleasant work environment. Having fewer workers on top of the SCC beam forms also increased the safety level.

To ensure an adequate connection between each flexure beam and its top flange, the top surface was roughened (raked). Unlike the SCC beams, it was possible to roughen the standard beams immediately after being poured. The SCC beams required approximately 1.5 hours set time for the paste to have sufficient stiffness to hold a roughened surface. As demonstrated by a greater amount of leakage of the concrete from the SCC beam forms than the standard beam forms, it is necessary to have watertight forms with SCC construction. Additionally, complete coverage of steel forms with form oil is important because the flowable nature of SCC causes increased adhesion and the possibility of damage upon form removal. The stronger bond is caused by the high flowability of SCC, enabling it to flow into very small surface irregularities of the forms. If forms are suitably coated with form-release agent and the formwork is watertight, then the SCC will provide a better formed finish.

3.4 CASTING MIX MATERIAL TESTS

The beams were constructed using concrete mixed in the prestressing supplier's batch plant, as was done for the verification mix. A number of fresh property tests were conducted on the SCC beam mix, and the results are shown in Table 6.

Table 6. Beam mix plastic properties

Test	Standard	Result
Standard slump	4.7 in.	n/a
Slump flow	n/a	24.7 in.
Slump flow T-20	n/a	1.6 sec
J-ring spread	n/a	25.3 in.
J-ring T-20	n/a	2.4 sec
J-ring H1/H2	n/a	5.75 in./5.25 in.
L-box H1/H2	n/a	4.0 in./4.0 in.
L-box T-200	n/a	0.5 sec
L-box T-400	n/a	1.0 sec
U-box H1/H2	n/a	13.0 in./14.0 in.
V-funnel flow	n/a	1.9 sec

Cylinders were taken from the beam mix casting for later compressive and tensile strength testing. One set of cylinders was shipped to the FDOT State Materials Office for storage and testing. The results of these tests are shown in Figure 17. The cylinders for these compressive test results were moist cured and tested at typical ages. An additional set of cylinders was transported with each beam to the FDOT Structures Laboratory and were tested when the respective beam was tested (Table 7). These cylinders were cured and stored with the beams until testing. Beam testing occurred approximately 8 to 10 months after the beams were constructed compared to the early age testing of the cylinders shown in Figure 17. The SCC beams all tested above 9,000 psi, while two of the three standard mix beams tested at approximately 7,500 psi. One of the standard mix beams, however, tested over 10,000 psi. It is not clear why there is such a difference in the standard mixes. Concrete top slabs (cap) were placed on four of the beam specimens prior to testing. The results are shown at the bottom of Table 7. The compressive strengths for these specimens were relatively consistent with the exception of the cap for SCCF2.

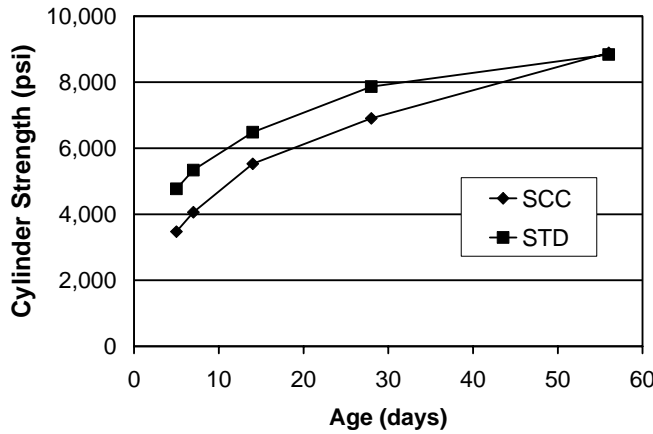


Figure 17. Beam mix average cylinder strength comparison

Table 7. Compressive strength results from cylinders tested on or near date of beam test.

Test-Beam	Strength 1 (psi)	Strength 2 (psi)	Average Strength (psi)
SCCF1	9,428	8,760	9,090
SCCF2	10,710	11,095	10,900
SCCS	9,910	10,155	10,030
STDF1	10,610	10,544	10,580
STDF2	7,461	7,854	7,660
STDS	7,219	7,762	7,490
SCCF1 Cap	7,886	7,603	7,740
STDF2 Cap	7,515	7,227	7,370
SCCF2 Cap	8,994	8,936	8,960
STDF1 Cap	7,923	6,967	7,440

Table 8. Twenty-eight day tensile strength test comparison

Test	Average Tensile Strength (psi)	
	Standard	SCC
Split cylinder (ASTM C496)	813	712
Beam (ASTM C78)	898	859

Additional hardened property tests conducted by the FDOT State Materials Office included shrinkage and surface resistivity. The results are shown in Figure 18 and Figure 19.

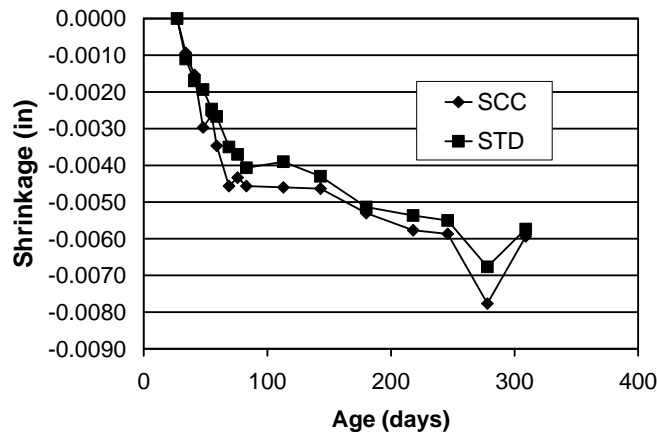


Figure 18. Comparison of SCC and standard mix shrinkage

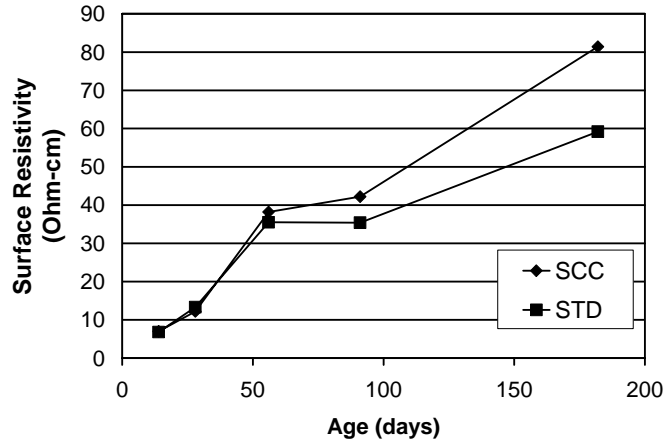


Figure 19. Comparison of surface resistivity

3.5 PRESTRESS TRANSFER LENGTH AND STRAND SLIP

Due to low early concrete strengths and scheduling conflicts, the prestress release was delayed until fifteen days after casting. The five-day cylinder compressive strengths from the precast plant were 3170 psi for the control concrete and 3810 psi for the SCC. It is not known why the early strengths were low.

The transfer length is the distance from the beam end to the point where the strand is at its full prestress force. The strain data were used to estimate this length. One technique is the 95% Average Maximum Strain (AMS) method developed by Russell and Burns (1997). The procedure is as follows:

Plot the strain profile.

1. Determine the AMS for the specimen by computing the numerical average of all the strains contained within the strain plateau of the fully effective prestress force.
2. Multiply the AMS by 0.95 and construct a line corresponding to this value.
3. Prestress transfer length is the intersection of the strain profile with the 95% AMS line. This step was modified slightly due to the low number of sensors used to measure strain. The transfer length is determined by the intersection of the 95% AMS and a best-fit line using the first two strain gage points and the origin (Figure 20 through Figure 23)

Long length vibrating wire strain gages necessitated the use of fewer gages that were staggered along the bottom of the beam. The strain readings of these gages were adjusted to the height of the tendon centroid using the strain profile and assuming that the strain profile remained linear. The strains from the innermost gauges clearly within the fully effective prestress force were used to calculate the 95% AMS. The first two strain points and the origin were used for a linear best-fit line. In one case, only one gauge was within the transition region due to another gauge being nonfunctional, and therefore the intersection of the strain profile with the 95% AMS was used to determine the transfer length (Figure 23). The instrumentation and

analysis methods used here are sufficient to compare the prestress transfer lengths of the SCC and control beams.

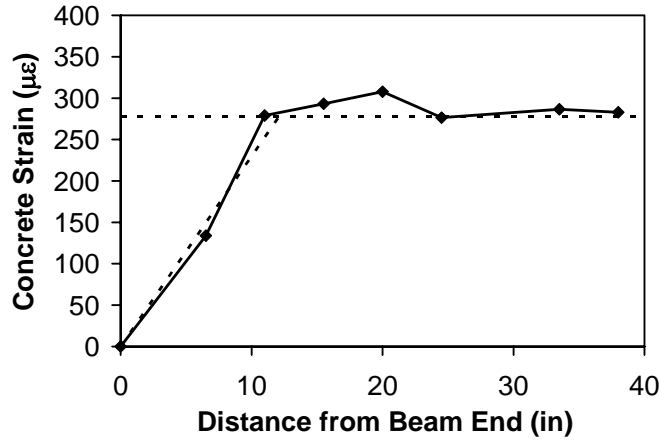


Figure 20. Transfer length determination plot for STDF2 north

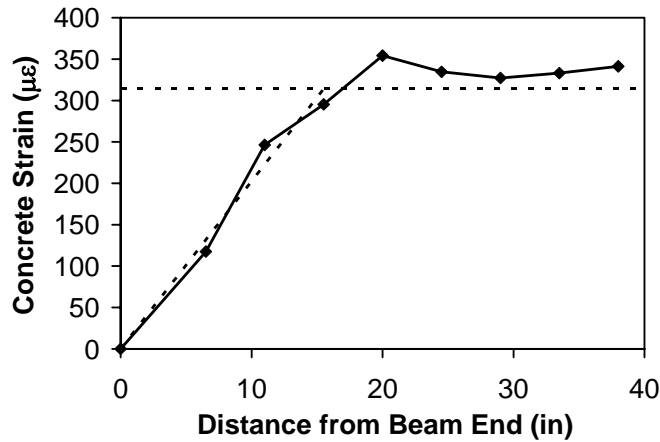


Figure 21. Transfer length determination plot for STDF2 South

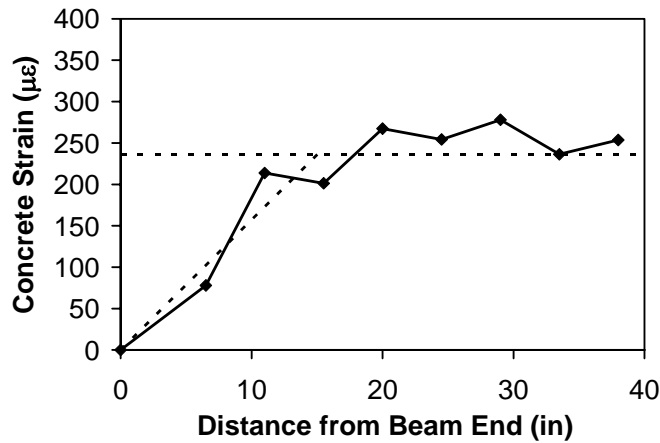


Figure 22. Transfer length determination plot for SCCF1 North

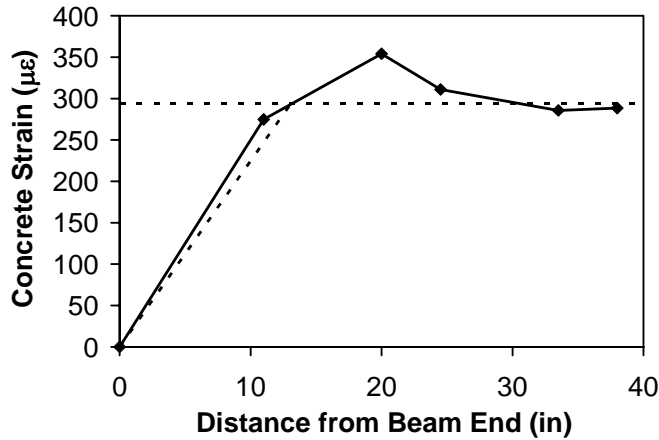


Figure 23. Transfer length determination plot for SCCF1 South

Transfer lengths calculated using the previously described procedure are shown in Table 9. Both beams in which the prestress transfer was sudden exhibited longer transfer lengths regardless of the concrete type. Similarly, the transfer lengths at the opposite ends from the sudden release exhibited shorter transfer lengths. Even with the additional transfer length caused by the sudden release, the measured transfer lengths are conservative compared to the AASHTO LRFD Bridge Design Specifications ($30 \cdot d_b = 60$ in.).

Table 9. Calculated prestress transfer lengths.

Test-Beam	Location	Torch cut	Transfer Length (in)
F1-STDF2	North	no	12.1
F2-STDF2	South	yes	15.5
F1-SCCF1	North	yes	15.0
F2-SCCF1	South	no	13.0

The average strand movements of the fully bonded strands caused by the transfer of prestress are shown in Figure 24. The results are quite variable, but they show that there is generally no difference in the materials with respect to strand movement.

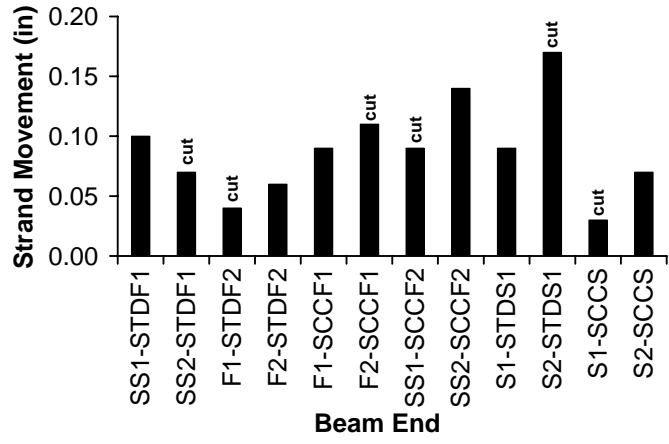


Figure 24. Prestress transfer average strand movement of fully bonded strands. *Cut* indicates tendon location that was torch-cut during prestress transfer.

3.6 CAMBER MONITORING

Figure 25 shows the mean camber of the SCC and standard beams over the camber test period. The plots are closely grouped indicating that there is little difference in the camber behavior between the SCC and standard beams. Theoretical camber was approximated using simplified multipliers at a standard erection age of 60 days (Nilson 1987). It is possible that the delay of prestress transfer resulted in lower camber than if an earlier release age was used. The results of these beam tests indicate that the camber approximation provides a good estimate of camber for both the SCC and standard beams.

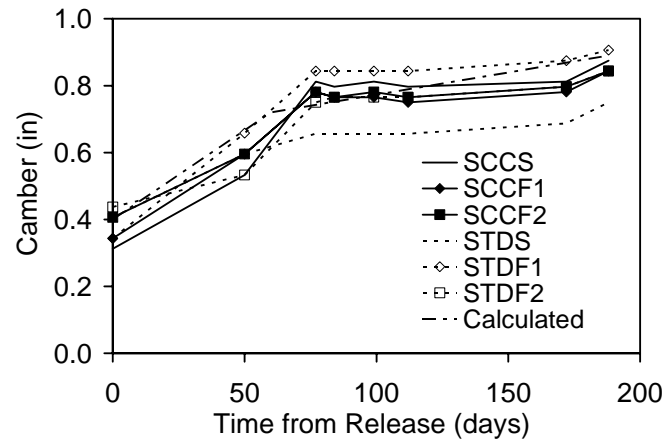


Figure 25. Camber versus time

3.7 SHEAR TEST

Both beams were loaded at a rate of 0.15 kips per second in three-point loading as described in Figure 11 and Table 1. Web cracking consistently formed suddenly in the beams when the load was between approximately 110 kips to 120 kips in both standard and SCC specimens. All four shear tests resulted in a single crack with a common angle of approximately 30° for each beam (Figure 26 and Figure 27). The load versus deflection remained linear until the loads were between approximately 155 kips and 220 kips (Figure 28). No movement of fully bonded strand was detected except for S2-STDS, in which the fully bonded strands began displacing at a load of 195 kips. The load versus deflection for all beams reached a plateau and had a very short inelastic range with failure loads between 180 kips and 230 kips with approximately one inch of deflection preceding a drastic loss in load. The failure mode for all four shear tests was a compression failure in the top flange under and adjacent to the load point.

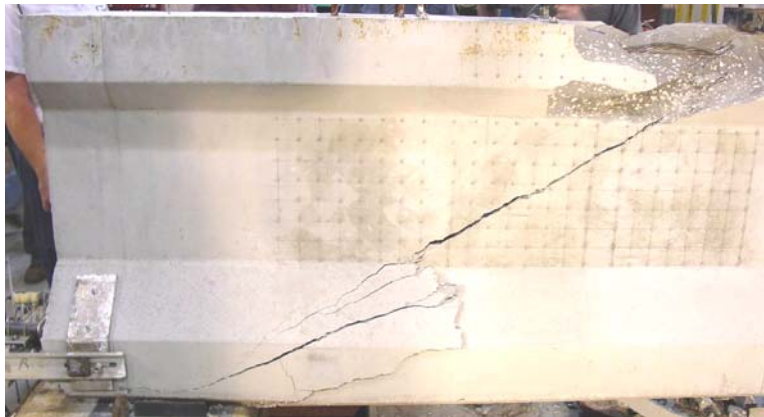


Figure 26. Failed S2-SCCS beam

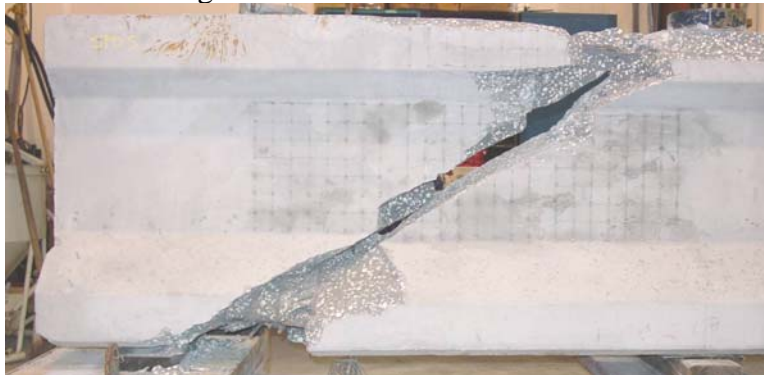


Figure 27. Failed S2-STDS beam

Table 10 shows the peak loads and maximum deflections. The maximum deflection was measured under the load and is the deflection just before the sudden loss in load. The S1-STDS beam performed slightly better with an 8.7% greater load carrying capacity than the S1-SCCS beam. The S1-STDS beam also deflected approximately 22% more than the S1-SCCS beam. The S2-SCCS and S2-STDS beams had nearly identical failure loads and deflections.

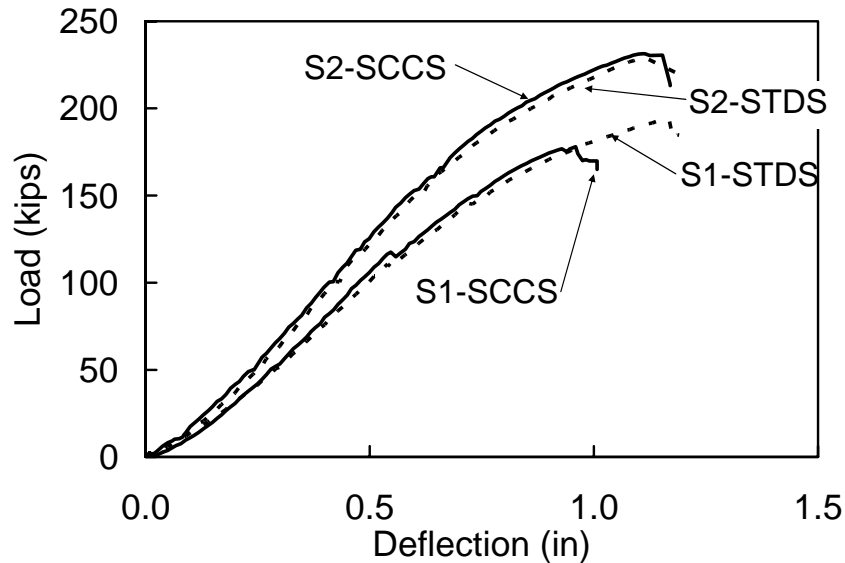


Figure 28. Comparison of beam behavior during shear tests. Deflection measured under load point.

Table 10. Maximum loads and deflections for shear tests

Test-Beam	Maximum Load (kips)	Cut*	Maximum Deflection (inches)
S1-SCCS	178.0	No	0.96
S1-STDS	193.4	Yes	1.17
S2-SCCS	231.4	Yes	1.17
S2-STDS	229.3	No	1.11

*Yes indicates this beam end was the cutting end during prestress transfer

Figure 29 through Figure 32 show the displacements of each strand for the shear tests. Only in test S2-STDS was slip noted in the instrumented fully bonded strands. In that test, strands one and two clearly began displacing at a load of 195 kips as shown in Figure 32. The SCC beam reached a slightly higher ultimate capacity than the standard beam, and the SCC beam reached this capacity without any strand slip. The strand movements of the sheathed strands were approximately the same for the SCC beams and the standard beams. The bonded strand displacement with the standard beam may be explained by considering the results from the transfer of prestress. There was a large amount of strand movement at the end of the beam during the transfer of prestress as shown in Figure 24. This large amount of strand movement during the prestress transfer may have contributed to the observed strand slip during the structural testing of the standard beam.

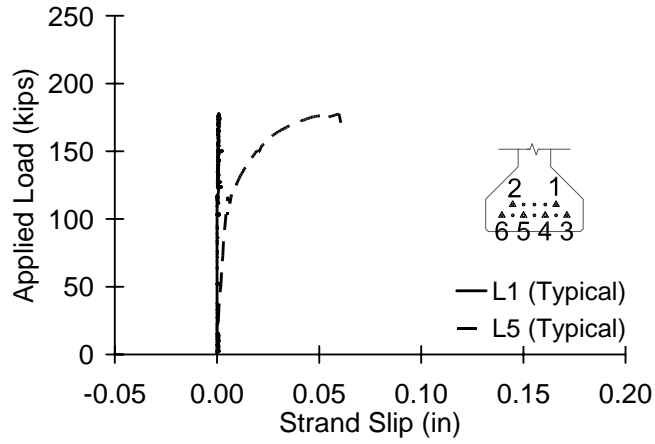


Figure 29. Strand slip for S1-SCCS

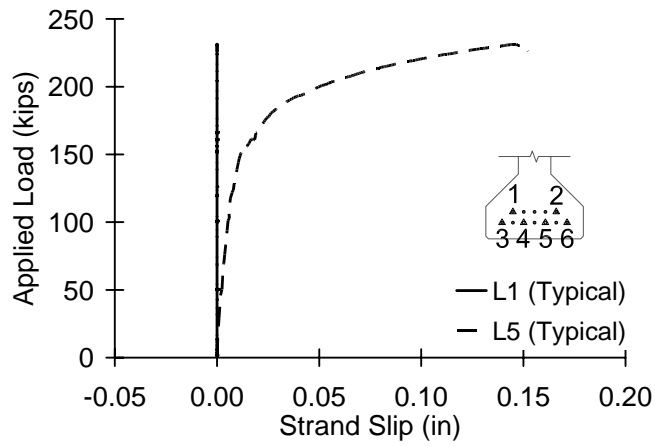


Figure 30. Strand slip for S2-SCCS

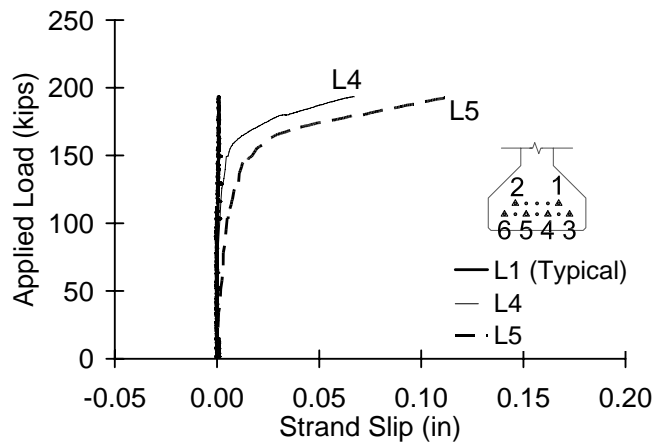


Figure 31. Strand slip for S1-STDS

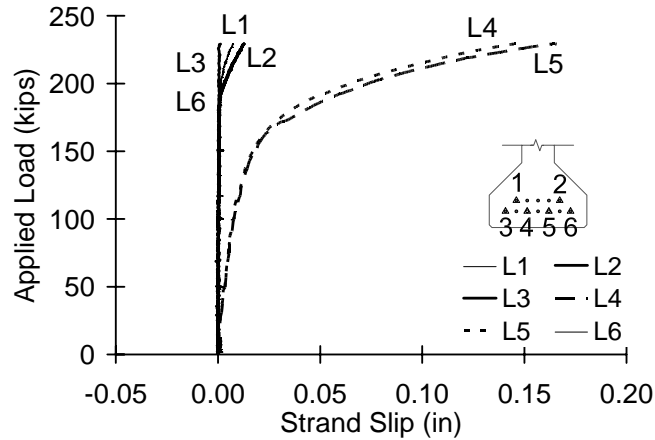


Figure 32. Strand slip for S2-STDS

In each of the four shear tests, a single diagonal crack formed in the web well before the ultimate load capacities were reached. This is likely due to the lack of shear reinforcement in the web in the high-shear region. The cracking did not significantly reduce the stiffness of the beam up to capacity with the exception of S1-SCCS. The web cracking and ultimate loads are compared in Table 11.

Table 11. Shear test web cracking and ultimate loads

Test-Beam	Cracking Load (kips)	Peak Load (kips)
S1-SCCS	117.6	178.0
S1-STDS	111.9	193.4
S2-SCCS	120.1	231.4
S2-STDS	114.0	229.3

The cracking loads are remarkably consistent among the four tests with a maximum difference of less than 10%. The compressive strength tests conducted on the day of the beam tests do not provide a good predictor of the cracking and ultimate loads (Table 7). The cylinder tests indicate that the SCC compressive strength is 33% greater than that of the STD. In contrast, the tensile strengths from Table 8 indicate a 14% or 5% difference in tensile strength considering the split cylinder and beam tests, respectively. Even though the STD tensile strength is greater than that of the SCC, the data suggests that the tensile strength is a better predictor of the shear behavior than that of compressive strength.

Table 12 shows a comparison of the measured ultimate capacities with the calculated capacities using three analytical models. The ACI theoretical capacity is calculated from the sectional shear strength of the beam given by ACI Section 11.4.1 (ACI 2002). The AASHTO theoretical capacity was calculated using the modified compression field theory from the shear strength provisions of the AASHTO Bridge Design Specification (AASHTO 1998). In both the ACI and AASHTO sectional analyses, it was assumed that three #5 stirrups contributed to the shear strength of the cross-section. The strut and tie analysis conforms to the approach given in ACI 318-02 Appendix A. A single strut was assumed to extend from the support to the load point with the prestressing strand providing the tie necessary to balance the strut force at the

support point. The strut angle for the shear test configuration was approximately 22 degrees, which is slightly less than the 25 degree minimum allowed by the ACI provisions. Since the load was very close to the support in each test, a strut and tie analysis is a more appropriate than a sectional analysis, which is intended for the B-region portions of the beam (away from concentrated loads). The results of the comparison indicate that the sectional models are conservative compared to the actual measured capacities while the strut and tie model provides a calculated capacity closer to that of the measured. In one case the strut and tie model is slightly unconservative (S1-SCCS). The compressive strength of the strut in the model controlled the strut-and-tie analysis, which matched the actual failure mode.

Table 12. Comparison of analytical models for shear dominated failure mode.

Test-Beam	P_{test} (kips)	P_{ACI} (kips)	P_{test}/P_{ACI}	P_{AASHTO} (kips)	P_{test}/P_{AASHTO}	P_{strut} (kips)	P_{test}/P_{strut}
S1-SCCS	178.0	124.0	1.44	145.0	1.23	182.8	0.97
S1-STDS	193.4	108.2	1.79	119.0	1.63	162.9	1.19
S2-SCCS	231.4	120.6	1.92	148.0	1.56	232.1	1.00
S2-STDS	229.3	105.3	2.18	128.0	1.79	196.3	1.17
Average			1.83		1.55		1.08

All three analysis methods incorporate the compressive cylinder strengths from Table 7 to calculate shear capacity. As such, all three methods predict different shear capacities for the SCC and standard specimens. The measured capacities for S1-SCCS and S1-STDS, however, are very close (within approximately 8%); much closer than predicted by the analytical methods. As discussed previously, the 28-day tensile strengths of the SCC and the standard are similar, indicating that the behavior and failure mode are perhaps dominated by the direct tensile strength rather than the term currently used in the sectional models to account for tensile strength ($\sqrt{f'_c}$). The difference is even more apparent when comparing the actual capacity of S2-SCCS and S2-STDS (less than 1% difference).

One final conclusion that can be drawn from the comparison of the test data is that little difference was noted when comparing the performance of SCC and standard concrete for this series of testing.

The aggregate distribution at the shear crack in SCCS girder was examined. Figure 33 shows the face of the crack after removal of the beam end. Although no quantitative measurements were made, there appears to be less aggregate in the top flange than at the bottom. Inspection of the crushed top portion of the beam at the opposite end, however, indicated that more aggregate remained in the top of the beam at that location.



Figure 33. SCCS girder after shear testing. Note higher density of aggregate in the bottom of beam than in the top.

3.8 *SHEAR-FLEXURE TEST*

Web cracking formed in the beams under a constant load application rate at a load in the range of 144 kips to 157 kips. The load-deflection response remained linear until a load of approximately 200 kips (Figure 34). The load versus deflection for all beams reached a plateau typical of a flexure dominated failure mode. The peak loads reached ranged between 248 kips and 263 kips with 1.6 to 3.1 inches of deflection preceding a sharp drop in load. In all four shear-flexure tests, the composite cap failed in compression due primarily to flexural compressive stress at the location directly under the load point. Figure 35 and Figure 36 show the F2-SCCF1 beam and F2-STDF2 beam following failure and unloading. Both beams had typical flexural tensile cracks emanating from the bottom of the beam under the load point. Visual observation indicated comparable cracking pattern and widths in the SCC and standard

specimens. Due to the short distance between the load point and support, the beams experienced high shear stresses simultaneously with the high flexural stresses, causing considerable diagonal cracking to form. This is in contrast to the shear tests, which had a negligible amount of shear reinforcement. The shear crack spacing and widths upon visual inspection appeared similar for both beams.

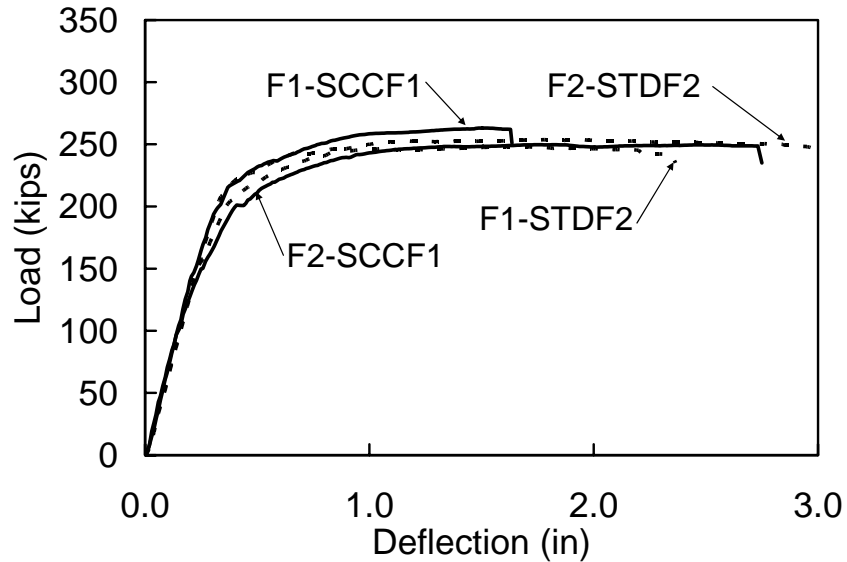


Figure 34. Comparison of beam behavior during shear-flexure tests. Deflection measured under load point.



Figure 35. Failed F2-SCCF1 beam

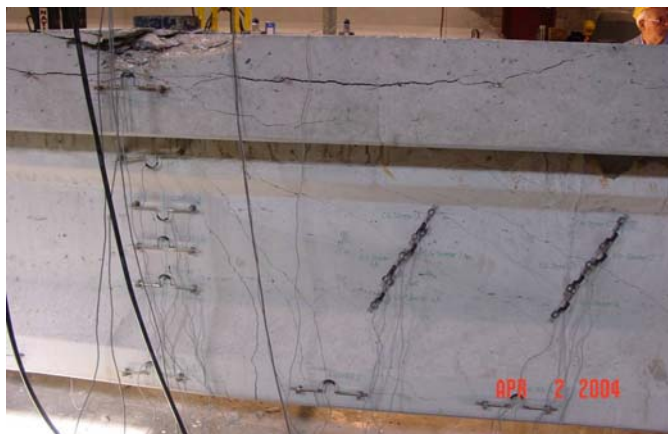


Figure 36. Failed F2-STDF2 beam

Table 13 shows the maximum loads and deflections for the four shear-flexure tests. The beam deflections were measured at the load point. F1-SCCF1 performed slightly better with a 6.0% greater load carrying capacity than the F1-STDF2 beam. F1-STDF2 outperformed F1-SCCF1 in terms of ductility with a 41.5% greater deflection immediately preceding failure. The F2-STDF2 beam performed slightly better than the F2-SCCF1 beam with a 1.6% greater load carrying capacity. The F2-STDF2 beam also outperformed the F2-SCCF1 beam in terms of ductility with a 9.3% greater deflection. In summary, the flexural capacity of the SCC and standard beams were comparable, but the displacement ductility of the standard beam was slightly better than that of the SCC beam.

Table 13. Maximum loads and deflections for shear-flexure tests

Test-Beam	Maximum Load (kips)	Cut*	Maximum Deflection (inches)
F1-SCCF1	263.1	No	1.64
F1-STDF2	248.2	Yes	2.32
F2-SCCF1	249.8	Yes	2.80
F2-STDF2	253.7	No	3.06

*Yes indicates this beam end cut during prestress transfer

Figure 37 through Figure 40 show the displacements of two of the strands during the four shear-flexure tests. No strand movement of the fully bonded strands (L1) was detected in any test. The sheathed strand (L5), however, began to slip at a load of approximately 200 kips leading to the plateau in the load-displacement relationship. The flexural capacity of these specimens was controlled by the compressive strength of the cap and the bond and yield strength of the prestressing strands. As the load increased beyond the elastic range, the strands begin to yield or slip, or both, which is apparent when the capacity of the beam ends adjacent to where the strands were cut are compared to those that were not. The abrupt release of the strands near the anchorage zone at the end of the beam will actually lengthen both the transfer and development length of the strands. This is especially true of the debonded strands. Consequently, the beam ends where the strands were cut have slightly lower flexural capacities than those that were away from the release. This is true regardless of whether the beam was SCC or standard mix.

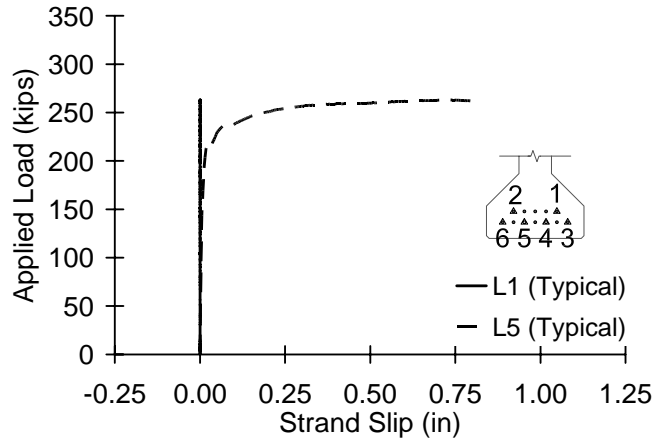


Figure 37. Strand slip for F1-SCCF1

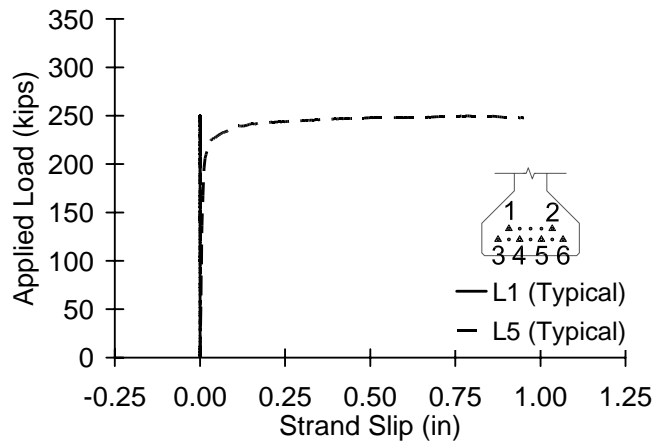


Figure 38. Strand slip for F2-SCCF1

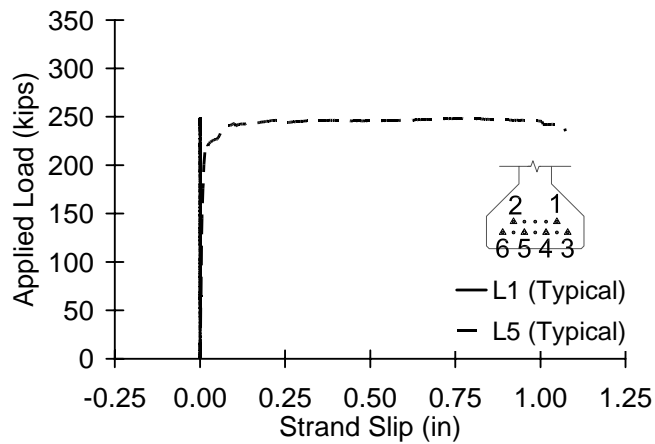


Figure 39. Strand slip for F1-STDF2

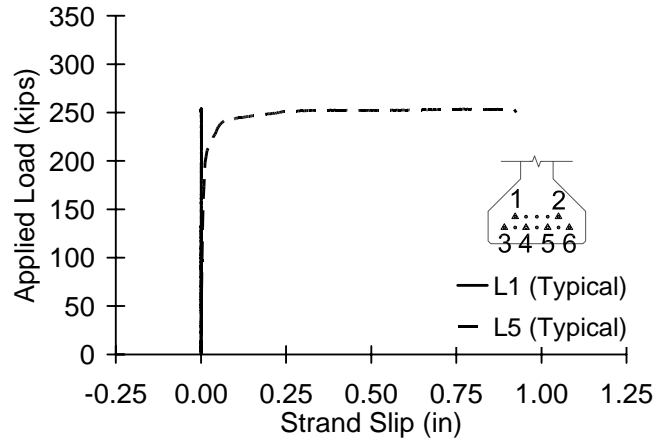


Figure 40. Strand slip for F2-STDF2

Table 14 compares the measured and theoretical capacities. Both ACI and AASHTO provisions require the use of first principles to calculate flexural capacity. The calculated capacities are based on the strength of the cap (Table 7).

Table 14. Comparison of analytical models for flexure dominated failure mode.

Test-Beam	P_{test} (kips)	P_{ACI} (kips)	P_{test}/P_{ACI}	P_{AASHTO} (kips)	P_{test}/P_{AASHTO}
F1-SCCF1	263	259	1.01	258	1.02
F1-STDF2	248	259	0.96	256	0.97
F2-SCCF1	250	247	1.01	246	1.02
F2-STDF2	254	246	1.03	244	1.04

The loads immediately before web cracking for all four shear-flexure tests are shown in Table 15. The cracking load was 3.6% more with the F1-STDF2 beam than the SCC beam, and the cracking load was 3.3% more with the F2-STDF2 beam than the SCC beam. In summary, there is no discernable difference in observed cracking behavior.

Table 15. Shear-flexure tests web cracking load

Test-Beam	Load (kips)
F1-SCCF1	144
F1-STDF2	149
F2-SCCF1	152
F2-STDF2	157

3.9 SHEAR-SLIP TEST

The four shear-slip tests are compared in Figure 41. Initial behavior was linear up to web cracking, which occurred between 124 and 134 kips. Even beyond initial cracking the response remained linear until a load of approximately 220 kips was reached. The load versus deflection

for all beams reached a plateau and had a failure load range of 269 kips to 314 kips with 0.9 to 1.2 inches of deflection preceding a sharp loss in load. With the exception of SS2-SCCF2 the failure mode was compression failure of the composite cap. SS2-SCCF2 failed prematurely due to strand slip at the beam end. Figure 42 and Figure 43 show the SS2-SCCF2 beam and SS2-STDF1 beam following failure and unloading.

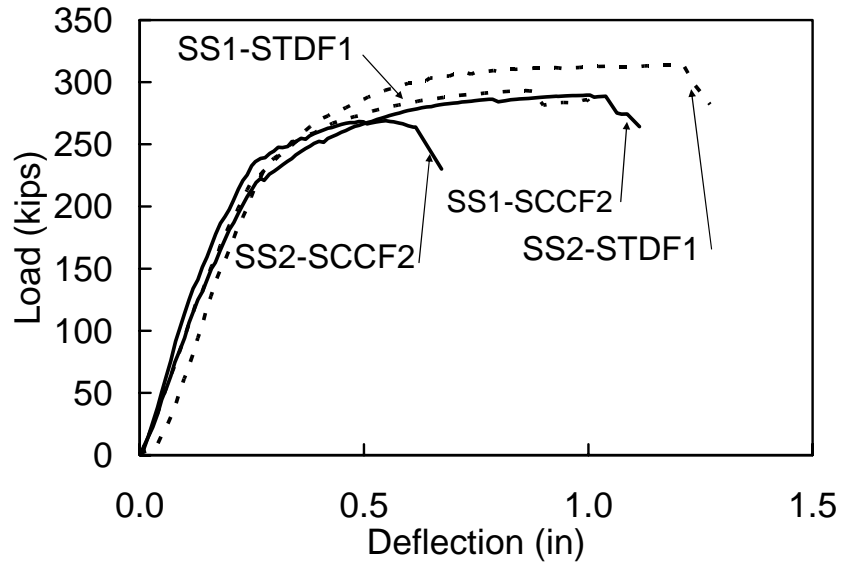


Figure 41. Comparison of beam behavior during shear-slip tests. Deflection measured under load point.



Figure 42. Failed SS2-SCCF2 beam



Figure 43. Failed SS2-STDF1 beam

Table 16 shows the maximum loads and deflections for all four shear-slip tests. Figure 41 is a plot of the deflections that occurred over the full range of loads. The SS1-SCCF2 beam was 18% more ductile than the SS1-STDF1 beam in terms of the beam deflection immediately before failure. SS2-STDF1 had nearly twice the maximum deflection as that of SS2-SCCF2, which was likely due to the strand slip in the latter specimen (discussion to follow).

Table 16. Maximum loads and deflections for shear-slip tests

Test-Beam	Maximum Load (kips)	Cut*	Maximum Deflection (inches)
SS1-SCCF2	290	No	1.04
SS1-STDF1	293	Yes	0.88
SS2-SCCF2	269	Yes	0.61
SS2-STDF1	314	No	1.21

*Yes indicates this beam end was the cutting end during prestress transfer

Table 17 shows the deflections near the end of the linear regions of the load-deflection curves for each beam. SS1-SCCF2 and SS1-STDF1 resulted in nearly equal deformations at 218 kips. The SS2-STDF1 beam had 17% more deflection than the SS2-SCCF2 beam at 228 kips.

Table 17. Load and deflections at end of elastic region for shear-slip tests

Test-Beam	Load (kips)	Deflection (inches)
SS1-SCCF2	218	0.26
SS1-STDF1	218	0.25
SS2-SCCF2	228	0.24
SS2-STDF1	228	0.28

Table 18 shows the strand displacement immediately before failure for the fully bonded strands in the bottom row of the strand arrangement. There was minimal slip in both beams with the SS1-SCCF2 beam performing slightly better than the SS1-STDF1 beam. The SS2-STDF1

beam performed much better than the SS2-SCCF2 beam in the second test due to the change in failure modes likely caused by a difference in the prestress transfer method. The SS2-SCCF2 beam end was at the cutting end during the prestress transfer, and the SS2-STDF1 beam end was at the free end during prestress transfer as shown in Figure 8. The measured transfer lengths presented in this report consistently indicate that there are longer transfer lengths at the cutting end. The large impact force of the quick cutting technique used may have produced sufficient permanent deformation to allow the SCC beam to fail by strand slip. Additionally, the SCC beam moved several inches during the prestress transfer due to the shock of unsynchronized release. STDF1, however, did not move during the prestress transfer.

Table 18. Shear-slip test strand slips at ultimate load

Test-Beam	Strand 3	Slip (in) Strand 6	Average
SS1-SCCF2	0.02	0.02	0.02
SS1-STDF1	0.05	0.07	0.06
SS2-SCCF2	0.30	0.38	0.34
SS2-STDF1	0.13	0.12	0.12

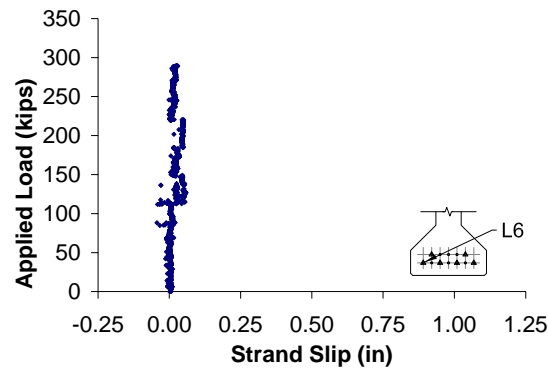


Figure 44. Typical fully bonded strand slip for SS1-SCCF2

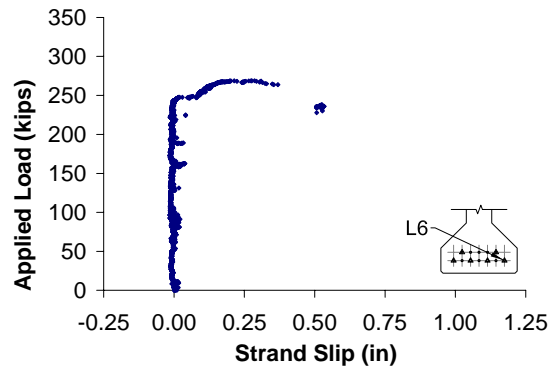


Figure 45. Typical fully bonded strand slip for SS2-SCCF2

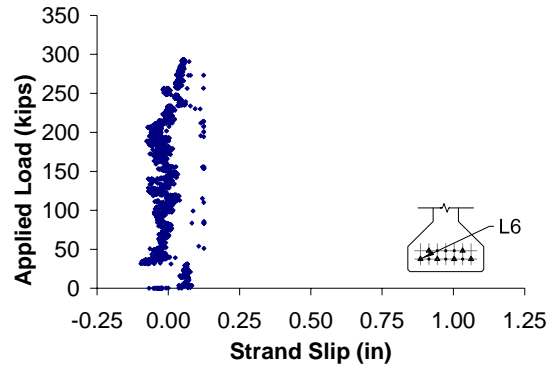


Figure 46. Typical fully bonded strand slip for SS1-STDF1

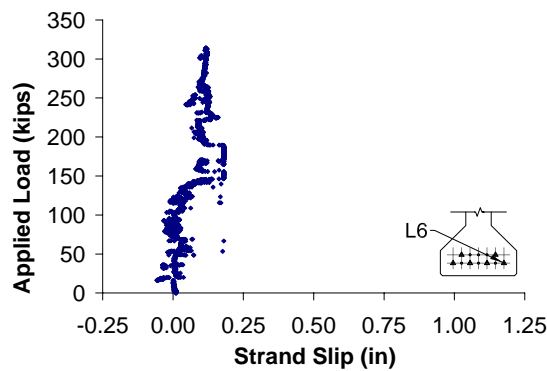


Figure 47. Typical fully bonded strand slip for SS2-STDF1

Table 19 shows the measured failure loads compared to the theoretical failure loads calculated as described previously for a shear dominated failure mode. The AASHTO and ACI capacities were calculated assuming 6 stirrups were actively engaged.

The load immediately before web cracking for each shear-slip test is shown in Table 20. The cracking load for the SS1-STDF1 beam was 5.2% more than the SS1-SCCF2 beam, and the cracking load was 0.9% more for the SS2-SCCF2 beam than the SS2-STDF1.

Table 19. Comparison of analytical models for shear dominated failure mode.

Test-Beam	P_{test} (kips)	P_{ACI} (kips)	P_{test}/P_{ACI}	P_{AASHTO} (kips)	P_{test}/P_{AASHTO}	P_{strut} (kips)	P_{test}/P_{strut}
SS1-SCCF2	290	240	1.21	243	1.19	273	1.06
SS1-STDF1	293	237	1.24	236	1.24	242	1.21
SS2-SCCF2*	269	236	1.14	253	1.06	283	0.95
SS2-STDF1	314	233	1.35	246	1.28	256	1.23
Average			1.23		1.19		1.11

*Strand slip occurred prior to crushing in cap.

Table 20. Shear-slip tests web cracking load

Test	Load (kips)
SS1-SCCF2	124
SS1-STDF1	131
SS2-SCCF2	134
SS2-STDF1	133

4 CONCLUSIONS

This testing program evaluated the mix design development and construction of AASHTO Type II girders using SCC. Six girders were constructed, three with SCC and three with a conventional concrete mix typically used by FDOT in AASHTO girders. Plastic and hardened properties of mix samples were tested. The prestress transfer length on each end of one SCC beam and one standard beam were determined. The camber of the three SCC beams and the three standard beams were monitored from the transfer of prestress to approximately 200 days after casting. Structural testing to destruction was performed with the target failure modes being shear and flexure. The following can be concluded from this testing program:

- Reduced construction time, improved labor efficiency, reduced noise, and improved safety were noted during the construction of the SCC beams.
- In general, the compressive strength of SCC is expected to be higher than that of a corresponding conventional concrete. This was found to be true in one of the two trial mixes prepared during the mix design phase. The other trial mix SCC compressive strengths were lower. SCC used to fabricate the beams was also found to have lower early age compressive strength than the standard concrete. Compressive strengths of the two concretes converged to approximately 8,800 psi at 56 days. Cylinders tested at the time of the beam tests indicated higher compressive strengths for the SCC in most cases. It was not clear why these differences in compressive strengths were noted. Variation in cylinder curing conditions may have contributed. In addition, the cement supplier was changed between the trial mix and beam construction, which may have contributed to the variation.
- No notable differences were found in prestress transfer length, mean camber growth, flexural capacity, shear capacity, or observed web cracking (during load testing) between the SCC and standard beams. One exception was the fully bonded strand slip in SS2-SCCF2, which resulted in a 15% lower ultimate capacity for SCC. It is believed that, based on the transfer length measurements, the abrupt prestress transfer conditions may have contributed to the early slip. Indeed, the prestress transfer conditions may have accounted for more variation in the beam performance than the difference in the type of concrete.
- Total deflections measured during the load tests indicated that the standard mix had slightly better ductility than SCC with the standard beams reaching an average of 17.1% more deflection than the SCC beams at the ultimate load.
- For flexure dominated failure modes, analytical models for flexure (both ACI and AASHTO approach, which are nearly identical) compare very well with the measured capacities with no more than 4% difference. Flexural failure modes consisted of some strand slip and yielding followed by a compression failure and sudden loss in capacity.
- Shear dominated failure modes were observed to consist of either a compression failure in the top of the section (either the top of the precast or topping, depending on the test specimen) near the point of applied load or, in one case, strand slip at the support. This is typical strut and tie behavior that has been commonly observed in previous research.

- Some aggregate segregation was noted in one of the SCC beams, but there was no indication of widespread problems.

5 RECOMMENDATIONS

This program did not encounter any issues that might render the use of SCC imprudent. The structural performance of the SCC test beams was very similar to that of the standard mixes. There are a number of methods that can be used to make concrete that has self-compacting qualities. Some of these methods are sensitive to the mixing procedures and conditions that make close quality control very important to a successful outcome. Consequently, in the current state of practice, it is recommended that SCC only be used in precast plant environment under carefully controlled conditions. The sensitivity of the plastic properties to the mixing procedures and environment make quality control indispensable. The same quality control that is usually exhibited in the precast plant environment may not be apparent under difficult field conditions. This may result in plastic property variation that can cause problems with concrete placement and quality.

6 REFERENCES

- American Association of State Highway and Transportation Officials, "AASHTO LRFD Bridge Design Specifications", Second edition, 1998.
- American Concrete Institute Committee 318, "Building Code Requirements for Structural Concrete (ACI 318-02)" 2002
- Chan, Y. W., Chen, Y. S., and Liu, Y. S., "Development of Bond Strength of Reinforcement Steel in Self-Consolidating Concrete," *ACI Structural Journal*, V. 100, No. 4, July 2003, pp. 490-498
- Khayat, K.H.; Manai, K.; and Trudel, A., "In-Situ Mechanical Properties of Wall Elements Cast Using Self-Consolidating Concrete," *ACI Materials Journal*, V. 98, No. 5, Sept.-Oct. 2001, pp. 371-378
- Martin, L. D., "A Rational Method for Estimating Camber and Deflection of Precast Prestressed Members," *J. PCI*, Jan-Feb, 1977, Vol. 22, No. 1, pp. 100-108
- Nilson, A., "Design of Prestressed Concrete," 1987, p. 346
- Okamura, H., "Self-Compacting High-Performance Concrete," *Concrete International*, July 1996, v 19, no. 7, pp. 50-54.
- Precast/Prestressed Concrete Institute, "Interim Guidelines for the Use of Self-Consolidating Concrete In Precast/Prestressed Concrete Institute Member Plants," *PCI*, TR-6-03, April 2003, 88 p.
- Russell, B. W., and Burns, N. H., "Measurement of Transfer Lengths on Pretensioned Concrete Elements," *Journal of Structural Engineering*, May 1997, pp. 541-549
- Sonebi, M., and Bartos, P. J. M., "Performance of Reinforced Columns Cast with Self-Compacting Concrete," *Recent Advances in Concrete Technology, Proceedings of the Fifth CANMET/ACI International Conference, SP-200*, V. M. Malhotra, ed., American Concrete Institute, Farmington Hills, Mich., pp. 415-431, 2001.
- Sonebi, M., Tamimi, A., and Bartos, P., "Performance and Cracking Behavior of Reinforced Beams Cast with Self-Consolidating Concrete," *ACI Materials Journal*, V. 100, No. 6, Nov.-Dec. 2003, pp. 492-500

APPENDIX A - MIX DESIGN AND TRIAL MIXES

The design, batching, and testing of trial mixes using the standard laboratory mixer shown in Figure 48 was used to determine a mix design for the SCC and control concrete that produced nearly the same strength and provided the targeted plastic properties. A mix design for the SCC and control concrete using the results from the trial mixes was then chosen for testing the mixes in the production-size mixer shown in Figure 49 to verify the plastic properties.



Figure 48. FDOT materials lab concrete mixer in Gainesville Florida

6.1 TRIAL MIX DESIGN AND PROPERTY TESTING

Two standard concrete mixes and two SCC mixes were developed by the FDOT State Materials Research Office for possible use in this project. The trial mixes were then batched and tested to determine the optimum mix design and determine if any adjustments to the constituent amounts in the design were necessary. The relative quantities of cement, fly ash, and water were the same for each design pair. The mixes were designed to achieve the same strength for both types of concrete. A FDOT class VI mix with a targeted concrete strength of 8,500 psi was used. The four final mix matrices are shown in Table 21. To achieve the targeted plastic properties for the mixes, it was necessary to add multiple small increments of glenium to the Pair A SCC mix and the Pair B control mix. The multiple incremental additions of glenium in these two mixes may have inflated the dosages, and therefore a smaller amount of glenium added using a single dose may have produced the same plastic-property influence of the admixture.



Figure 49. Gate concrete products processing and mixing facility

Table 21. Trial mix designs

Constituents*	Description	Pair A		Pair B	
		Control	SCC	Control	SCC
Standard Constituents		(lbs)	(lbs)	(lbs)	(lbs)
Cement	Lehigh Type I/II	686	686	752	752
Fly ash	ISG Class F	154	154	168	168
Coarse aggregate	Tarmac #67	1725	1400	1307	1307
Fine aggregate	Florida Rock silica sand	1047	1400	1414	1414
Water	Local	252	252	258	258
Admixtures		(ozs)	(ozs)	(ozs)	(ozs)
Air entrainer	MBVR-S	5.0	1.7	1.8	1.8
Set retarding water reducer	Pozzolith 100 XR	25.2	12.6	13.8	13.8
High range water reducer	Glenium 3200 HES	25.2	73.5	62.1	64.4

*Amounts are shown per cubic yard

The plastic property testing included unit weight, slump, spread, J-Ring, and L-Box tests. The hardened property testing included compressive and tensile strength tests at different concrete ages. The results from the trial mix property testing are shown in Table 22. After conducting the plastic and hardened property tests, it was determined that mix design Pair B would be used for the verification batch with the necessary modification to the amount of high-range water reducing admixture due to the original incremental additions.

Table 22. Trial mix properties

Plastic properties	Pair A		Pair B	
	Control	SCC	Control	SCC
Unit weight	138.5 pcf	142.5 pcf	145.8 pcf	146.6 pcf
Air content	5.50 %	4.25 %	2.50 %	2.25 %
Temperature	73 °F	74 °F	74 °F*	73 °F
Workability	5.3" slump	26.8" spread	5.0" slump	27.5" spread
Workability T-20	N/A	3.7 sec	N/A	13.2 sec
J-ring spread	N/A	21.5"	N/A	23.5"
J-ring T-20	N/A	15.2 sec	N/A	40.3 sec
J-ring H1/H2	N/A	5.8"/4.3"	N/A	6.0"/4.3"
L-box T-20	N/A	2.4 sec	N/A	6.0 sec
L-box T-40	N/A	5.8 sec	N/A	14.1 sec
L-box H1/H2	N/A	5.3"/3.5"	N/A	5.3"/3.3"
Hardened properties**	(psi)	(psi)	(psi)	(psi)
1 day compressive strength	3,130	5,100	5,960	5,880
7 day compressive strength	6,380	8,740	9,880	9,170
14 day compressive strength	7,209	9,442	10,749	9,892
28 day compressive strength	8,231	10,147	11,762	10,899
28 day tensile strength	705	835	860	815

*Approximate value

**Average values

6.2 VERIFICATION MIX DESIGN AND PROPERTY TESTING

A verification mix was necessary to insure the plastic properties were adequate with the use of a production-size mixer. Previous studies have shown that SCC plastic properties can change significantly depending on the mixing method. The control and SCC mix designs shown in Table 23 were used to create full-size batches at the Gate Concrete Products precasting plant in Jacksonville, Florida. The verification mix design was also used for the actual casting mix. The plastic property testing included slump, spread, J-ring, L-box, and V-funnel tests.

Table 23. Verification mix design

Constituents*	Description	Control	SCC
Standard Constituents		(lbs)	(lbs)
Cement	Lehigh Type I/II	752	752
Fly ash	ISG Class F	168	168
Coarse aggregate	Tarmac #67	1307	1307
Fine aggregate	Florida Rock silica sand	1414	1414
Water	Local	258	258
Admixtures		(ozs)	(ozs)
Air entrainer	MBVR-S	1.8	1.8
Set retarding water reducer	Pozzolith 100 XR	13.8	13.8
High range water reducer	Glenium 3200 HES	27.6	64.4

*Amounts are shown per cubic yard

APPENDIX B - BEAM DESIGN AND CONSTRUCTION

The beams were designed using prestressed beam design software (LRFD P Beam Version 1.85) furnished by the Florida Department of Transportation (FDOT). The design output was then hand checked for flexural strength, shear strength, and prestress release strength. The input values in the program coincided with the design of a typical bridge beam, and the input values are shown in Table 24. The flexural test beams were designed to include a 12-inch composite cap to prevent a premature compressive failure during testing, and the cap simulates the actual use of an AASHTO beam with a composite slab. Due to the beams being tested without the use of diaphragms, no mild reinforcing steel protruded from the ends of the beams. The prestressing tendons protruded one inch from the end of the beams to facilitate the attachment of instrumentation to monitor strand movement during structural testing. A minimal amount of shear reinforcement was used in the shear-test beams in order to investigate the concrete structural response and not to include excessive steel-property influence on the shear behavior of each type of concrete.

Table 24. Assumed section geometry and material properties used in design

Plan and Section Properties		Concrete Properties	
Beam length	42 ft	f'_c slab	6.0 ksi
Bearing distance	12 in	f'_c beam	8.5 ksi
Pad width	6.0 in	f'_{ci} beam	6.0 ksi
Beam spacing	6.0 ft	Unit weight slab	150 pcf
Overhang	3.0 ft	Unit weight beam	160 pcf
Slab thickness	10.0 in		
Slab buildup	0.0 in		
Overhang to parapet	1.5 ft		
Beam position	Interior		
Beam type	II		
Wearing surface thickness	0.0 in		
Number of beams	7		
Bridge skew	0 deg		
Stirrup Size and Spacing		Steel Properties	
End cover	2.0 in	fpu tendons	270 ksi
Stirrup spacing A	3.0 in	Ep tendons	28500 ksi
Number of spaces A	4	fy mild steel	60 ksi
Stirrup area A	0.62 sq in	Es mild steel	29000 ksi
Stirrup spacing 1	12 in	Relative humidity	75 %
Number of spaces 1	8	Time jacking to transfer	1.5 days
Stirrup area 1	0.31 sq in	Slab rebar area	0.31 sq in/ft
Stirrup spacing 2	18 in	Slab depth to rebar	5.0 in
Number of spaces 2	7		
Stirrup area 2	0.31 sq in		

Four 42-foot long AASHTO Type II girders were constructed for flexural and shear testing using a composite cap, and two 42-foot long Type II girders were constructed for shear testing without a composite cap. The beams were constructed at the Gate Concrete Products precasting plant in Jacksonville, FL. The as-built beam details are shown at the end of this appendix. Quality assurance personnel were present to insure the beams were cast with the correct procedures and tolerances. All of the beams were cast on the same day. The schedule of key events leading to structural testing is shown in Table 25.

Table 25. Key events leading to structural testing

Event	Date
Trial mix	04/02/2003
Verification mix	06/05/2003
Beam casting	06/25/2003

Prestress transfer and begin camber monitoring	07/10/2003
Beam transportation to Tallahassee	07/17/2003
End camber monitoring	12/29/2003
SCC shear tests	02/03/2004
STD Shear tests	03/03/2004
SCC Shear-flexure tests	03/31/2004
STD Shear-flexure tests	04/02/2004
SCC Shear-slip tests	04/29/2004
STD Shear-slip tests	04/27/2004

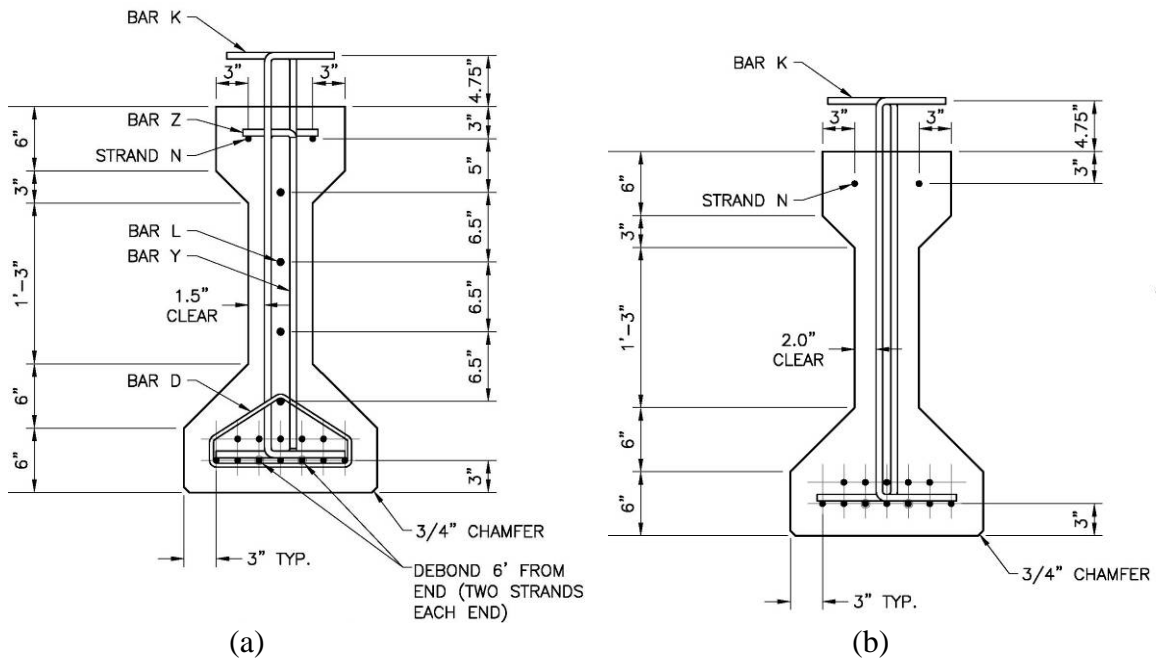


Figure 50. Prestressed beam design (a) end section (b) middle section



Figure 51. Stirrup and confinement reinforcement at end of non-capped shear beam



Figure 52. Stirrup and confinement reinforcement at end of capped flexure beam

To eliminate a vibration carry-over effect from the consolidation of the standard concrete due to the continuously connected forms, all standard concrete beams were cast and consolidated before the SCC beams were poured. No consolidation was utilized on the SCC beams.

The SCC beams were poured in approximately 40% less time, and they required approximately 50 % fewer workers than the control beams due to the increased flow rate of the concrete and the elimination of side mounted and internal vibrators. The elimination of the vibrators also caused a dramatic decrease in the noise level of the casting process, resulting in a more pleasing work environment. Having fewer workers on top of the SCC beams also increased the safety level.

To insure an adequate connection between each flexure beam and its composite cap, the top of the beams had a standard roughened surface. Unlike the SCC beams, it was possible to roughen the control beams immediately after being poured. The SCC beams required approximately 1.5 hours set time for the paste to have sufficient free-standing cohesion to hold the shape required to form the ridges of the roughened surface. As demonstrated by a greater amount of leakage of the concrete from the SCC beam forms than the control beam forms, it is necessary to have very tight forms with SCC construction. Additionally, there is a greater importance to grease all areas of the steel forms when using SCC, due to SCC causing a stronger bond between the beams and the forms requiring excessive force when removing the forms. The stronger bond is caused by the highly flowable ability of SCC, enabling it to flow into very small surface irregularities of the forms. The highly flowable characteristic is also a benefit of SCC with regards to a better and smoother formed finish.

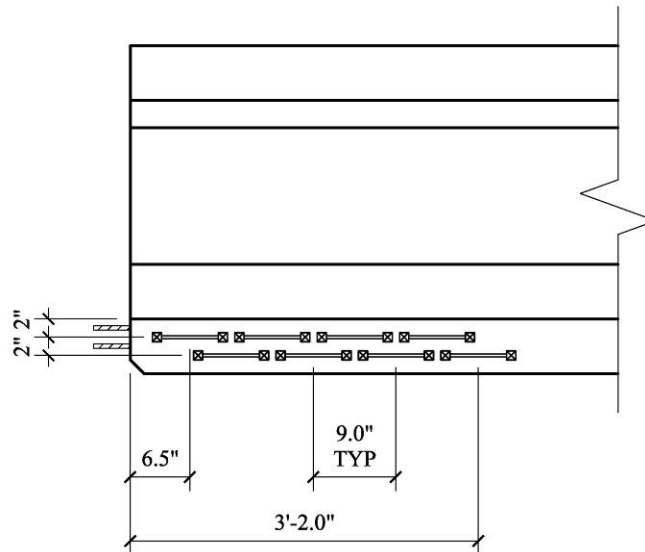
PRESTRESS TRANSFER LENGTH AND TRANSFER STRAND SLIP

The beams were cast in a single line on a single casting bed. The transfer of prestress was accomplished by torch-cutting one strand at a time simultaneously between every other pair of beam ends and at each far end of the casting bed as shown in Figure 53. This pattern resulted in each beam having a cutting end and a free end. As other researchers have found, and as the results of the transfer length analysis shows, the transfer lengths are significantly larger at the cutting end (Russell and Burns 1997).



Figure 53. Specimen configuration in prestressing bed

Due to low early concrete strengths and scheduling conflicts, the prestress transfer was delayed until fifteen days after casting. The five-day cylinder compressive strengths from the precasting plant were 3170 psi for the control concrete and 3810 psi for the SCC. It is not known why the early strengths were low. Strain gauges were installed before the transfer of prestress on each end of one control beam and one SCC beam on the bottom flanges in order to measure the prestress transfer lengths (Figure 54).



NOTES:

DIMENSIONS USE GAUGE \varnothing

THIS DETAIL IS TYPICAL FOR FOUR BEAM ENDS

Figure 54. Transfer length instrumentation setup

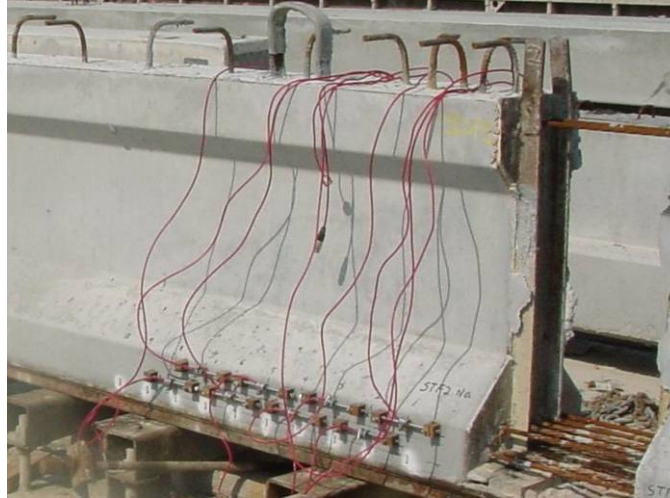


Figure 55. Installed transfer length strain gauges

An analysis was performed on the strain data to determine where the strain transitions from increasing in the longitudinal direction to a constant value using the 95% AMS method (Russell and Burns 1997). The execution of the 95% AMS method was as follows:

1. Plot the strain profile.
2. Determine the AMS for the specimen by computing the numerical average of all the strains contained within the strain plateau of the fully effective prestress force.
3. Multiply the AMS by 0.95 and construct a line corresponding to this value.
4. Prestress transfer length is determined by the intersection of the 95% line with a best-fit line through 0,0 and the first two points of the strain profile.

This is a modified version of the 95% AMS method due to having slightly higher variations in the measured strains than others have found when determining transfer lengths and due to using fewer gauges than most transfer length measurements. The slightly higher variations were caused by using crack gauges and using multiple vertical placements of the gauges as shown in Figure 55. Also, it was necessary to change the vertical locations of the gauges from the planned positions in the field. The vertical placements of the gauges, therefore, were determined from photographs, which added some error to the measurements. After the vertical locations of the gauges were determined, the strain readings from each gauge were used to calculate the strains at the height of the strand centroid using the assumption that plain sections remain plane. The strains from the innermost gauges clearly within the fully effective prestress force were used to calculate the 95% AMS. The first two strain points and the origin were used for a linear best-fit line. In one case, only one gauge was within the transition region due to another gauge being nonfunctional, and therefore the intersection of the strain profile with the 95% AMS was used to determine the transfer length. The instrumentation and analysis methods used here are sufficient to compare the prestress transfer lengths of the SCC and control beams.

The results shown in Table 26 show that the transfer length for the control beam on the cutting end was 0.5 inches higher than the SCC beam, and the transfer length for the SCC beam

on the free end was 0.9 inches higher than the control beam. The results show that there is an insignificant difference between the SCC and control beams with respect to prestress transfer lengths.

Table 26. Prestress transfer lengths

Test-Beam	Location	End Condition	Transfer Length (in)
F1-STDF2	North	Free	12.1
F2-STDF2	South	Cutting	15.5
F1-SCCF1	North	Cutting	15.0
F2-SCCF1	South	Free	13.0

An approximate measurement of the strand movement due to the transfer of prestress to the beams was conducted by marking the strands three inches away from the beam ends and measuring the mark with a ruler after the prestress transfer. The resulting strand movements of the fully bonded strands are shown in Table 27. The strand movements of the sheathed strands for some of the beams are shown in Table 28. The results show that the SCC beams were able to transfer the prestress as efficiently as the control beams.

Table 27. Prestress transfer strand movement of fully bonded strands

Beam End	Strand										
	1	2	3	4	5	6	7	9	11	12	Average
	(in)	(in)	(in)	(in)	(in)	(in)	(in)	(in)	(in)	(in)	(in)
STDF1North	0.06	0.13	0.06	0.19	0.13	0.06	0.00	0.13	0.13	0.13	0.10
STDF1 South	0.06	0.00	0.00	0.00	0.13	0.13	0.13	0.06	0.13	0.06	0.07
STDF2 North	0.00	0.00	0.00	0.00	0.06	0.06	0.06	0.06	0.06	0.13	0.04
STDF2 South	0.13	0.06	0.06	0.13	0.13	0.06	0.00	0.00	0.06	0.00	0.06
SCCF1 North	0.06	0.06	0.06	0.13	0.19	0.06	0.06	0.13	0.19	0.00	0.09
SCCF1 South	0.06	0.13	0.06	0.06	0.19	0.06	0.13	0.13	0.13	0.13	0.11
SCCF2 North	0.13	0.13	0.13	0.06	0.13	0.00	*	0.00	0.13	0.13	0.09
SCCF2 South	0.13	0.13	0.19	0.19	0.13	0.31	0.00	0.06	0.19	0.13	0.14
STDS North	0.00	0.13	0.25	0.06	0.13	0.06	0.06	0.00	0.06	0.19	0.09
STDS South	0.25	0.25	0.25	0.19	0.38	*	0.00	0.06	0.06	0.06	0.17
SCCS North	0.06	0.06	0.06	0.00	0.00	0.00	0.00	0.00	*	0.06	0.03
SCCS South	*	*	0.13	0.13	0.00	*	*	0.06	0.06	0.06	0.07

* No data

Table 28. Prestress transfer strand movement for sheathed strands

Beam End	Strand		
	8	10	Average
	(in)	(in)	(in)
STDF1 North	0.50	No data	0.50
STDF1 South	No data	0.56	0.56
STDF2 North	0.44	0.50	0.47
STDF2 South	0.50	0.50	0.50
SCCF1 North	0.63	No data	0.63
SCCF2 North	0.38	No data	0.38
STDS North	No data	0.50	0.50
STDS South	0.25	0.31	0.28
SCCS North	No data	0.41	0.44
SCCS South	0.69	0.50	0.59

APPENDIX C - CAMBER MONITORING

Table 29. Camber data

Beam	Day							
	0	50	77	84	99	112	172	188
SCS	0.31	0.53	0.81	0.80	0.81	0.80	0.81	0.88
SCF1	0.34	0.60	0.78	0.77	0.77	0.75	0.78	0.84
SCF2	0.41	0.60	0.78	0.77	0.78	0.77	0.80	0.84
STS	0.41	0.60	0.66	0.66	0.66	0.66	0.69	0.75
STF1	0.34	0.66	0.84	0.84	0.84	0.84	0.88	0.91
STF2	0.44	0.53	0.75	0.77	0.77	0.77	0.80	0.84

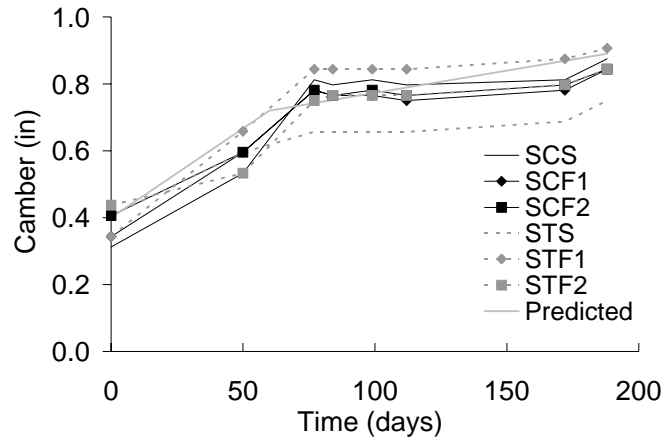


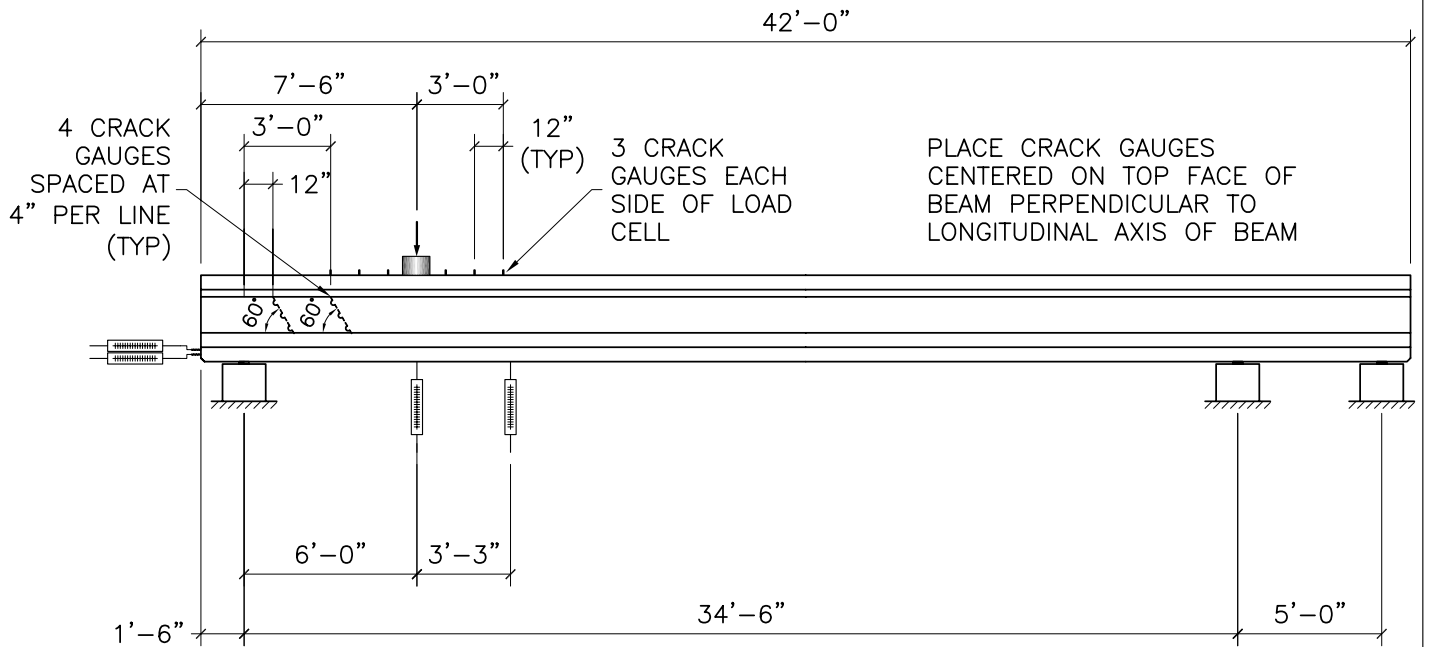
Figure 56. Camber versus time

APPENDIX D - SHEAR TEST

TEST SETUP

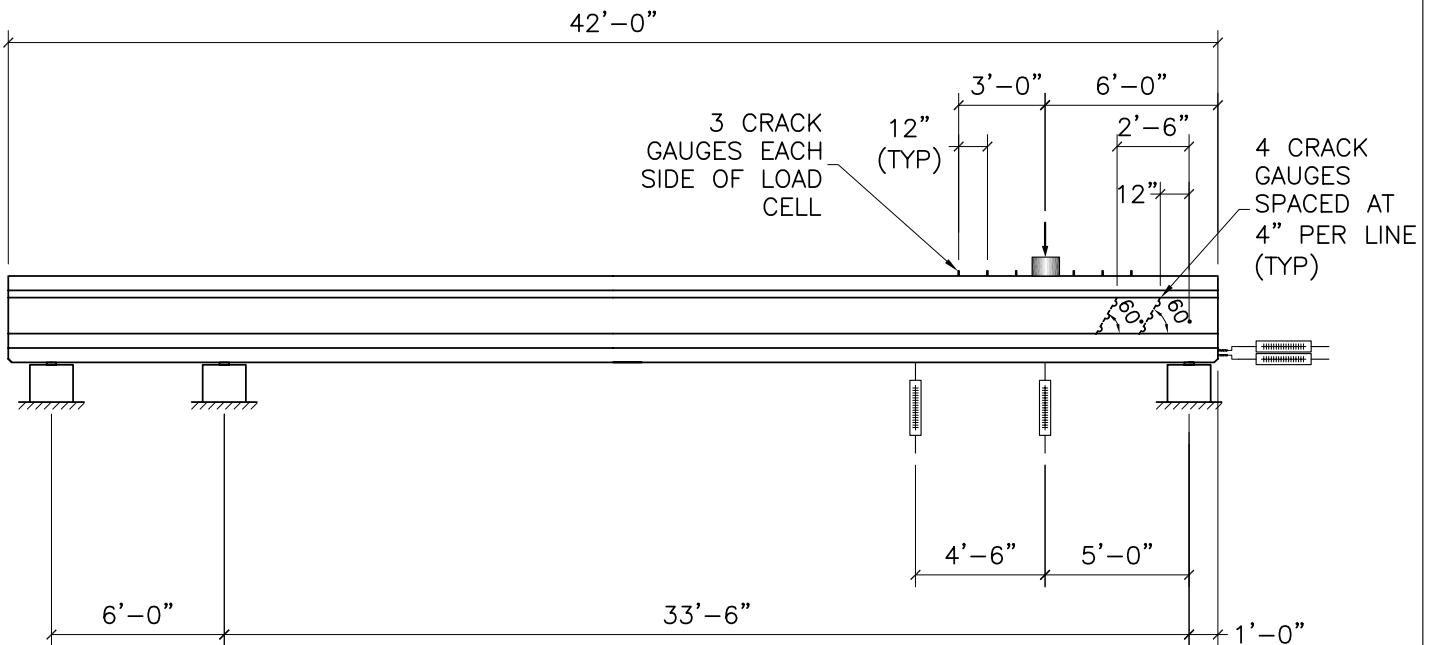
Two of the six beams were constructed and tested to investigate the shear behavior of SCC as compared to the control concrete. As shown in Appendix B, one SCC beam and one control beam with a stirrup spacing of 48 inches were used. The normally unacceptable wide spacing of stirrups was used to minimize the steel behavior influence on the performance of the beams. The detailed as-built figures of the shear beams are shown in Appendix C.

The test setup for the shear tests is shown in Figure 57. In order to compare the structural performance of the two types of concrete, instrumentation to measure deflection and strain in the concrete was installed as shown. Linear variable displacement transducers (LVDTs) were placed on the beam to measure vertical displacement with increasing load. LVDTs were also installed on the strands to monitor strand movement. Additionally, crack gauges were installed on the vertical face of the beam web and oriented to measure tension strain due to shear. Finally, crack gauges were installed on top of the beam and oriented to measure strain in the transverse direction. The load was gradually increased as each gauge was sampled until a failure condition was reached. Each end of both beams was tested. When testing the first beam end, the load was placed six feet from the center of the support, and the center of the support was placed 18 inches from the end of the beam. When testing the second beam end, the load was placed five feet from the center of the support, and the center of the support was placed 12 inches from the end of the beam. The geometry of the beam ends was chosen to create a condition of high shear and an available strand development length just sufficient to accommodate the required development length. It was intended that this geometry would create a concrete strut or node crushing failure mode, along with the possibility of some bonded strand movement.



SINGLE BEAM - TEST 1 LAYOUT

SCALE: NTS



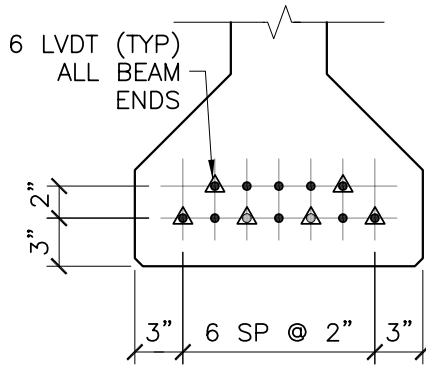
SINGLE BEAM - TEST 2 LAYOUT

SCALE: NTS

SCC Instrumentation 7.dwg L4 5/13/04

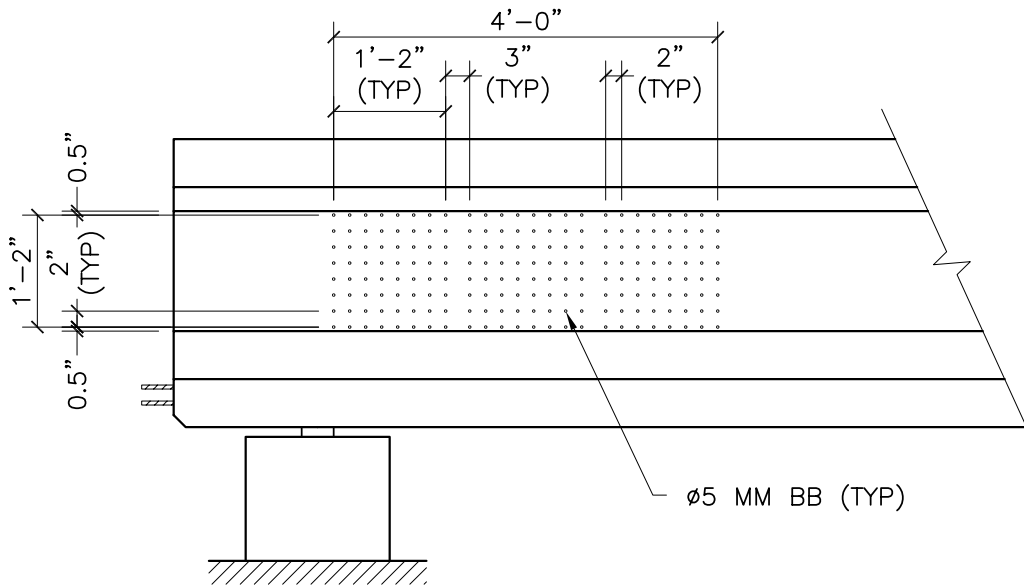
Figure 57a
 Shear Test
 Loads and Instrumentation
 AASHTO Type II Girder

Research Project 982
Self-Consolidating Concrete For
Use In FDOT Bridge Elements



STRAND INSTRUMENTATION

SCALE: 1" = 1'-0"




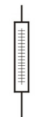

THIS DETAIL IS
TYPICAL FOR EACH
END OF BOTH BEAMS

APPLY BEADS TO
OPPOSITE SIDE OF
INCLINED GAUGES

BEAD LAYOUT

SCALE: 1/2" = 1'-0"

Legend

-  PI200-5-X Crack Gauge
-  SDP200D or SDP200R LVDT
-  Load Cell (400 kip)

SCC Instrumentation 7.dwg L5 5/13/04

Figure 57b
Shear Test
Loads and Instrumentation
AASHTO Type II Girder

Research Project 982
Self-Consolidating Concrete For
Use In FDOT Bridge Elements

RESULTS

Table 30. Shear tests web cracking strain

Gauge	S1-SCCS		S1-STDS		S2-SCCS		S2-STDS	
	Line 1	Line 2	Line 1	Line 2	Line 1	Line 2	Line 1	Line 2
	Strain ($\mu\epsilon$)	Strain ($\mu\epsilon$)	Strain ($\mu\epsilon$)	Strain ($\mu\epsilon$)	Strain ($\mu\epsilon$)	Strain ($\mu\epsilon$)	Strain ($\mu\epsilon$)	Strain ($\mu\epsilon$)
1	94.3	80.5	86.9	131.3	85.9	62.9	82.1	172.8
2	8.3	147.2	79.9	104.0	62.1	169.7	91.0	81.2
3	222.2	321.0	131.0	132.1	280.0	176.4	145.0	340.1
4	102.4	312.8	113.6	107.8	78.5	183.7	111.2	-30.6
Average	106.8	215.4	102.8	118.8	126.6	148.2	107.3	140.9

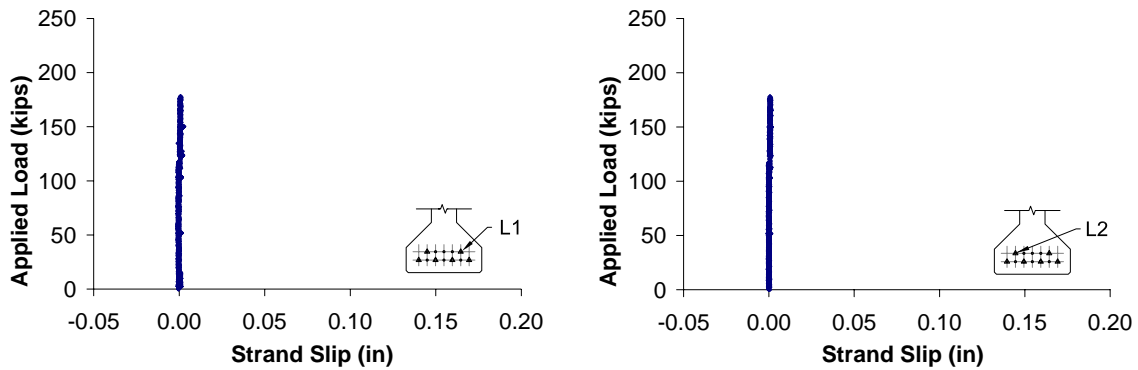


Figure 58. Strand slip for strands one and two in S1-SCCS

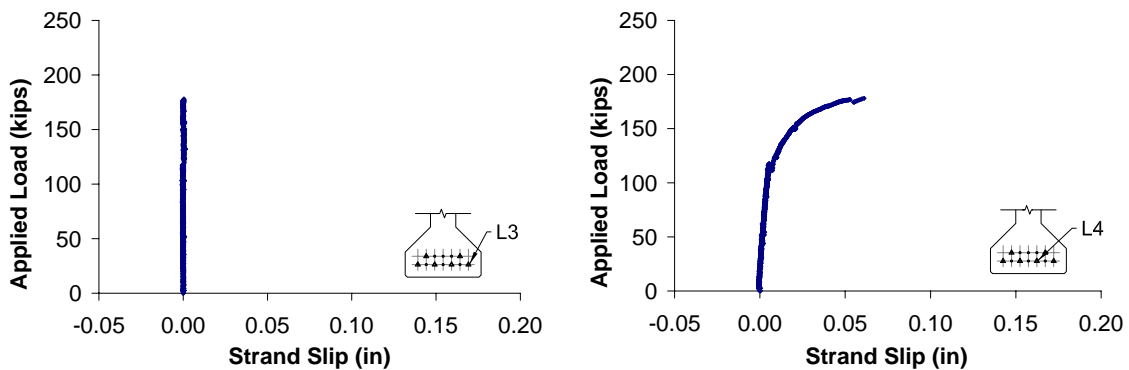


Figure 59. Strand slip for strands three and four in S1-SCCS

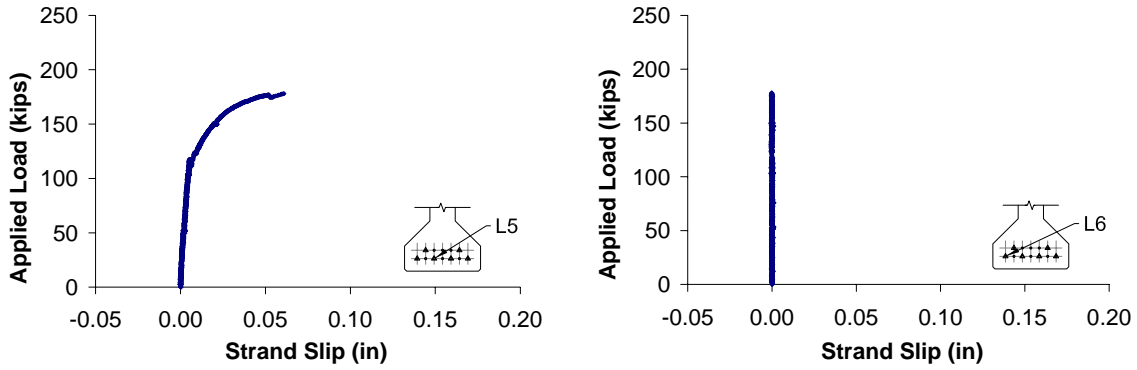


Figure 60. Strand slip for strands five and six in S1-SCCS

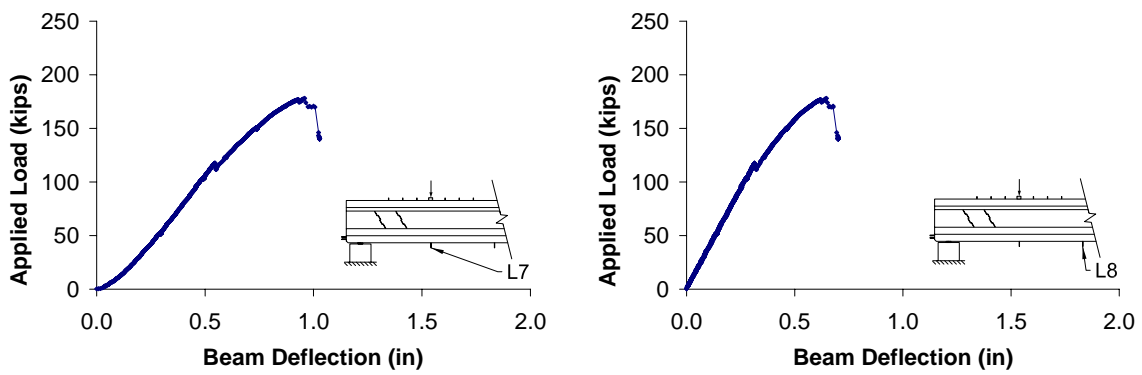


Figure 61. Beam deflections in S1-SCCS

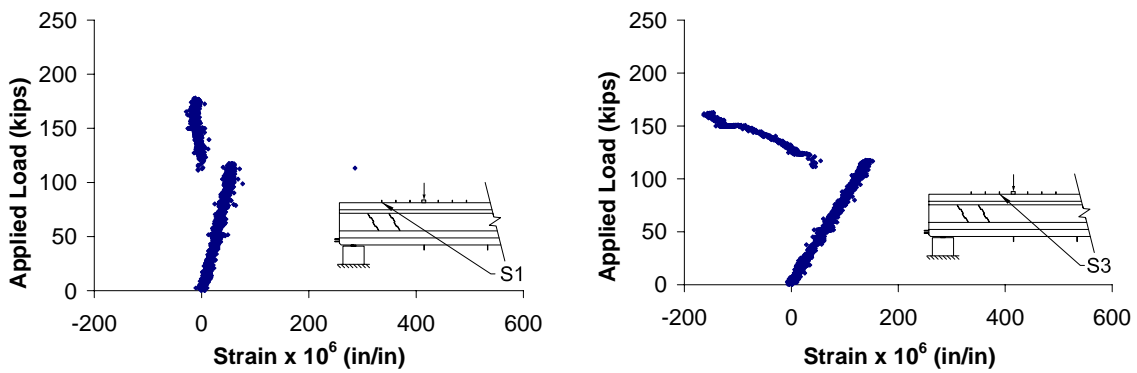


Figure 62. Top face transverse strain positions one and three in S1-SCCS

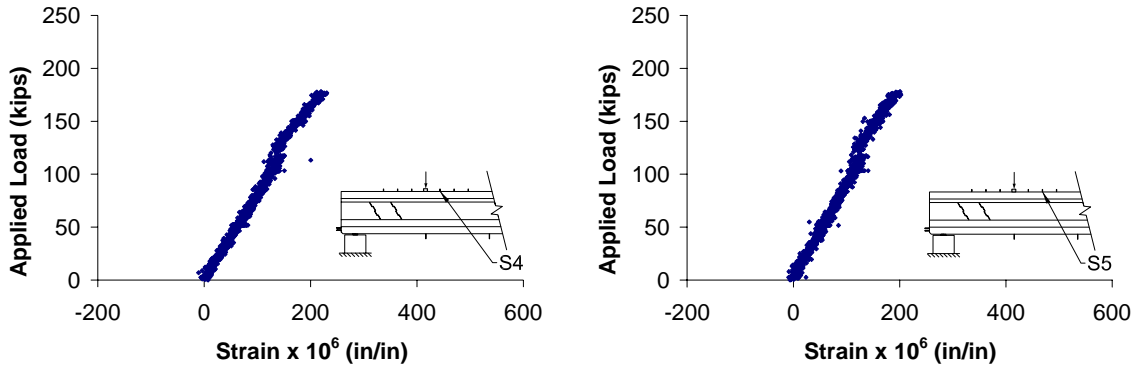


Figure 63. Top face transverse strain positions four and five in S1-SCCS

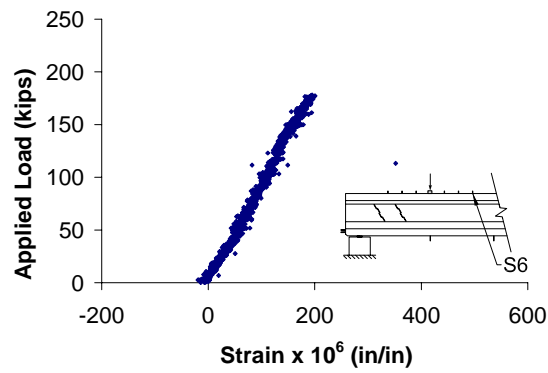


Figure 64. Top face transverse strain position six in S1-SCCS

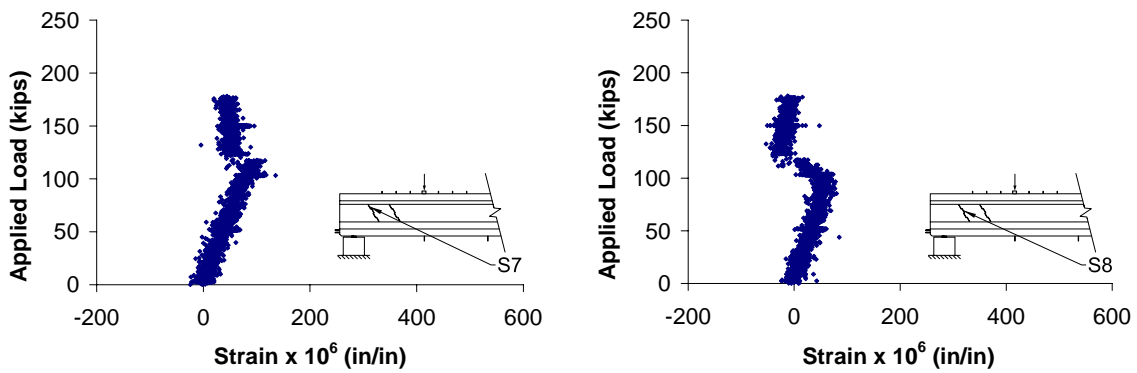


Figure 65. Web shear strain positions seven and eight in S1-SCCS

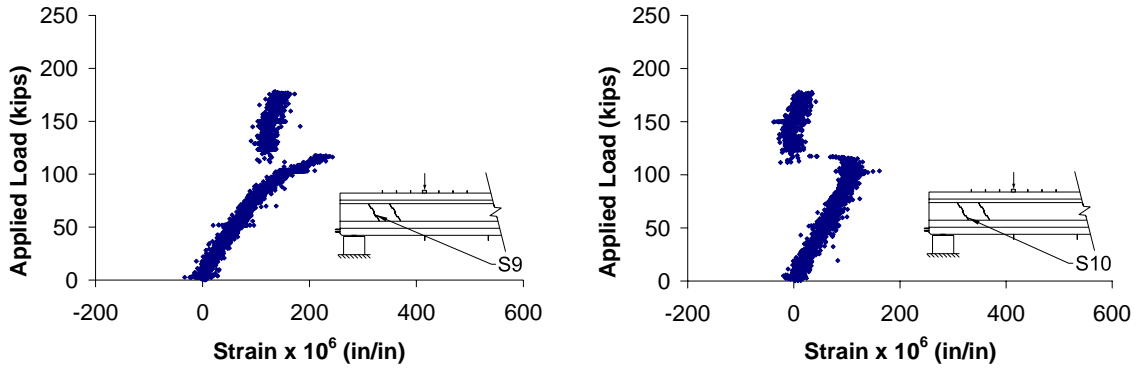


Figure 66. Web shear strain positions nine and ten in S1-SCCS

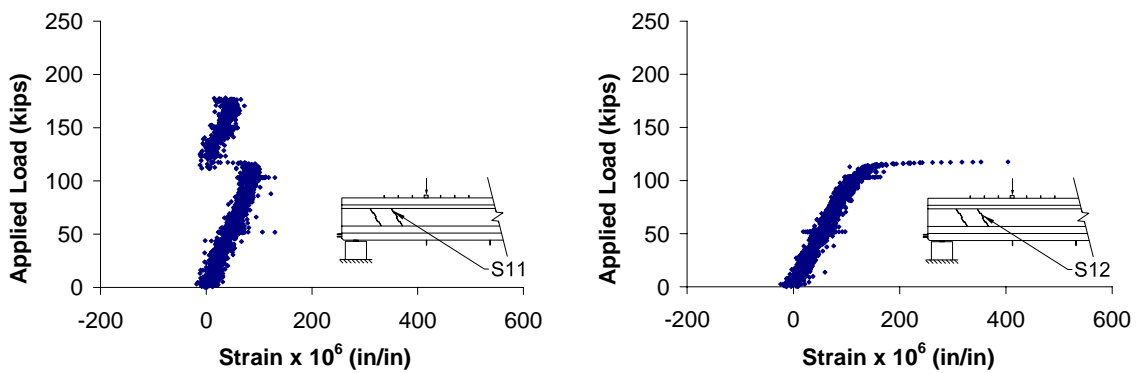


Figure 67. Web shear strain positions eleven and twelve in S1-SCCS

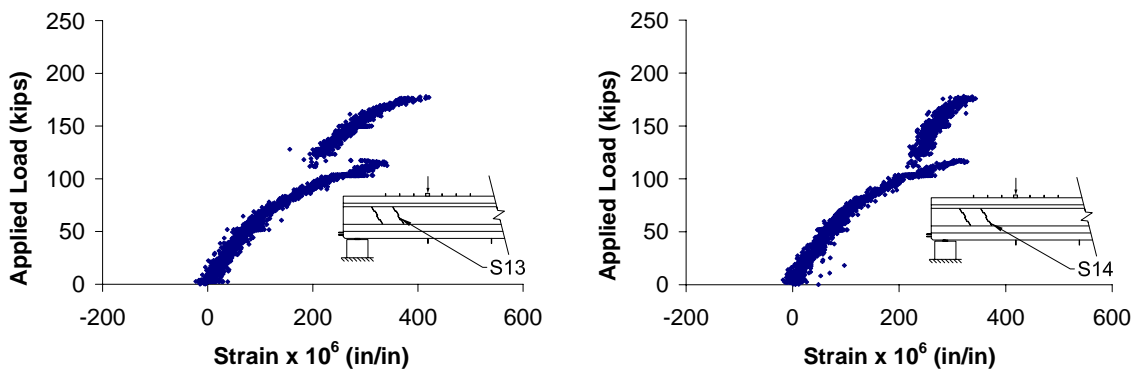


Figure 68. Web shear strain positions thirteen and fourteen in S1-SCCS

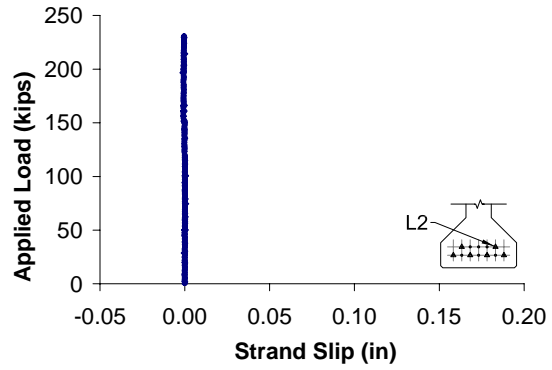
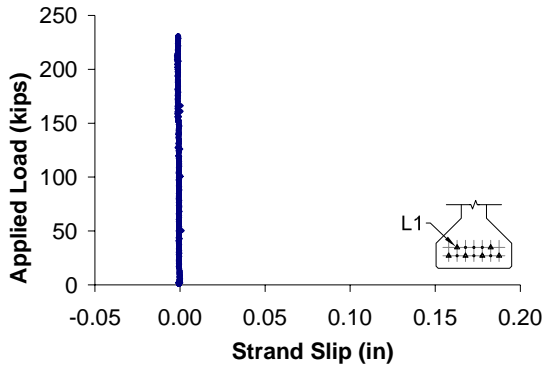


Figure 69. Strand slip for strands one and two in S2-SCCS

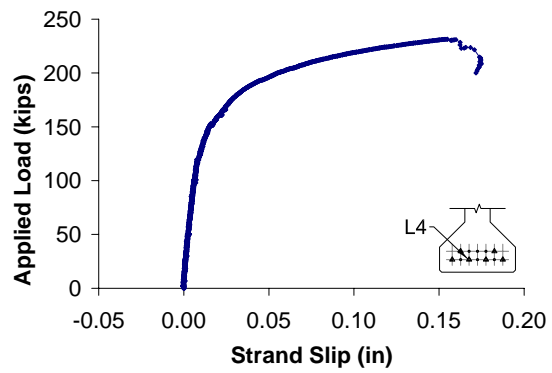
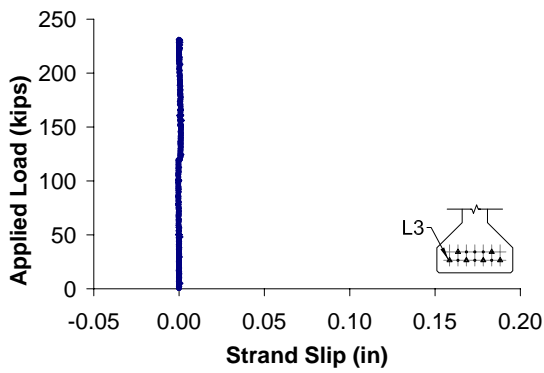


Figure 70. Strand slip for strands three and four in S2-SCCS

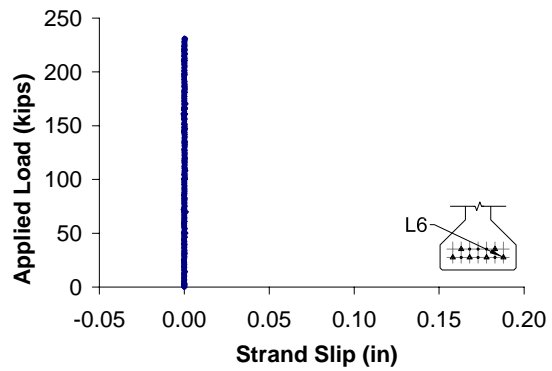
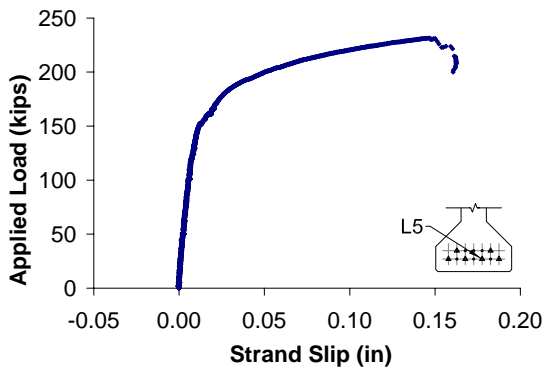


Figure 71. Strand slip for strands five and six in S2-SCCS

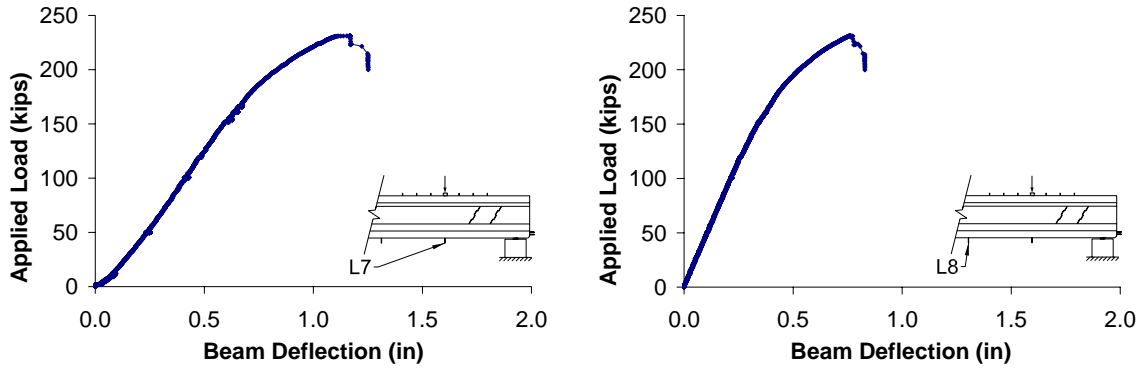


Figure 72. Beam deflections in S2-SCCS

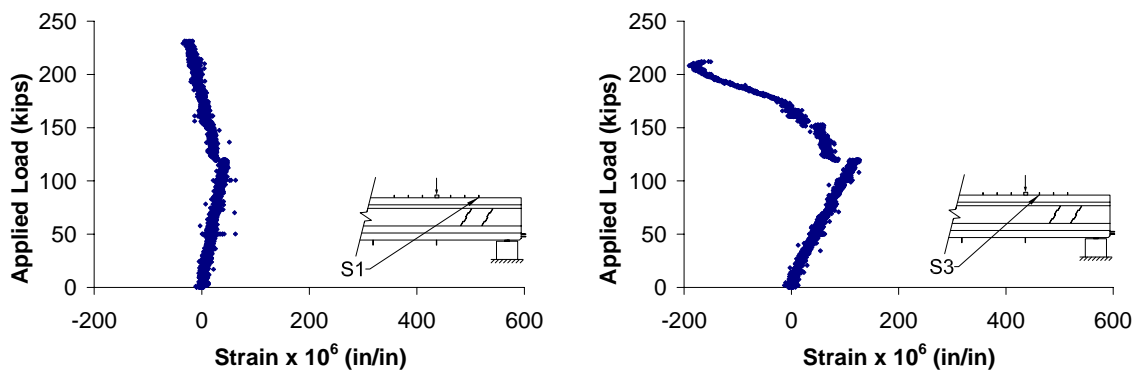


Figure 73. Top face transverse strain positions one and three in S2-SCCS

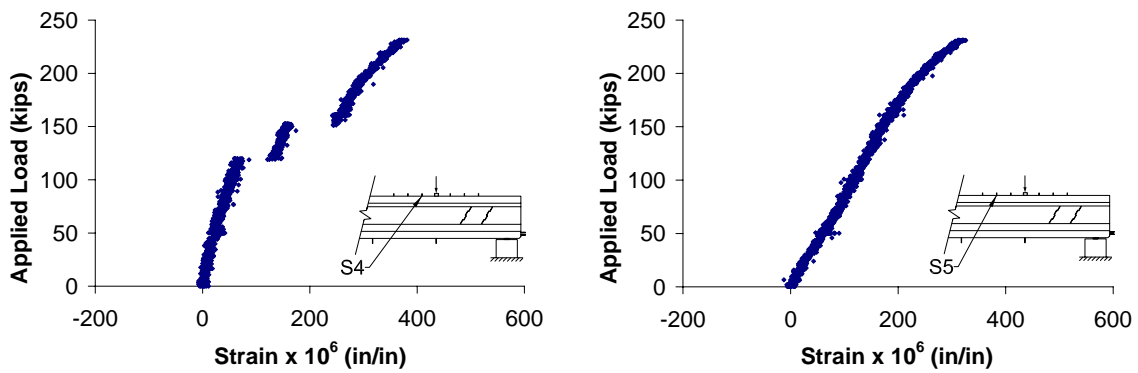


Figure 74. Top face transverse strain positions four and five in S2-SCCS

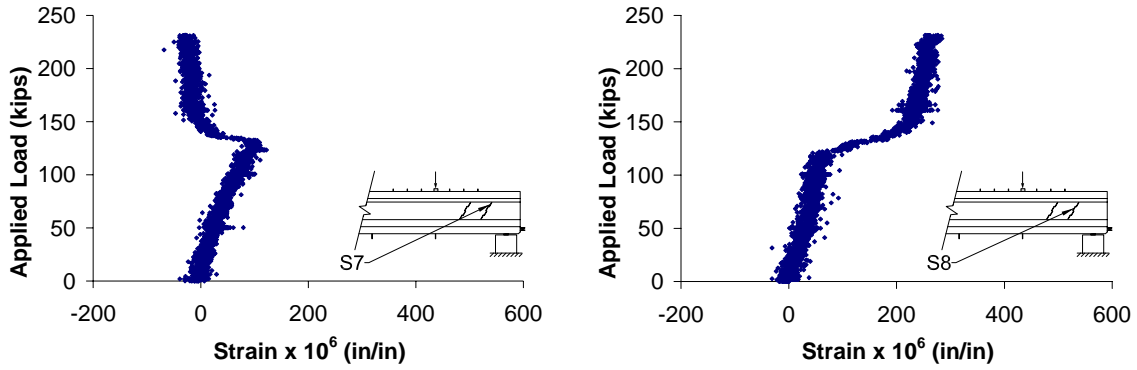


Figure 75. Web shear strain positions seven and eight in S2-SCCS

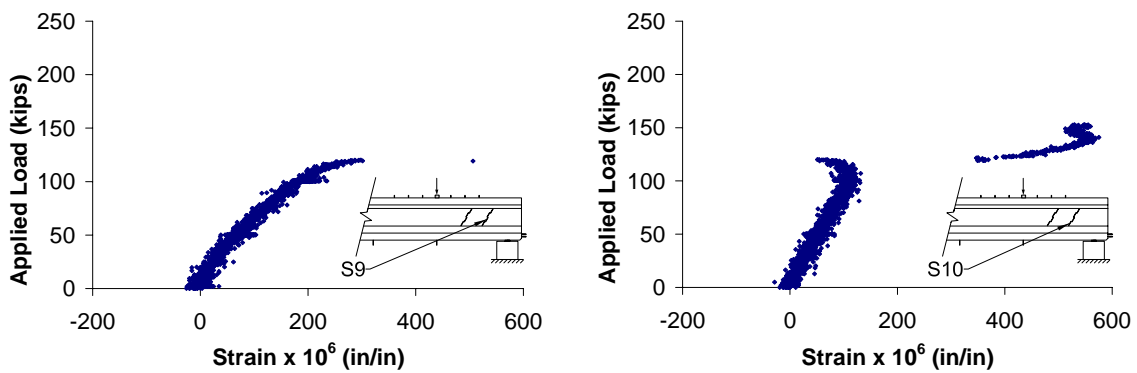


Figure 76. Web shear strain positions nine and ten in S2-SCCS

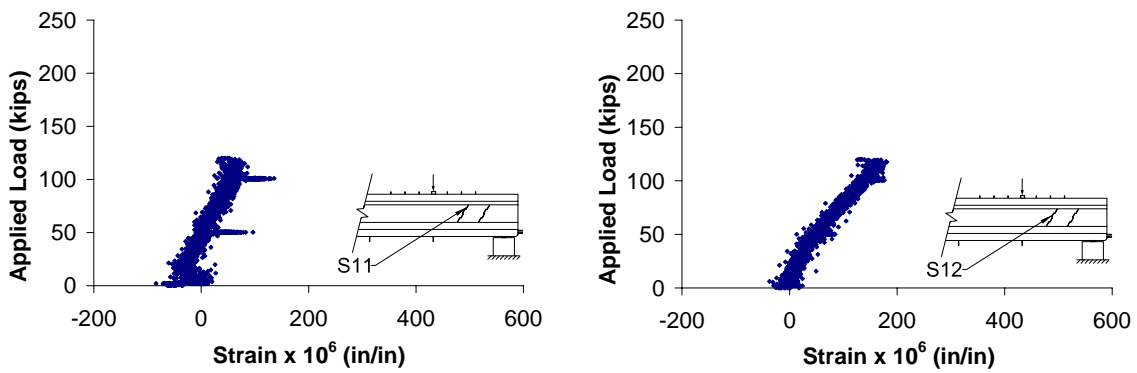


Figure 77. Web shear strain positions eleven and twelve in S2-SCCS

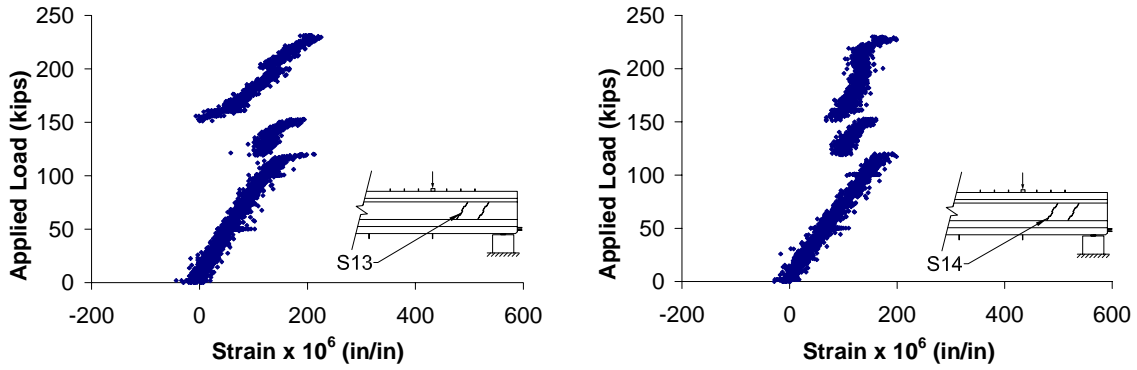


Figure 78. Web shear strain positions thirteen and fourteen in S2-SCCS

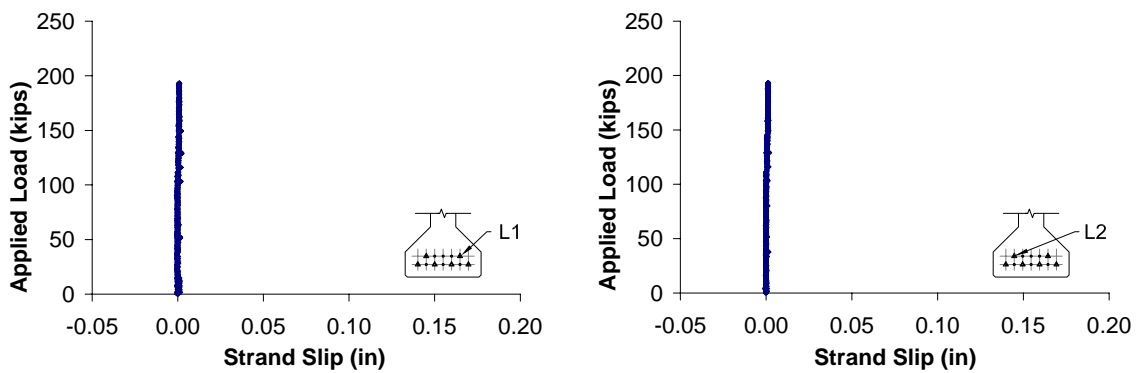


Figure 79. Strand slip for strands one and two in S1-STDS

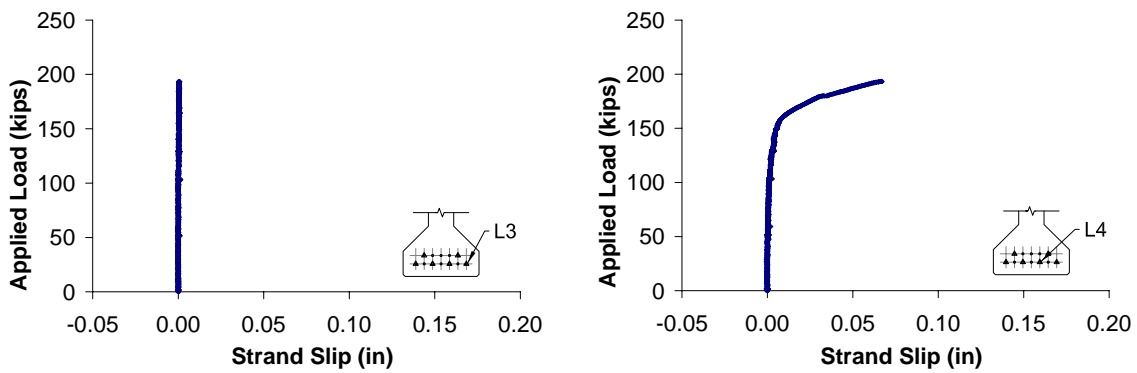


Figure 80. Strand slip for strands three and four in S1-STDS

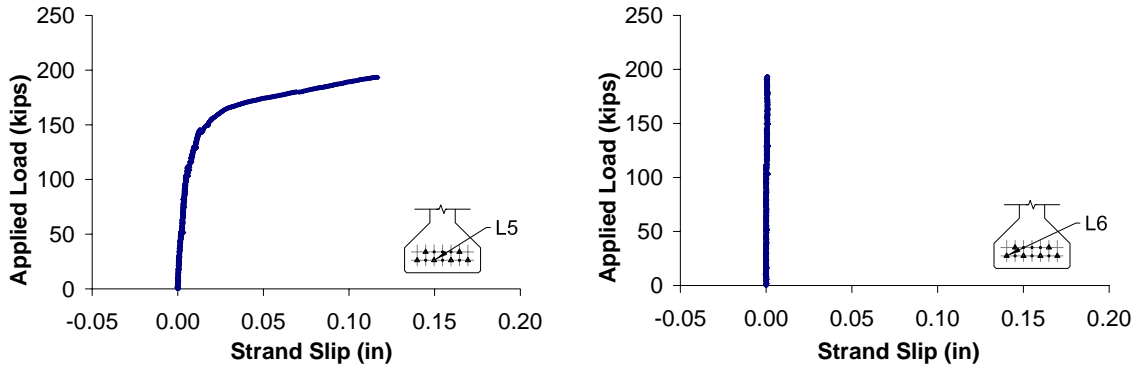


Figure 81. Strand slip for strands five and six in S1-STDS

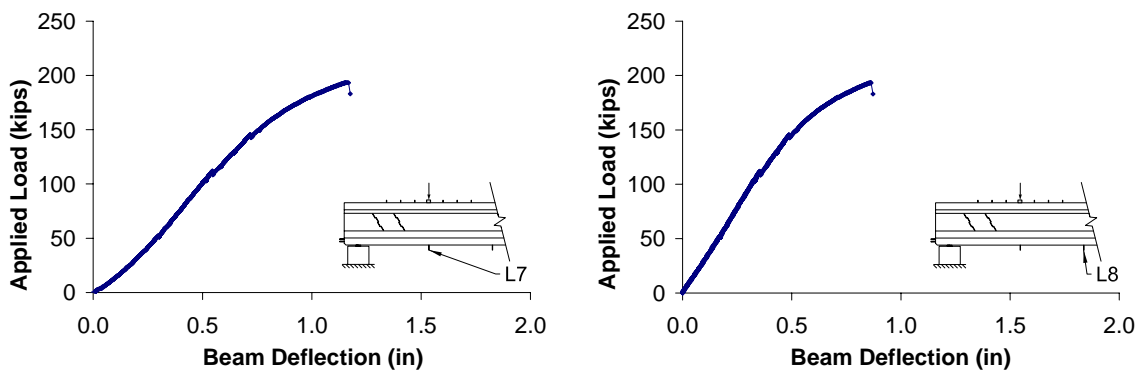


Figure 82. Beam deflections in S1-STDS

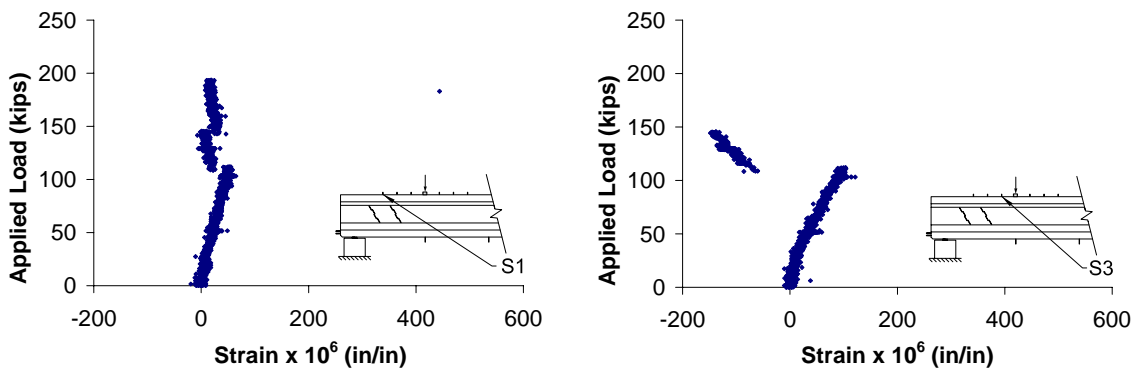


Figure 83. Top face transverse strain positions one and three in S1-STDS

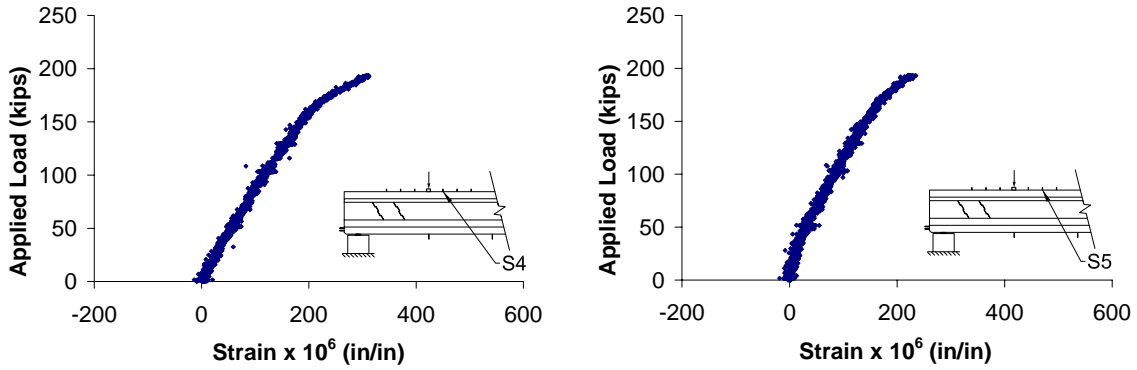


Figure 84. Top face transverse strain positions four and five in S1-STDS

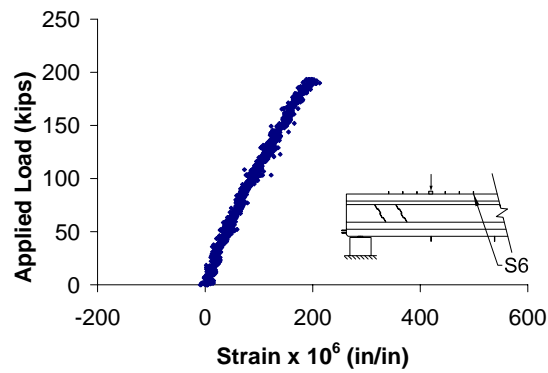


Figure 85. Top face transverse strain position six in S1-STDS

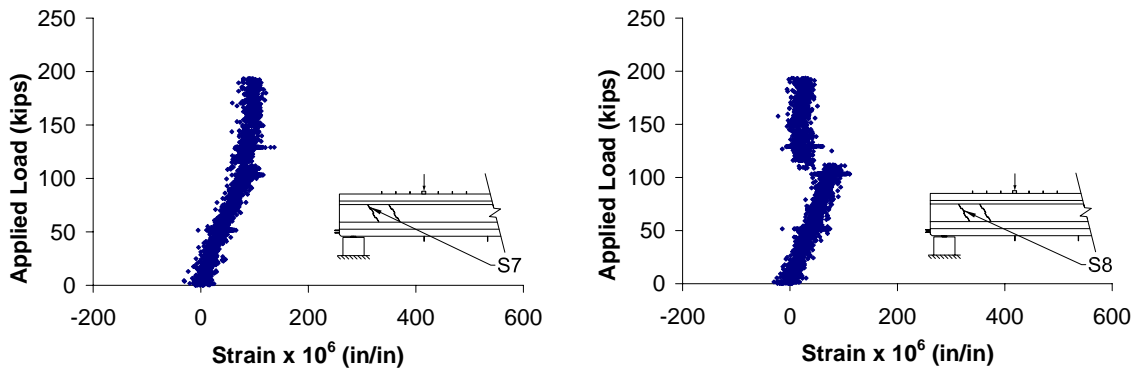


Figure 86. Web shear strain positions seven and eight in S1-STDS

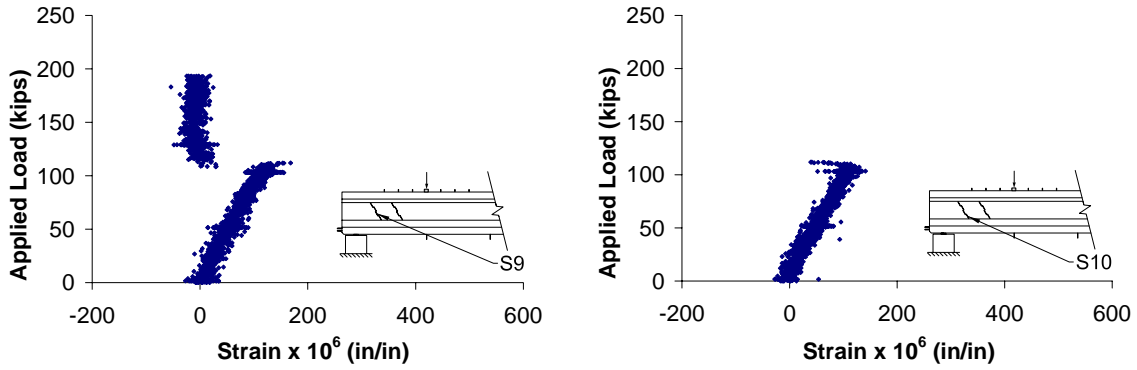


Figure 87. Web shear strain positions nine and ten in S1-STDS

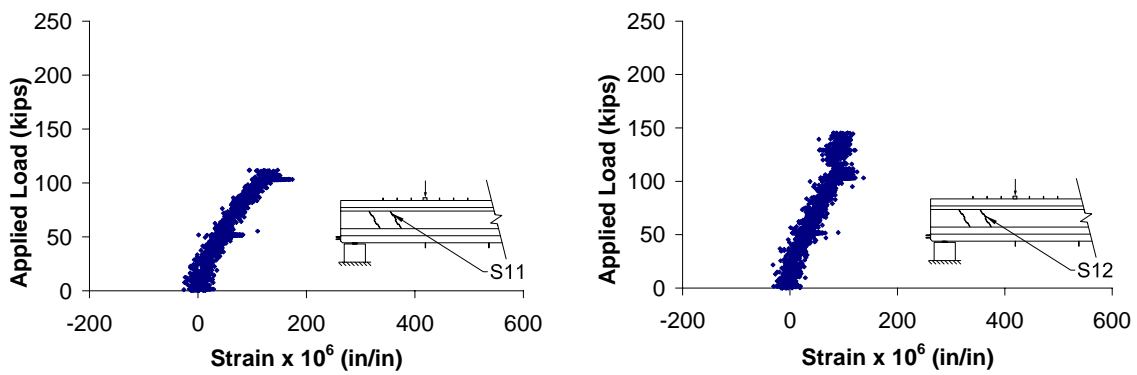


Figure 88. Web shear strain positions eleven and twelve in S1-STDS

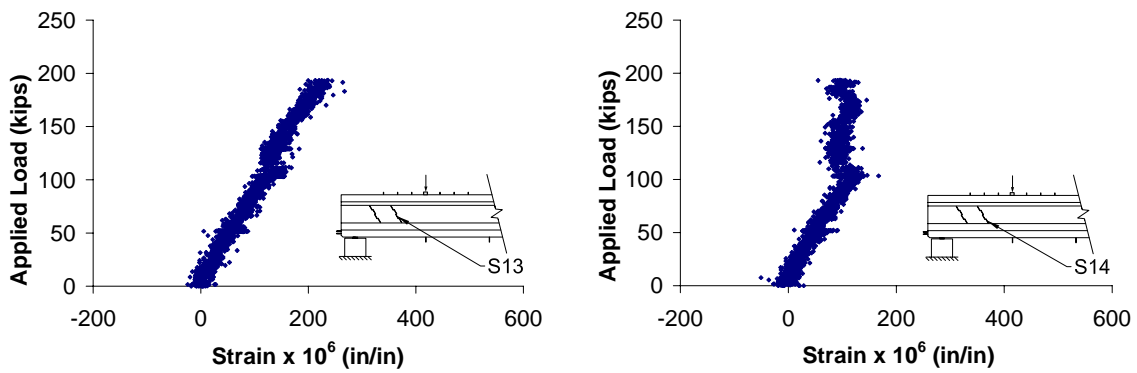


Figure 89. Web shear strain positions thirteen and fourteen in S1-STDS

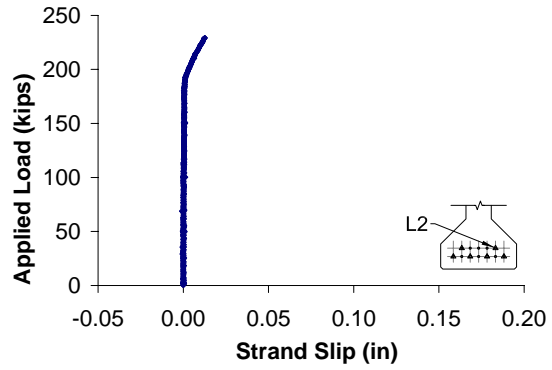
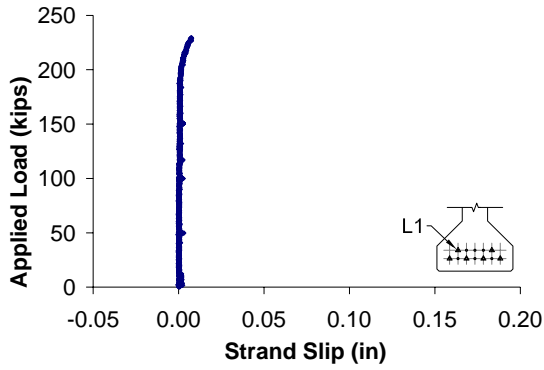


Figure 90. Strand slip for strands one and two in S2-STDS

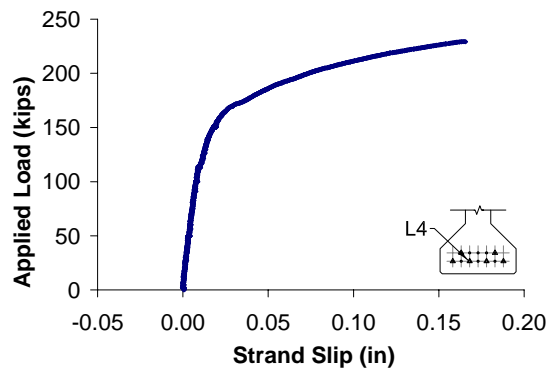
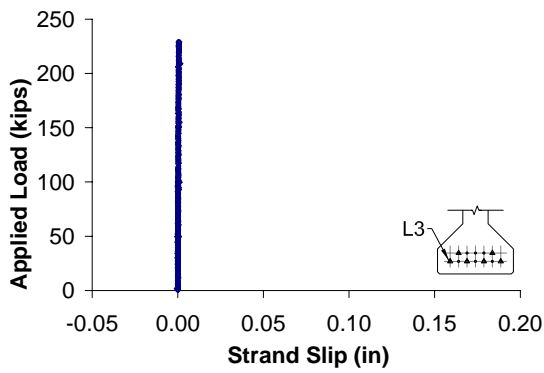


Figure 91. Strand slip for strands three and four in S2-STDS

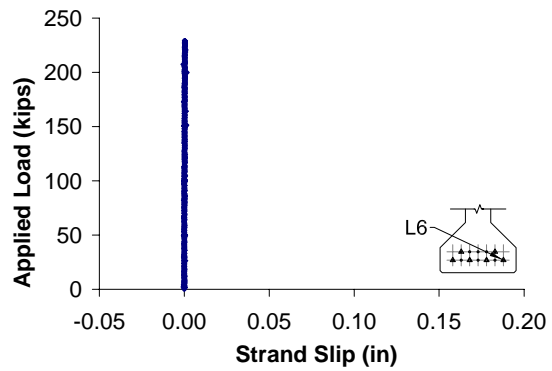
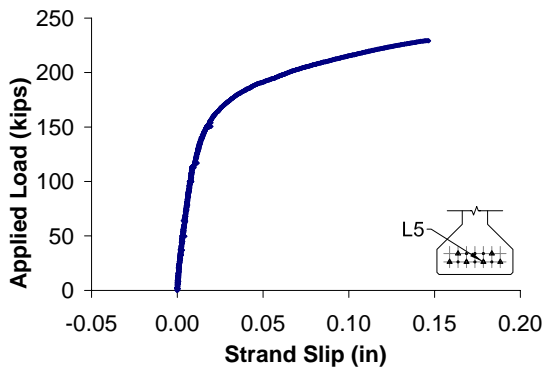


Figure 92. Strand slip for strands five and six in S2-STDS

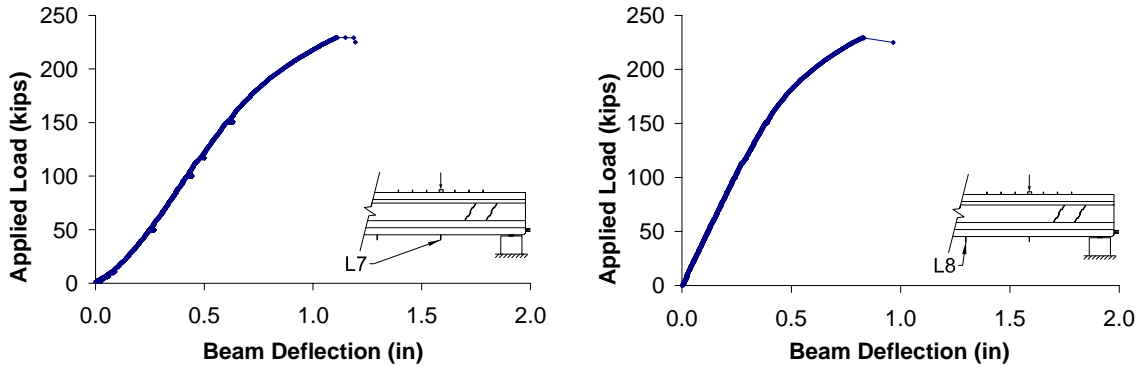


Figure 93. Beam deflections in S2-STDS

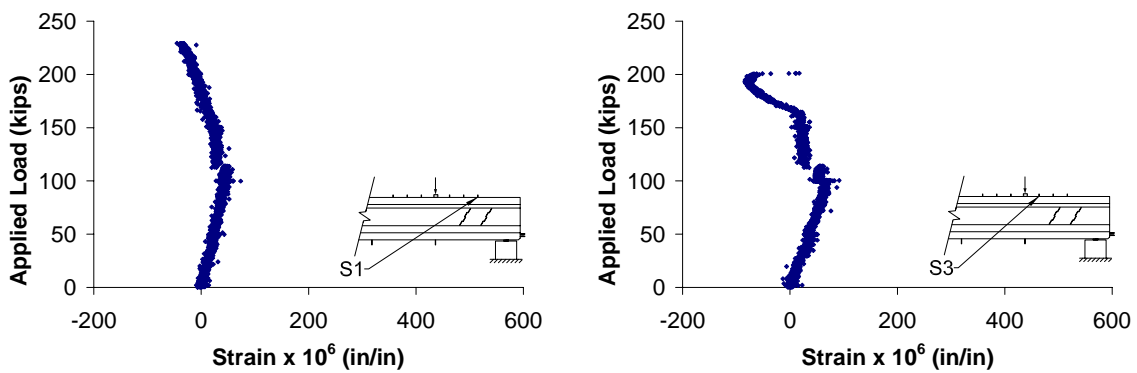


Figure 94. Top face transverse strain positions one and three in S2-STDS

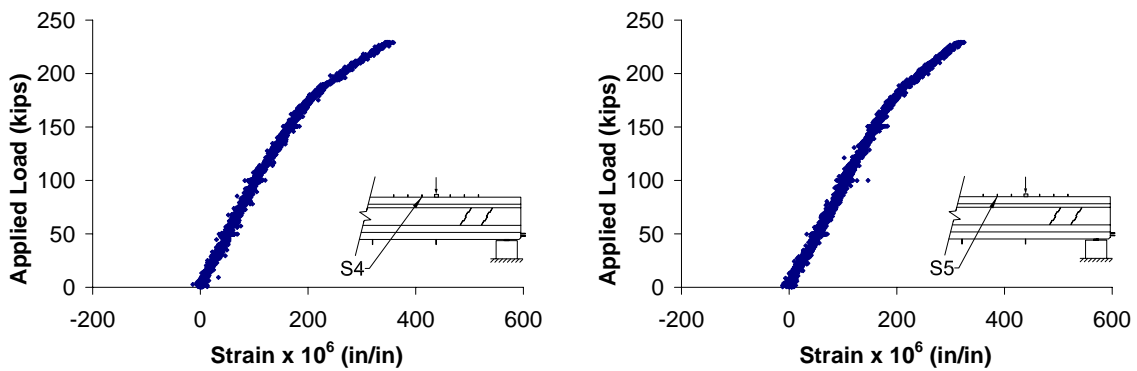


Figure 95. Top face transverse strain positions four and five in S2-STDS

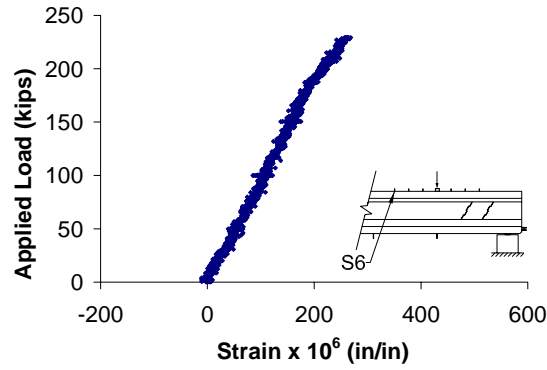


Figure 96. Top face transverse strain position six in S2-STDS

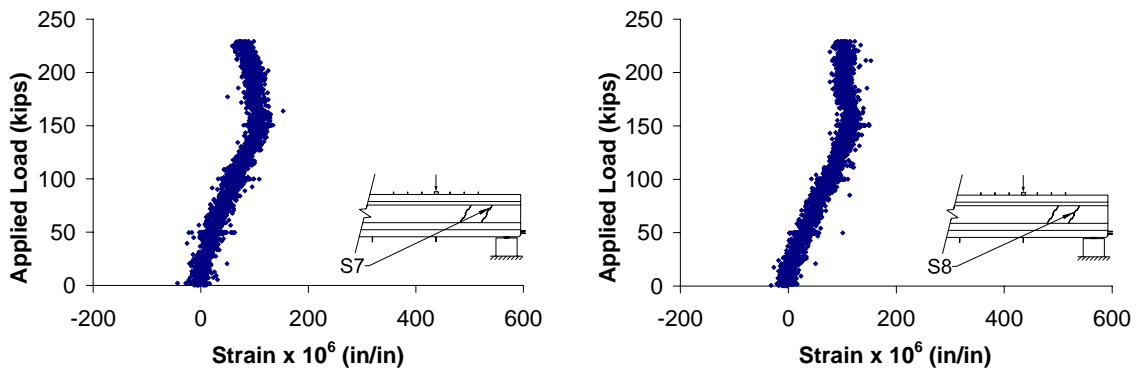


Figure 97. Web shear strain positions seven and eight in S2-STDS

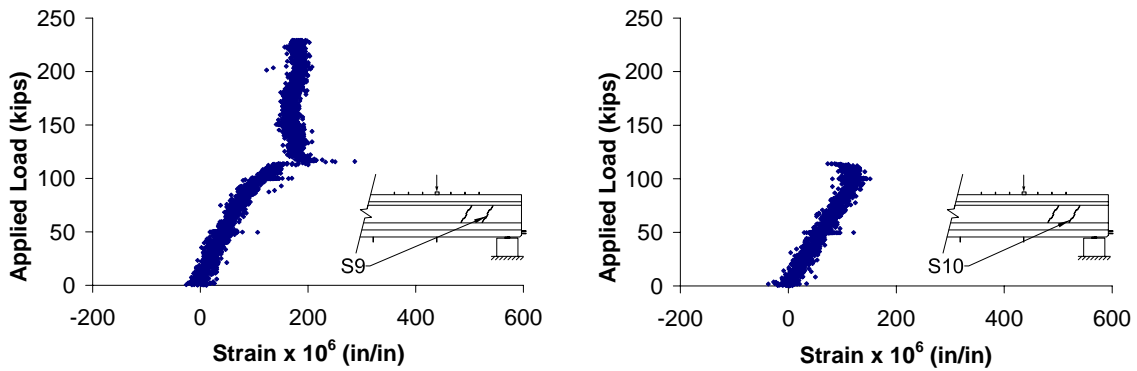


Figure 98. Web shear strain positions nine and ten in S2-STDS

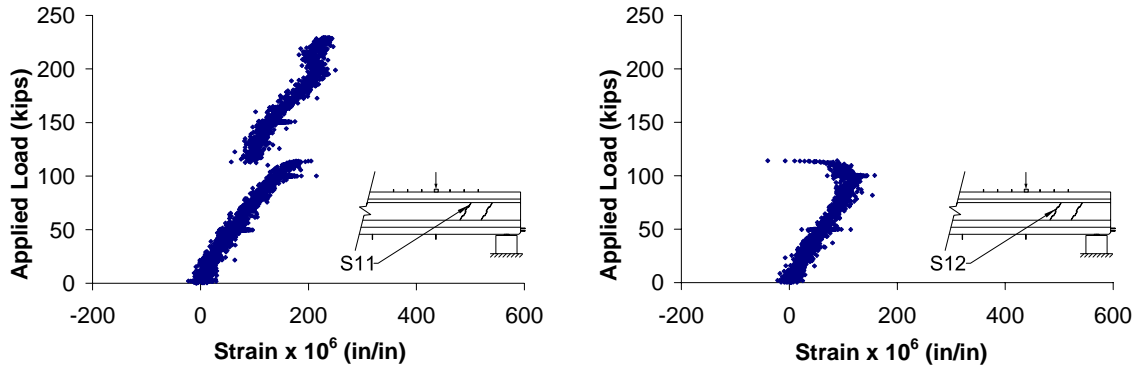


Figure 99. Web shear strain positions eleven and twelve in S2-STDS

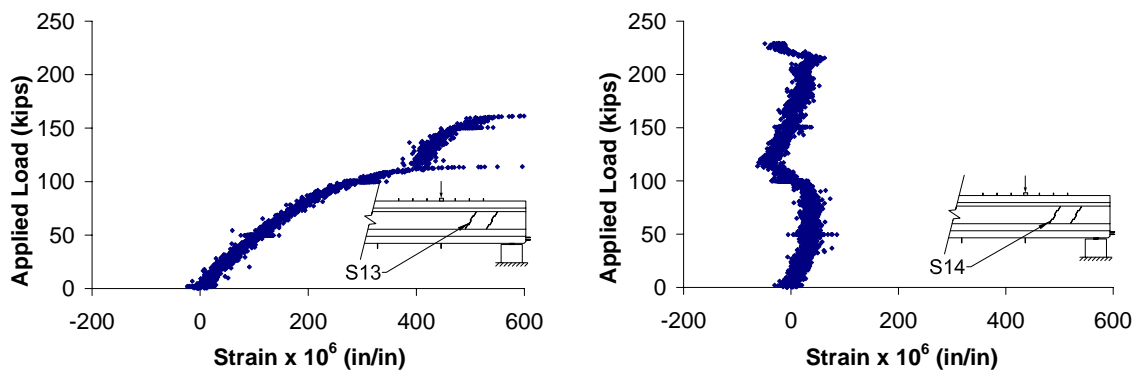


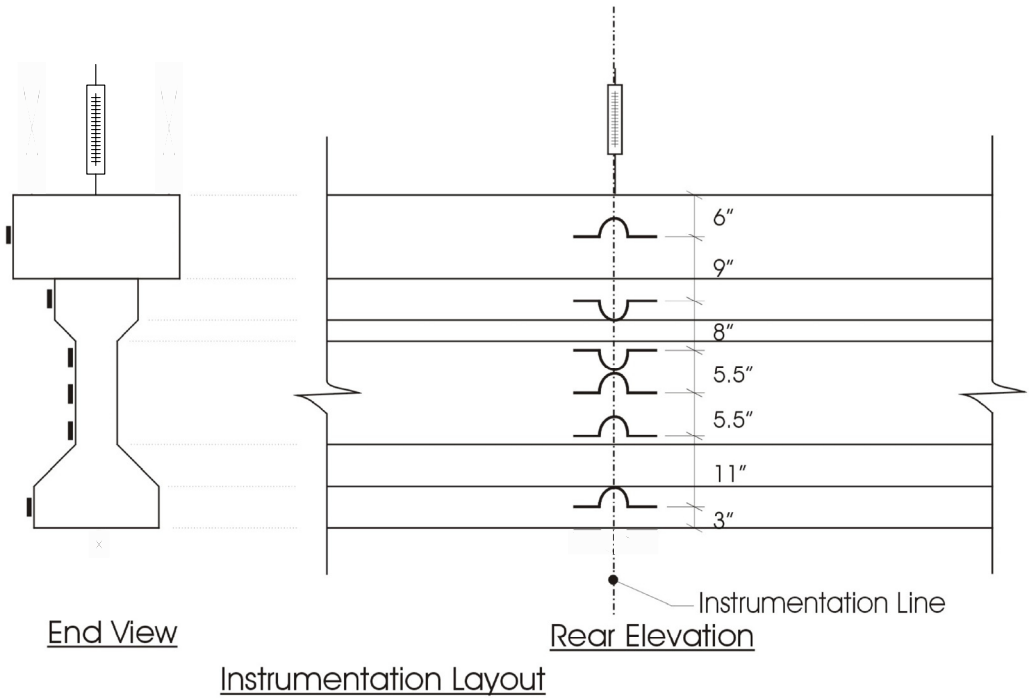
Figure 100. Web shear strain positions thirteen and fourteen in S2-STDS

APPENDIX E - SHEAR- FLEXURE TEST

TEST SETUP


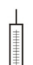

Two of the Type II AASHTO beams were constructed and tested to investigate the structural behavior of SCC as compared to the control concrete in a condition of combined shear and flexure. As shown in the detailed as-built figures in Appendix C, the beams incorporated a standard arrangement of stirrups and strands. Single-leg number five stirrups spaced at 18 inches were used at the position of the load cell, which coincides with the location of the highest moment. An available development length of over 12 inches, with the center of the support 12 inches from the end of the beam, was provided to minimize the chance of the bonded strands slipping. Additionally, a non-SCC composite cap was constructed on top of each beam to match an actual application of an AASHTO Type II beam.

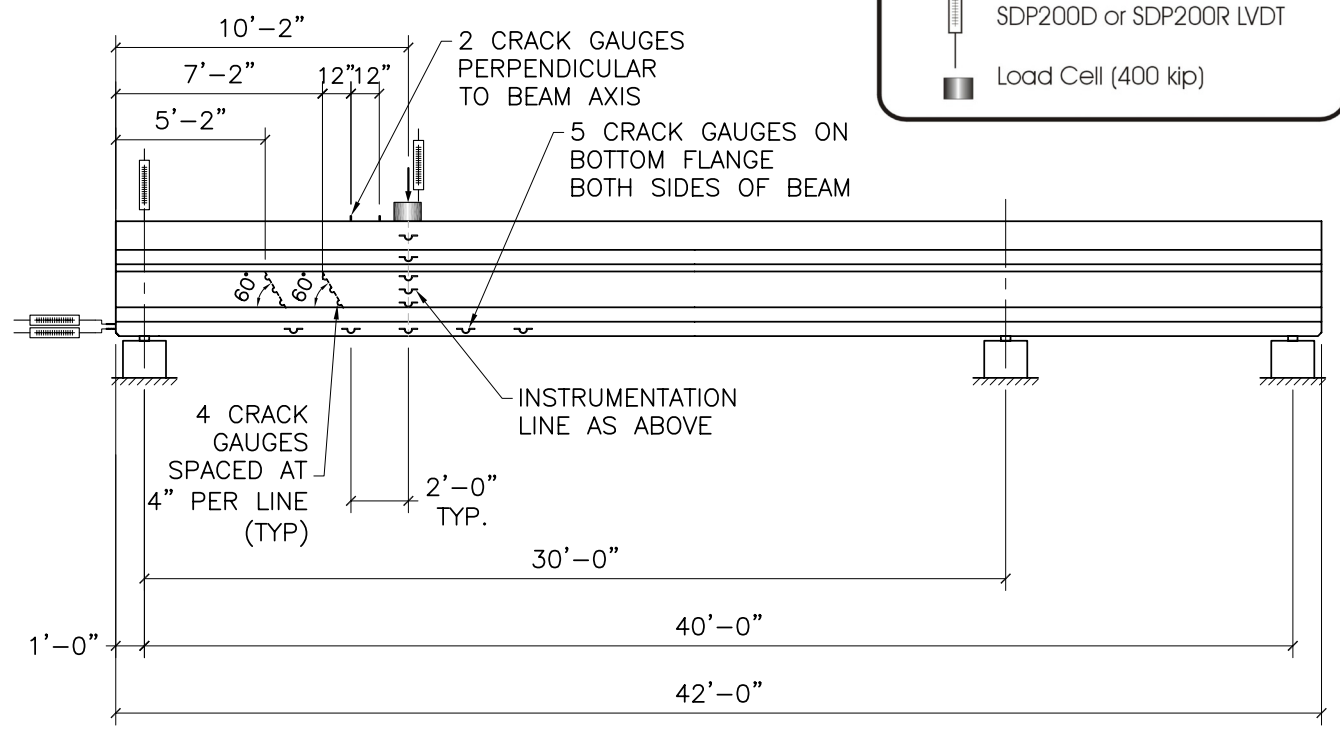
The test setup for the shear-flexure tests is shown in Figure 101. Crack gauges were installed in a line on the vertical faces of the beam under the position of the load cell to monitor the strain due to flexure. Additionally, crack gauges were installed on the vertical face of the beam web and oriented to measure tension strain due to shear. A LVDT was used to monitor beam deflection with increasing load. LVDTs were also installed on the strands at the ends of the beams to confirm that a negligible amount of strand slip of the fully bonded strands would occur. Additional crack gauges were installed as shown to compare the two types of concrete. The load was increased until a failure condition was reached.



Instrumentation Layout

Legend

-  PI200-5-X Crack Gauge
-  SDP200D or SDP200R LVDT
-  Load Cell (400 kip)

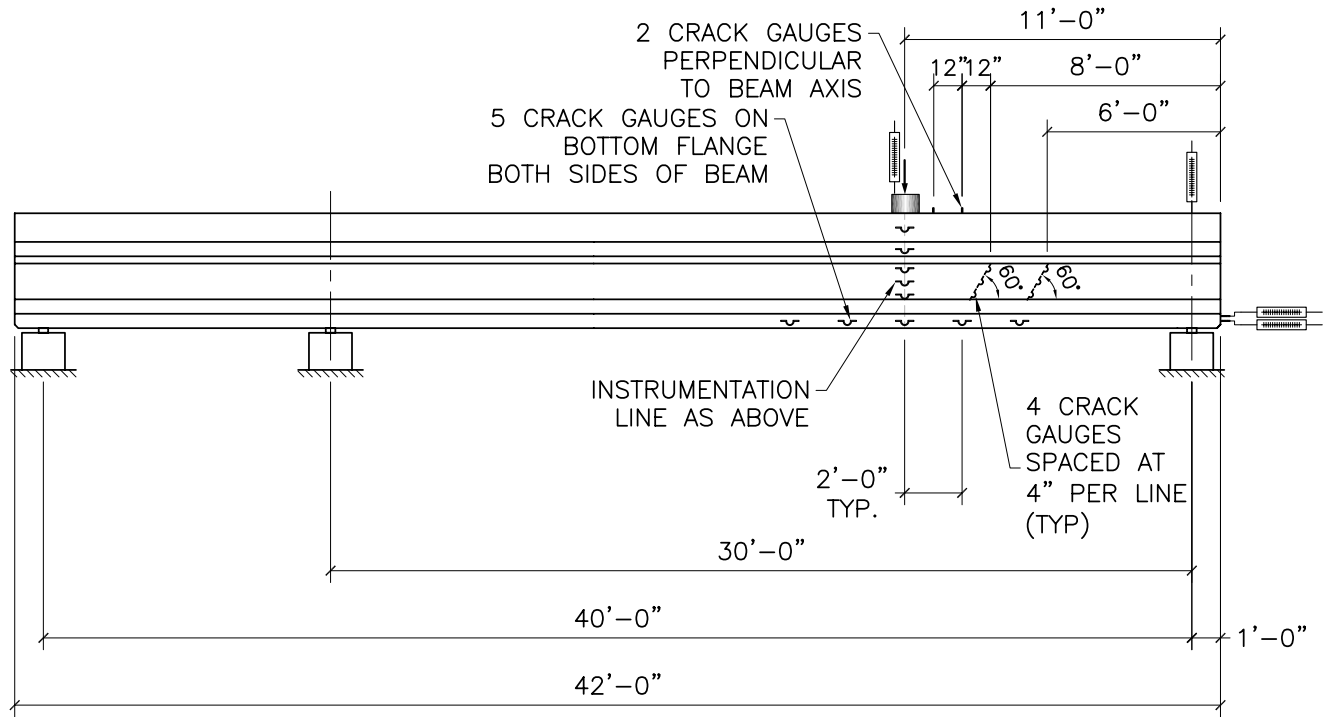


SINGLE BEAM - TEST 1 LAYOUT
SCALE: NTS

SCC Instrumentation 7.dwg L6 5/13/04

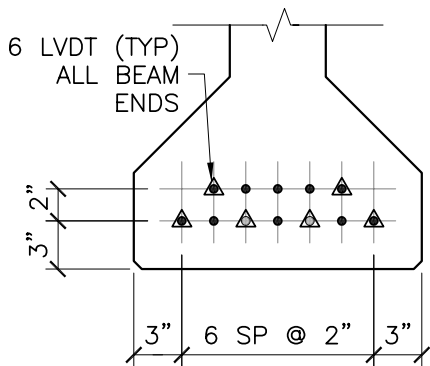
Figure 101a
Shear-Flexure Test
Load Positioning and Instrumentation
AASHTO Type II Girder

Research Project 982
Self-Consolidating Concrete For
Use In FDOT Bridge Elements



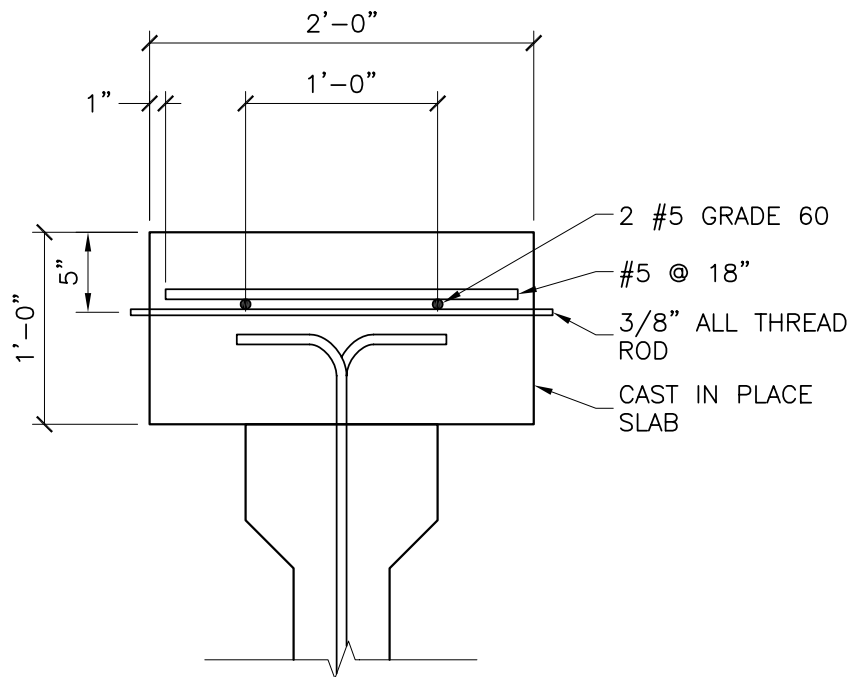
SINGLE BEAM - TEST 2 LAYOUT

SCALE: NTS



STRAND INSTRUMENTATION

SCALE: 1" = 1'-0"



COMPOSITE CAP DESIGN

SCALE: 1" = 1'-0"

SCC Instrumentation 7.dwg L3 5/13/04

Figure 101b
 Shear-Flexure Test
 Strand Instrumentation and Composite Cap Design
 AASHTO Type II Girder

Research Project 982
Self-Consolidating Concrete For
Use In FDOT Bridge Elements

RESULTS

Table 31. Shear-flexure tests web cracking strain

Gauge	F1-SCCF1		F1-STDF2		F2-SCCF1		F2-STDF2	
	Line 1 Strain ($\mu\epsilon$)	Line 2 Strain ($\mu\epsilon$)	Line 1 Strain ($\mu\epsilon$)	Line 2 Strain ($\mu\epsilon$)	Line 1 Strain ($\mu\epsilon$)	Line 2 Strain ($\mu\epsilon$)	Line 1 Strain ($\mu\epsilon$)	Line 2 Strain ($\mu\epsilon$)
1	31.2	-0.5	24.8	7.8	54.5	8.4	20.3	23.3
2	3.6	53.6	-3.3	37.3	-3.6	58.6	28.3	29.5
3	56.1	14.4	43.0	35.9	15.9	3.4	40.3	33.9
4	21.6	22.5	15.8	15.2	27.0	13.3	17.7	30.9
Average	28.1	22.5	20.1	24.0	23.4	20.9	26.6	29.4

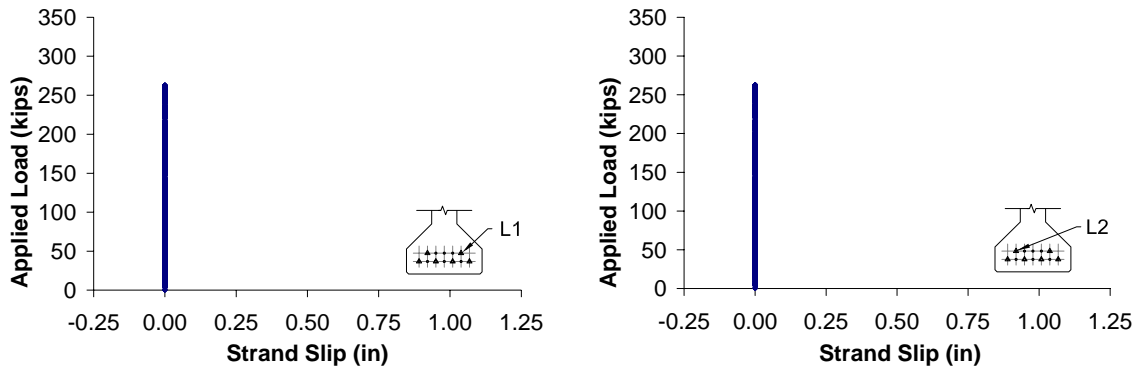


Figure 102. Strand slip for strands one and two in F1-SCCF1

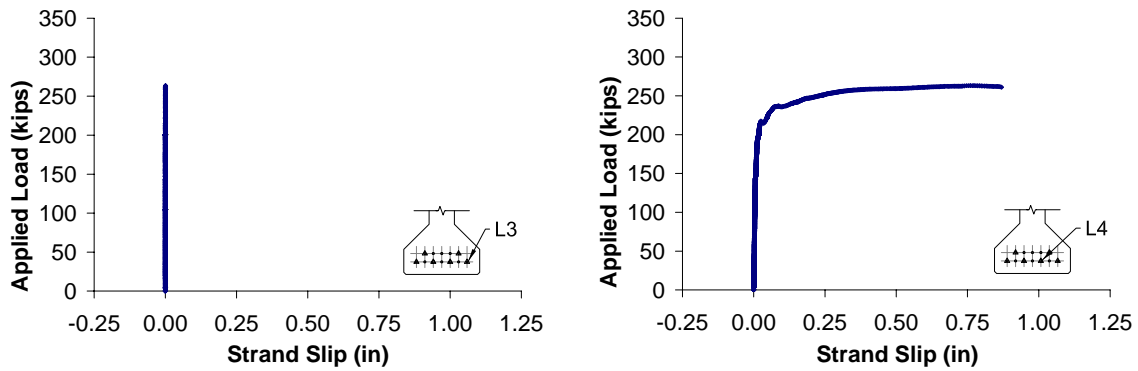


Figure 103. Strand slip for strands three and four in F1-SCCF1

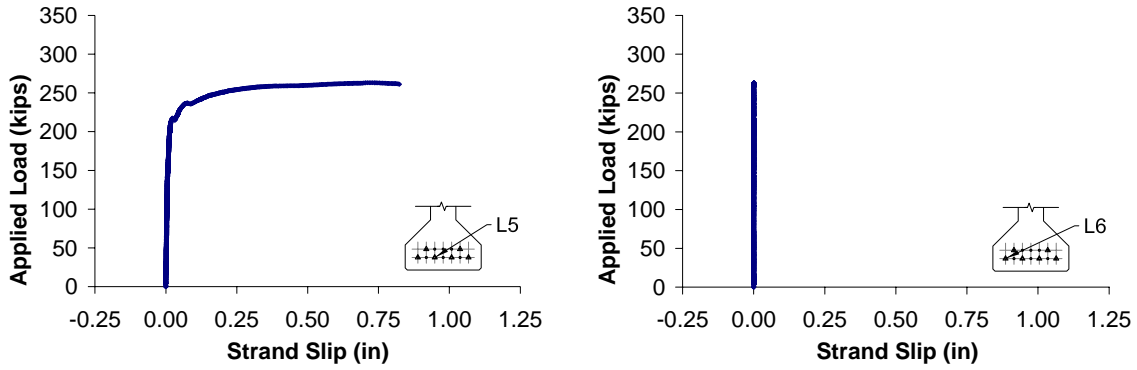


Figure 104. Strand slip for strands five and six in F1-SCCF1

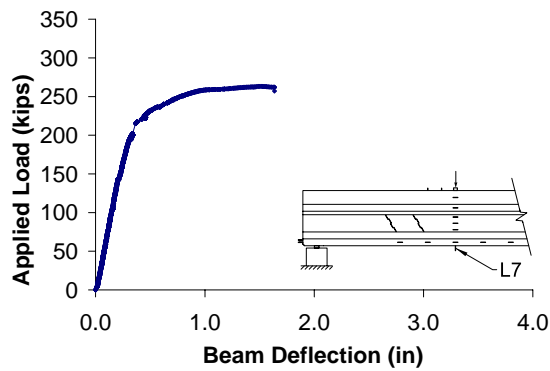


Figure 105. Beam deflection in F1-SCCF1

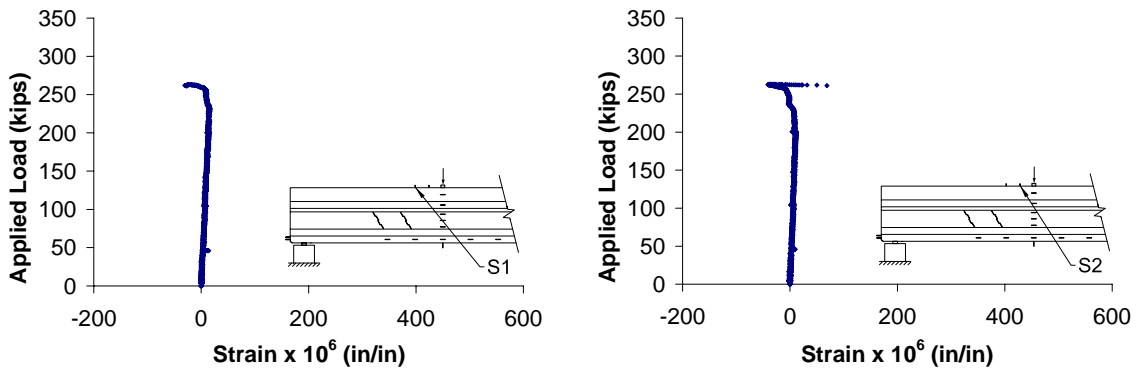


Figure 106. Top face transverse strain positions one and two in F1-SCCF1

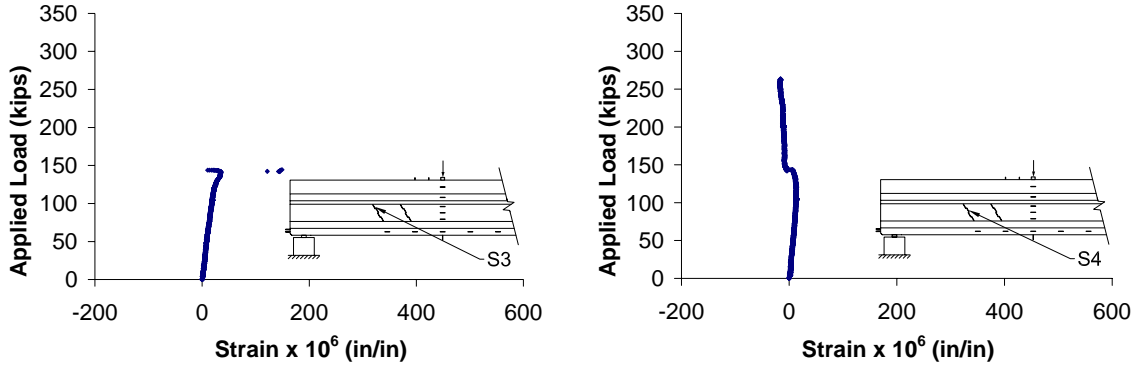


Figure 107. Web shear strain positions three and four in F1-SCCF1

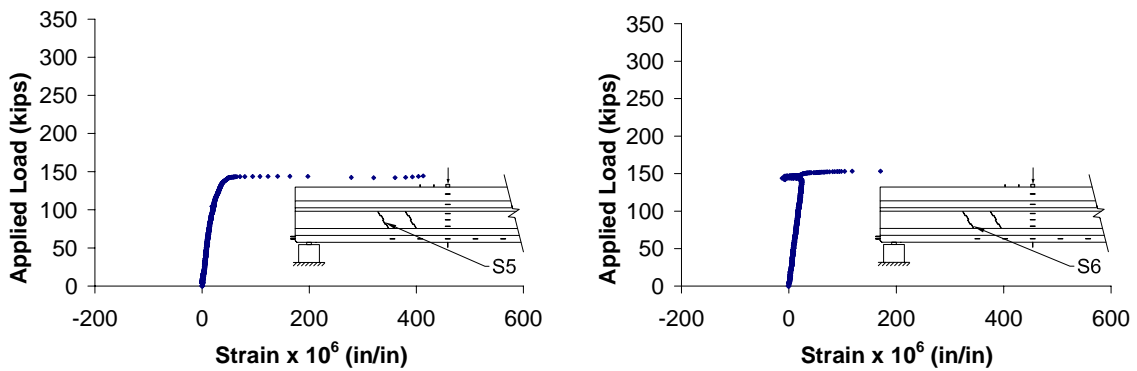


Figure 108. Web shear strain positions five and six in F1-SCCF1

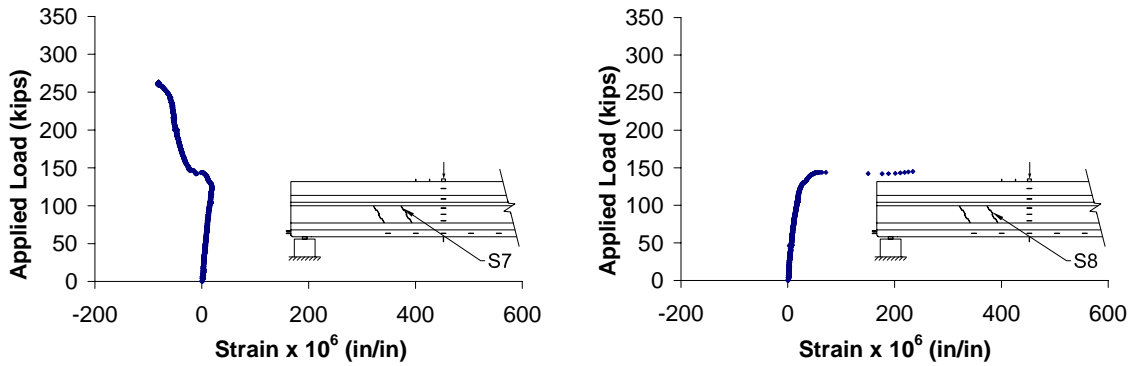


Figure 109. Web shear strain positions seven and eight in F1-SCCF1

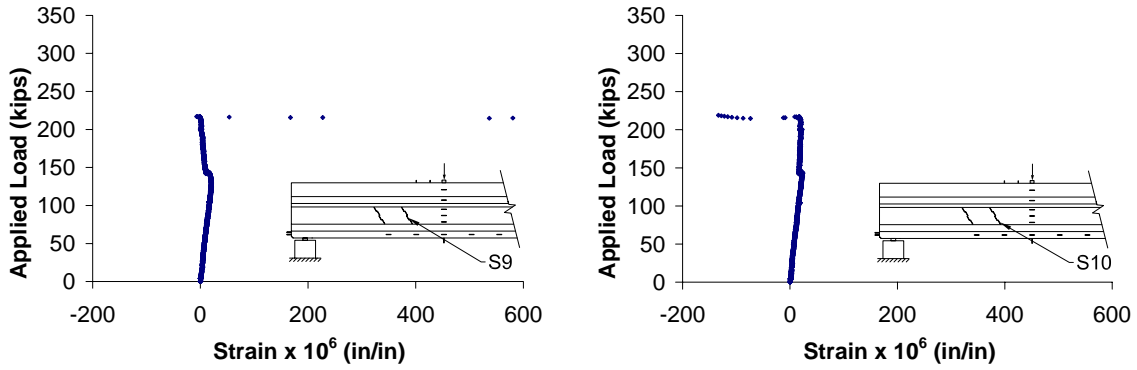


Figure 110. Web shear strain positions nine and ten in F1-SCCF1

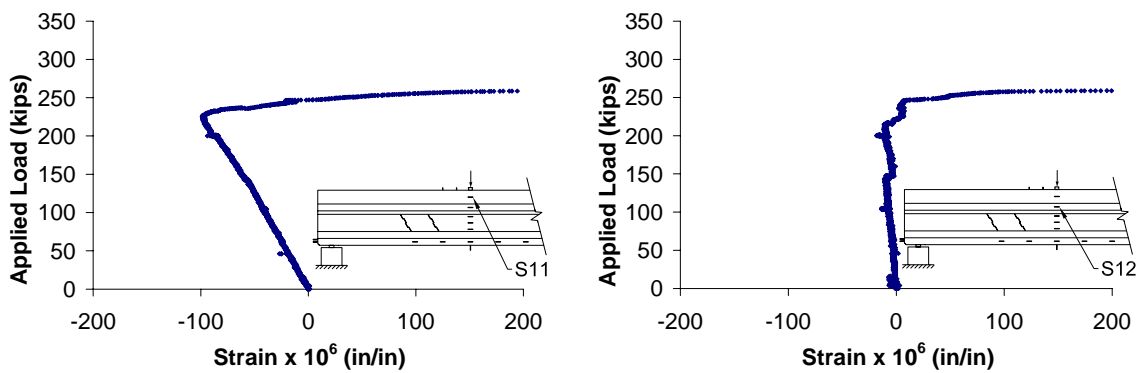


Figure 111. Flexural strain positions eleven and twelve in F1-SCCF1

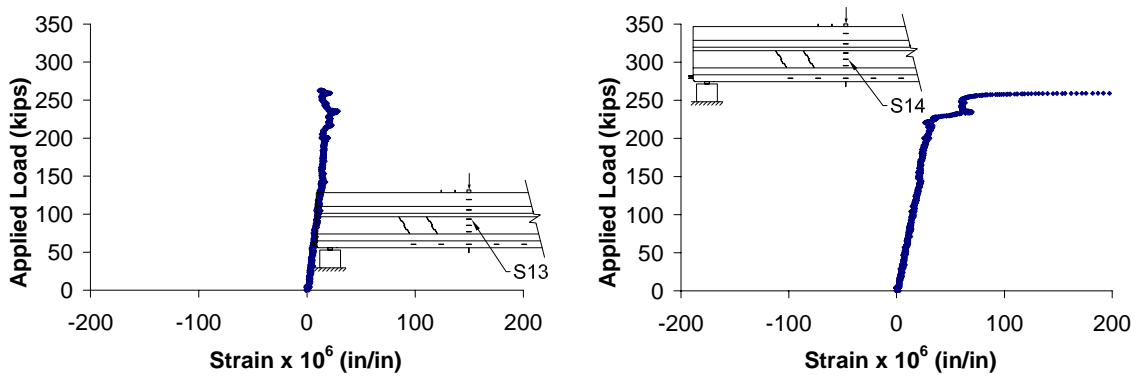


Figure 112. Flexural strain positions thirteen and fourteen in F1-SCCF1

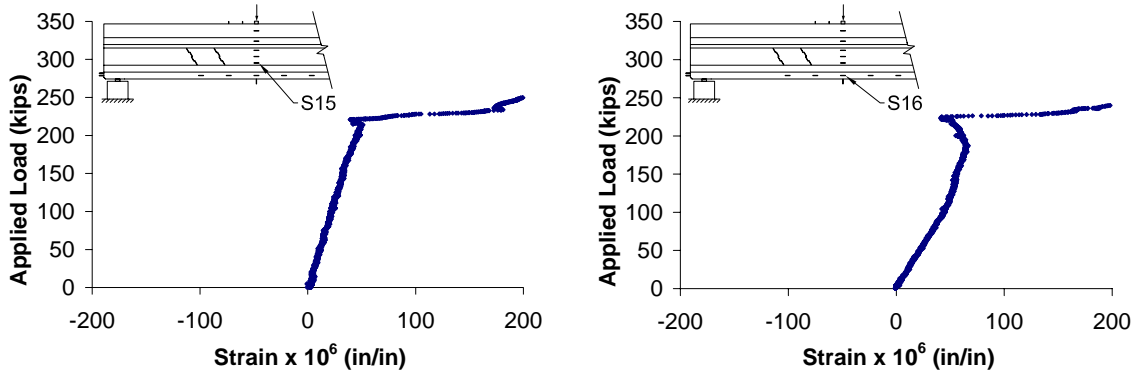


Figure 113. Flexural strain positions fifteen and sixteen in F1-SCCF1

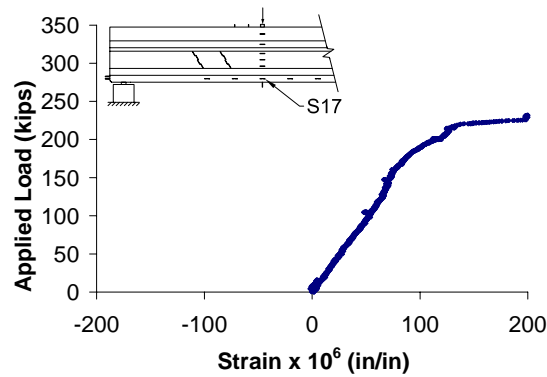


Figure 114. Flexural strain position seventeen in F1-SCCF1

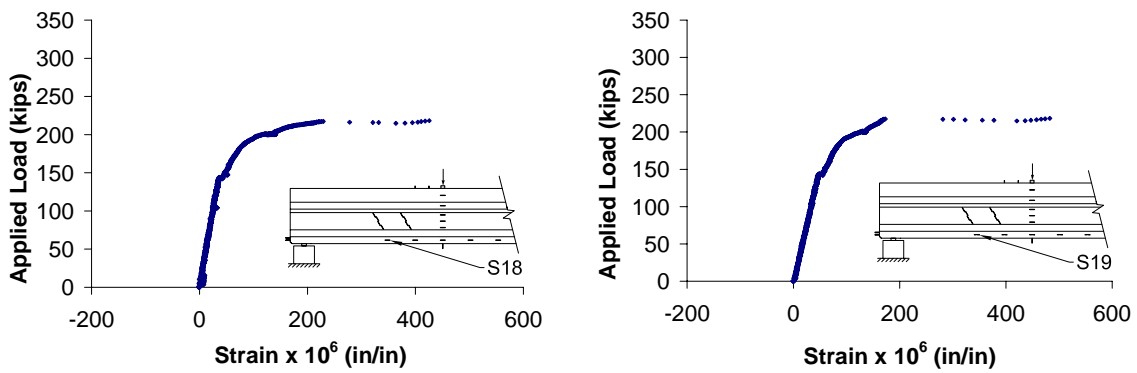


Figure 115. Strain positions eighteen and nineteen in F1-SCCF1

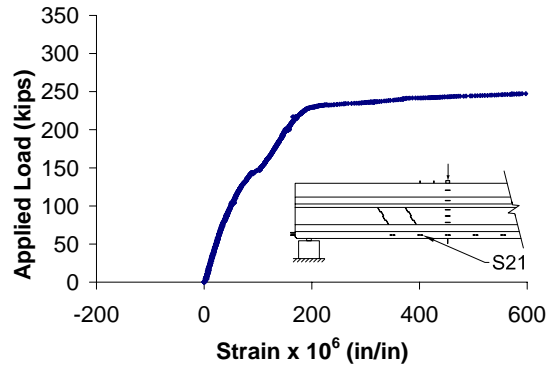
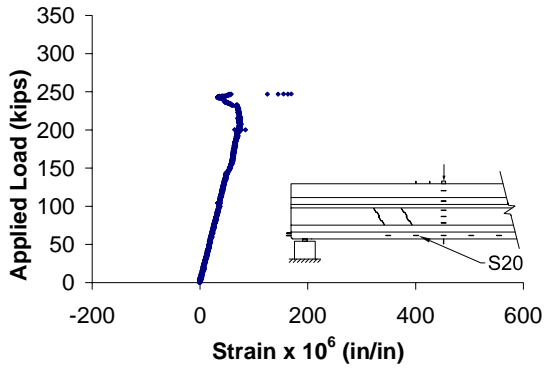


Figure 116. Strain positions 20 and 21 in F1-SCCF1

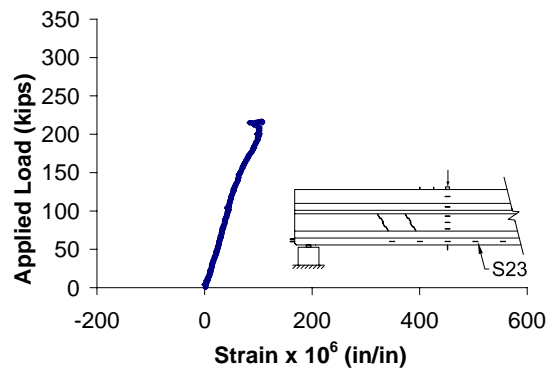
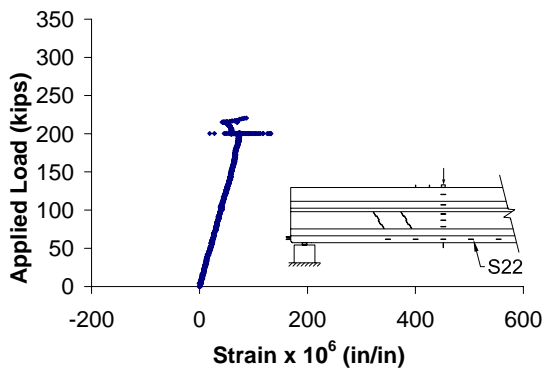


Figure 117. Strain positions 22 and 23 in F1-SCCF1

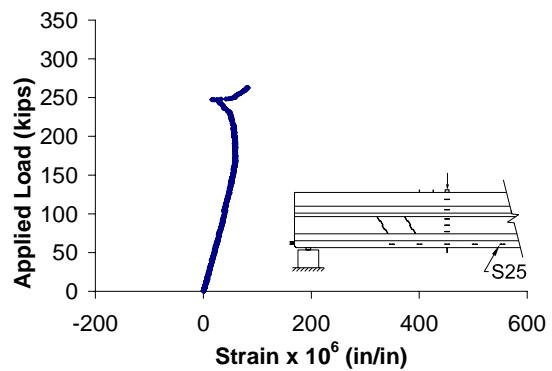
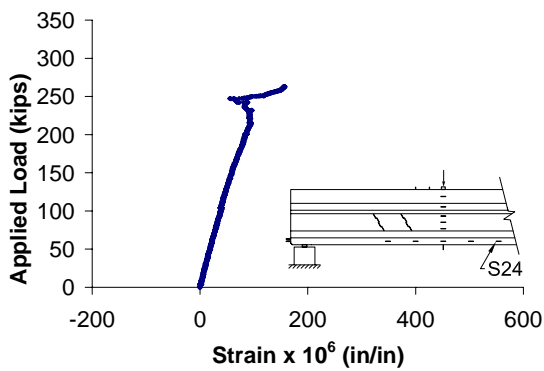


Figure 118. Strain positions 24 and 25 in F1-SCCF1

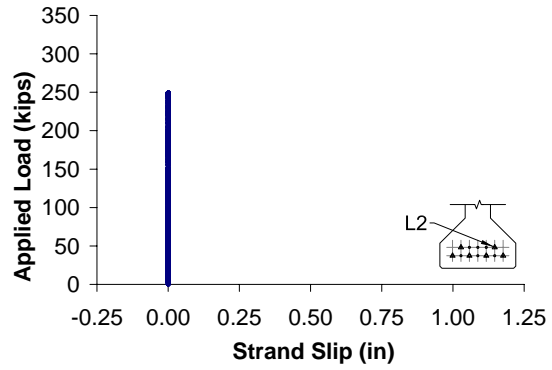
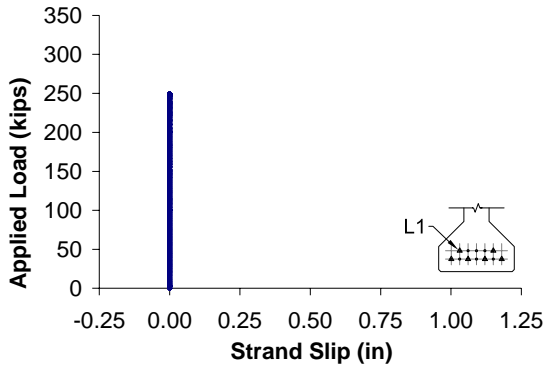


Figure 119. Strand slip for strands one and two in F2-SCCF1

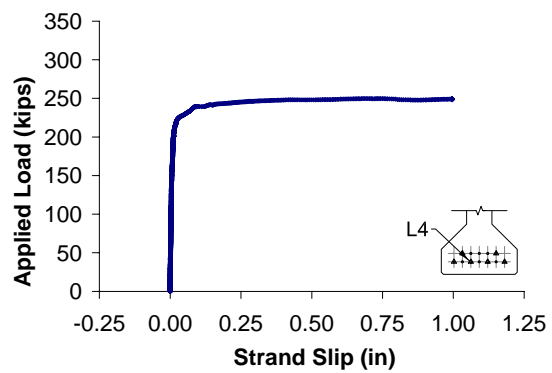
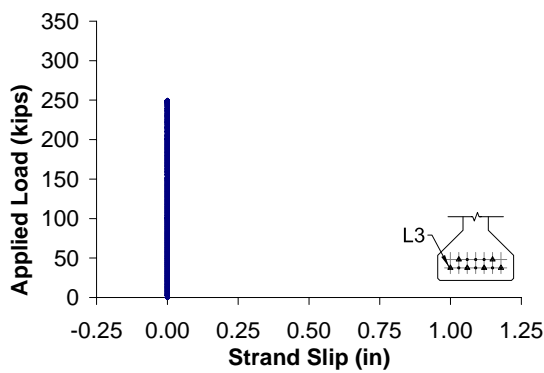


Figure 120. Strand slip for strands three and four in F2-SCCF1

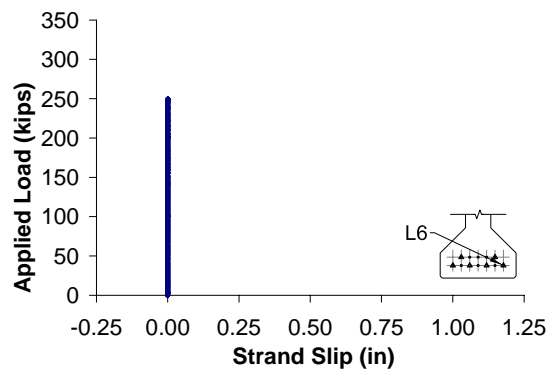
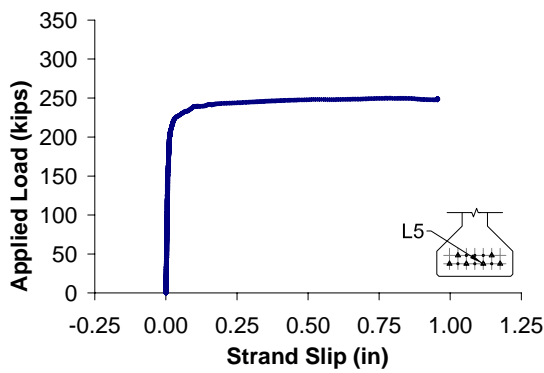


Figure 121. Strand slip for strands five and six in F2-SCCF1

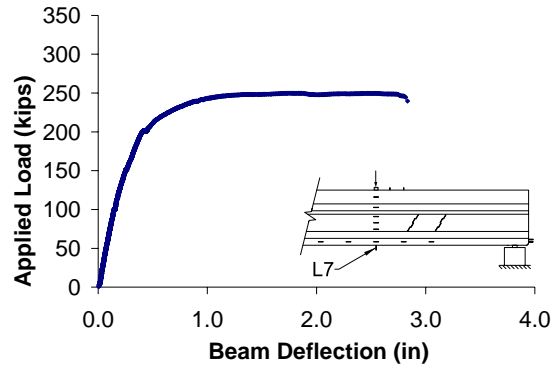


Figure 122. Beam deflection in F2-SCCF1

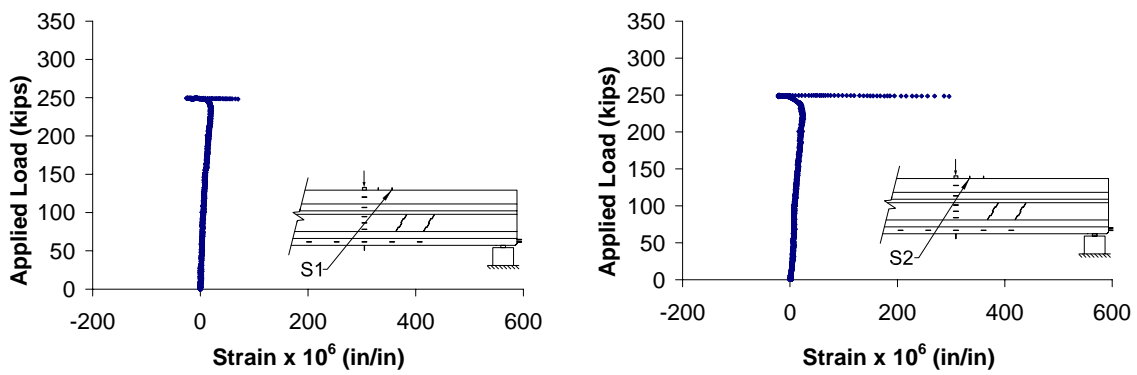


Figure 123. Top face transverse strain positions one and two in F2-SCCF1

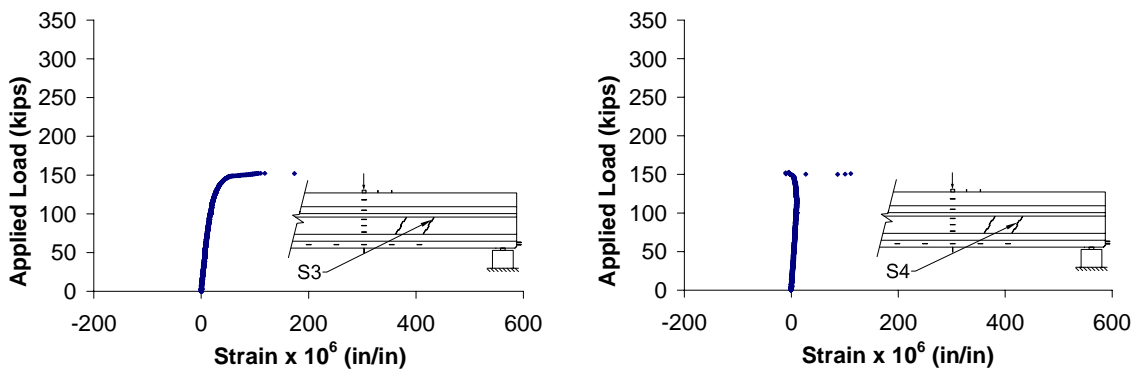


Figure 124. Web shear strain positions three and four in F2-SCCF1

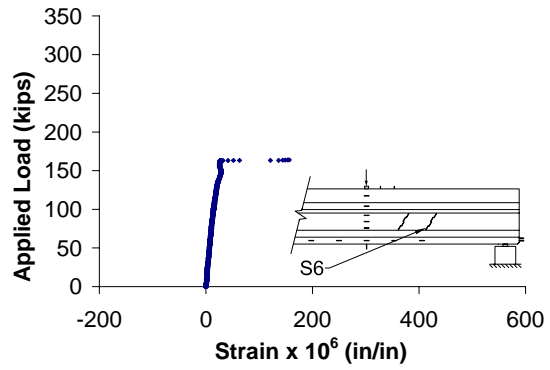
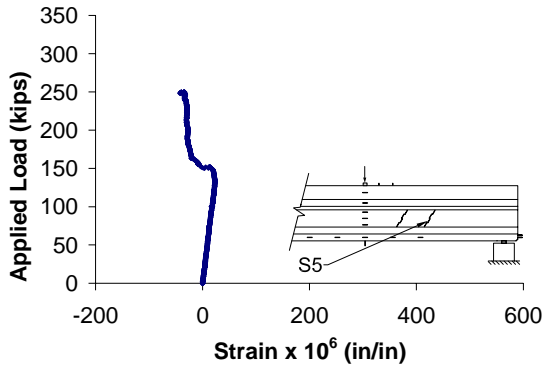


Figure 125. Web shear strain positions five and six in F2-SCCF1

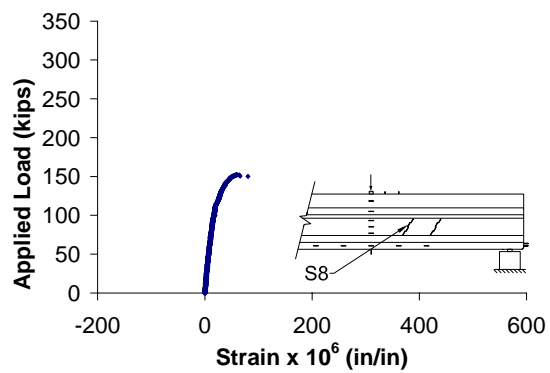
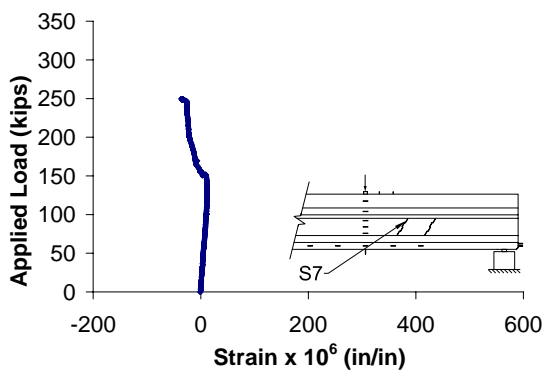


Figure 126. Web shear strain positions seven and eight in F2-SCCF1

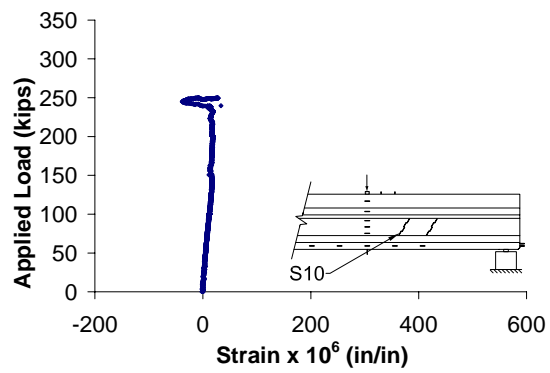
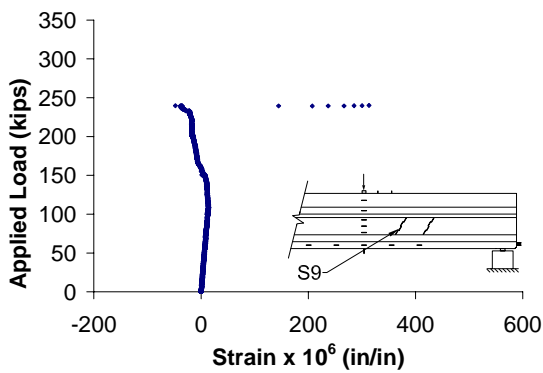


Figure 127. Web shear strain positions nine and ten in F2-SCCF1

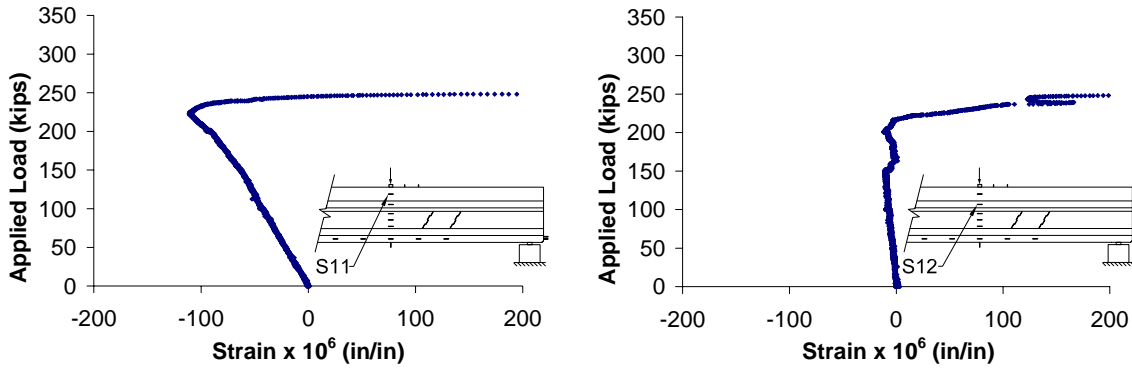


Figure 128. Flexural strain positions eleven and twelve in F2-SCCF1

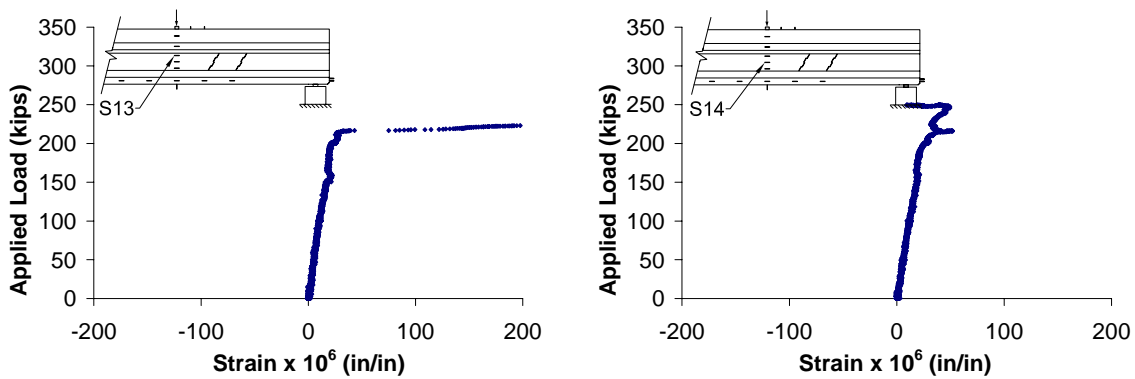


Figure 129. Flexural strain positions thirteen and fourteen in F2-SCCF1

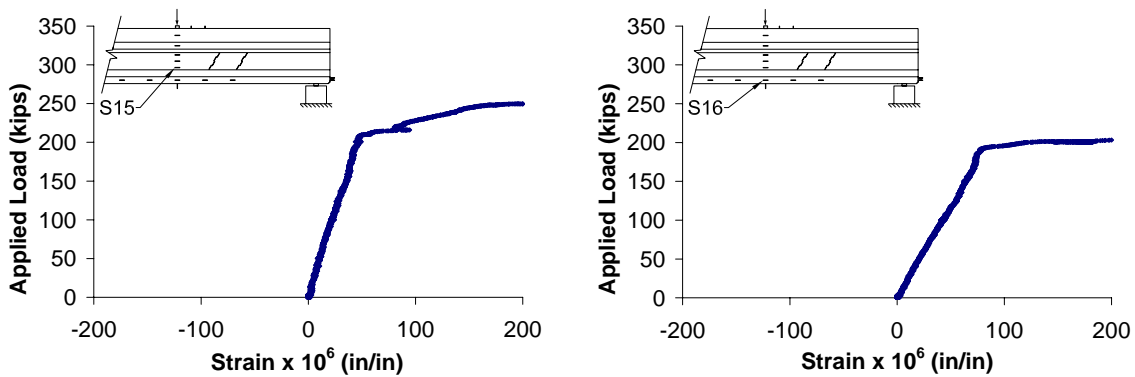


Figure 130. Flexural strain positions fifteen and sixteen in F2-SCCF1

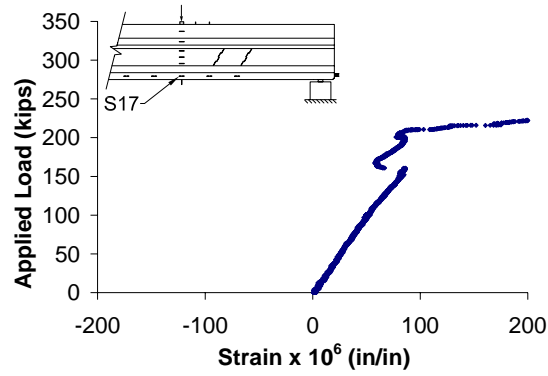


Figure 131. Flexural strain position seventeen in F2-SCCF1

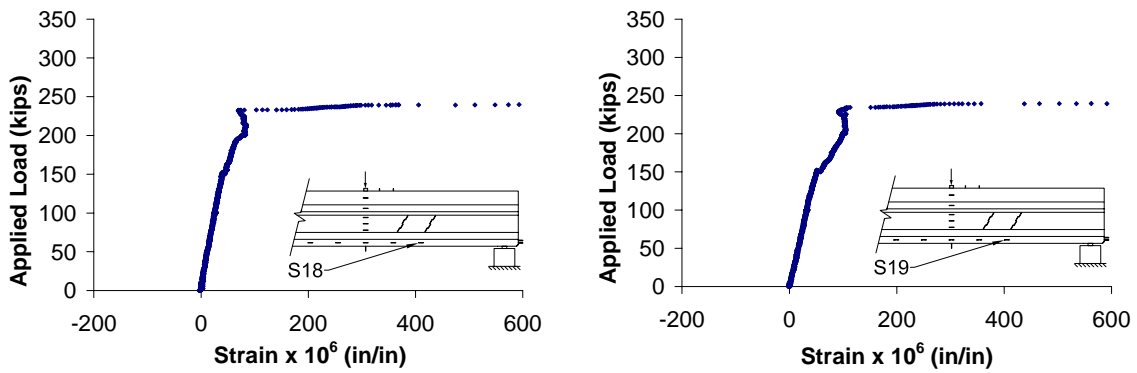


Figure 132. Strain positions eighteen and Ninteen in F2-SCCF1

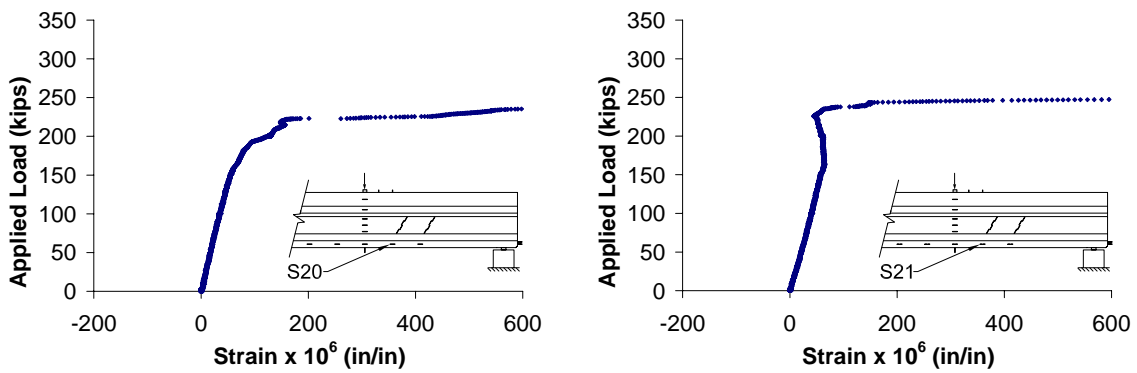


Figure 133. Strain positions 20 and 21 in F2-SCCF1

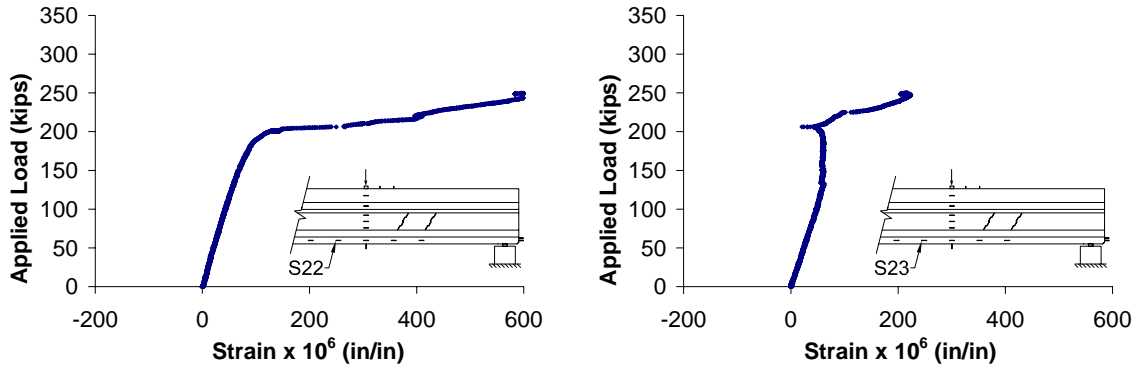


Figure 134. Strain positions 22 and 23 in F2-SCCF1

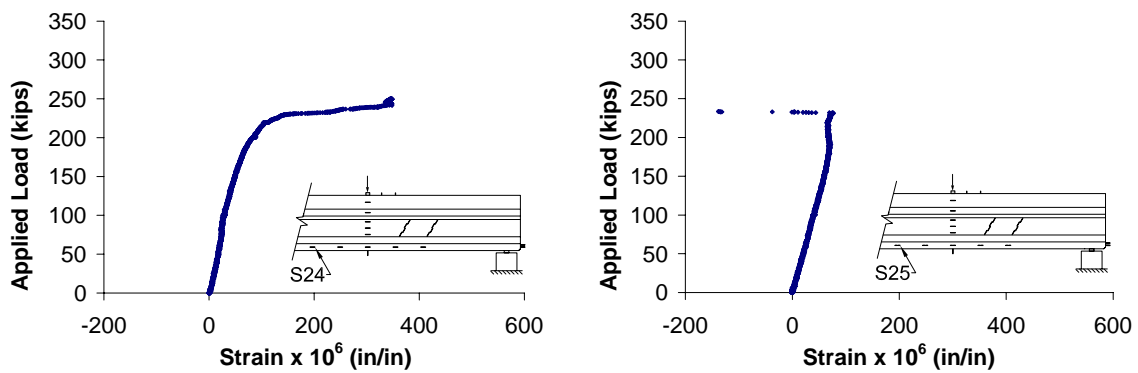


Figure 135. Strain positions 24 and 25 in F2-SCCF1

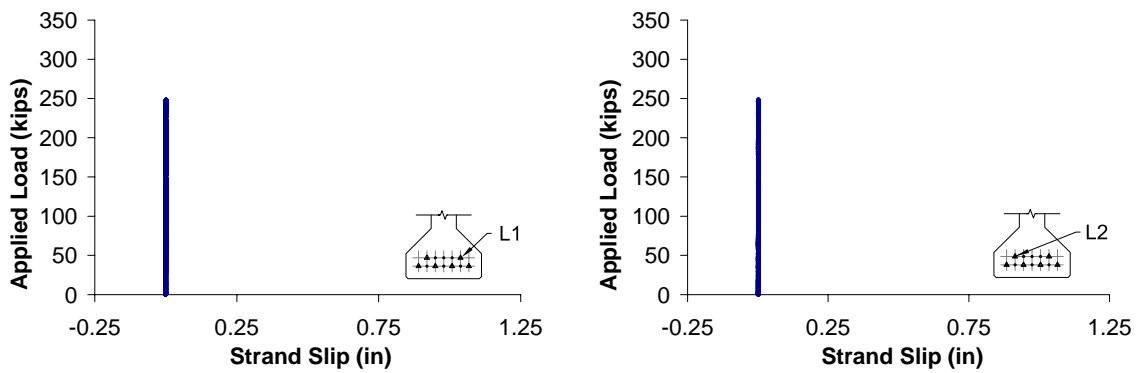


Figure 136. Strand slip for strands one and two in F1-STDF2

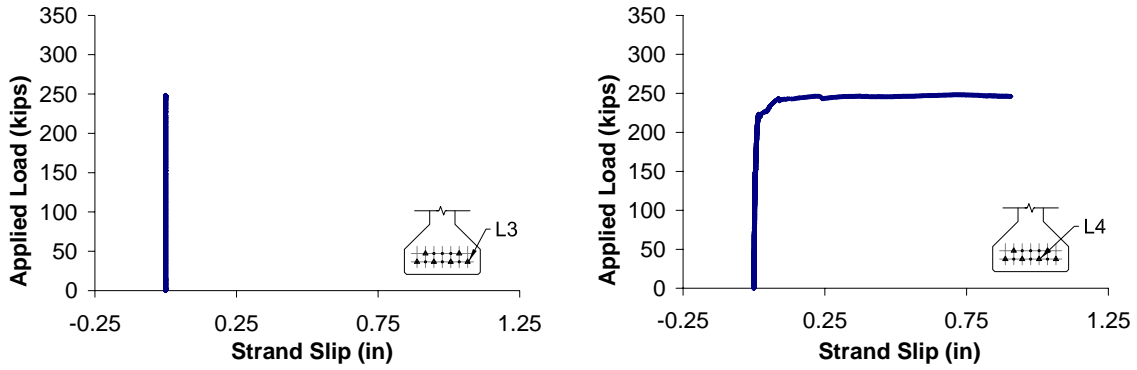


Figure 137. Strand slip for strands three and four in F1-STDF2

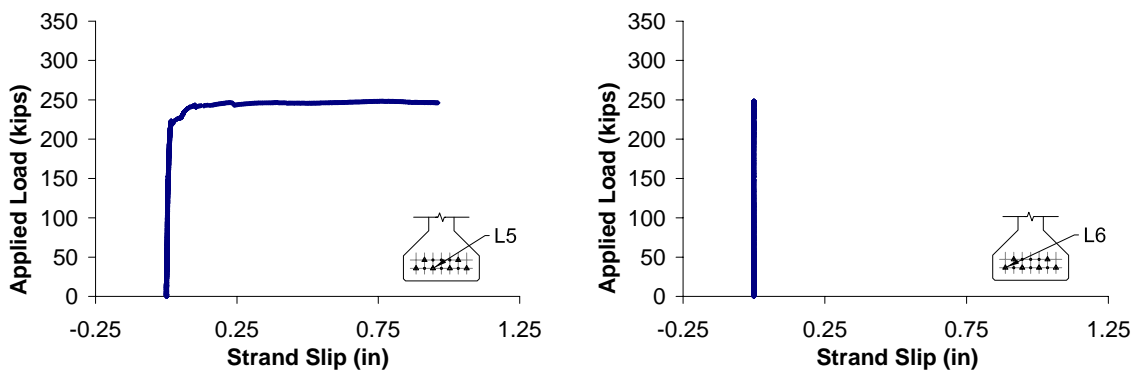


Figure 138. Strand slip for strands five and six in F1-STDF2

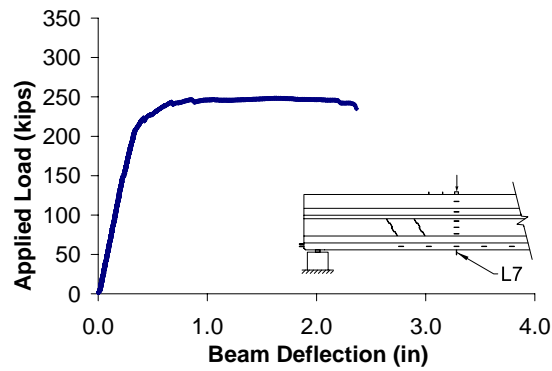


Figure 139. Beam deflection in F1-STDF2

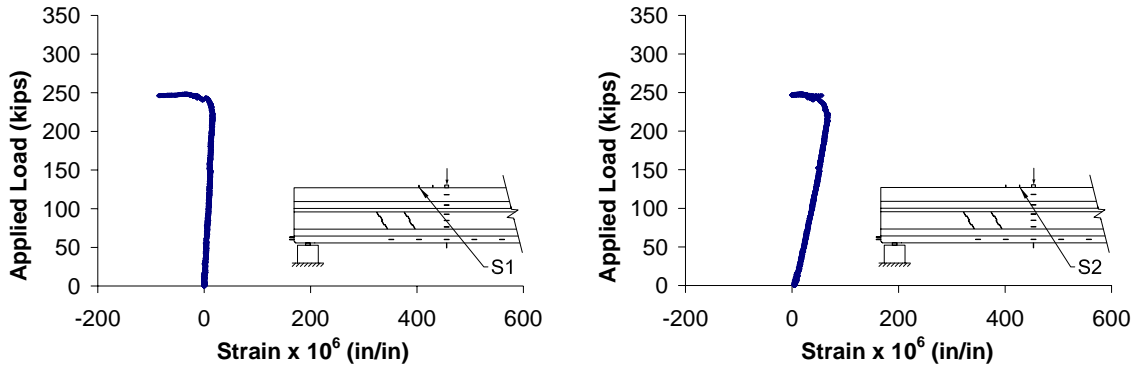


Figure 140. Top face transverse strain positions one and two in F1-STDF2

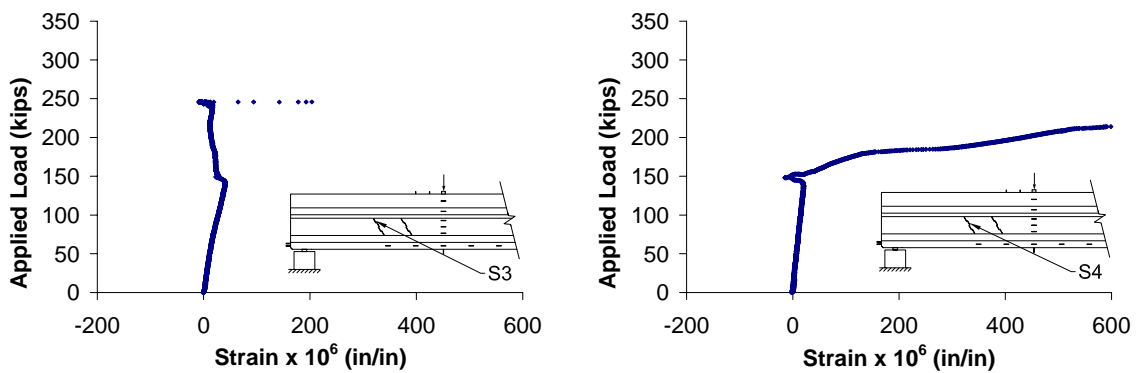


Figure 141. Web shear strain positions three and four in F1-STDF2

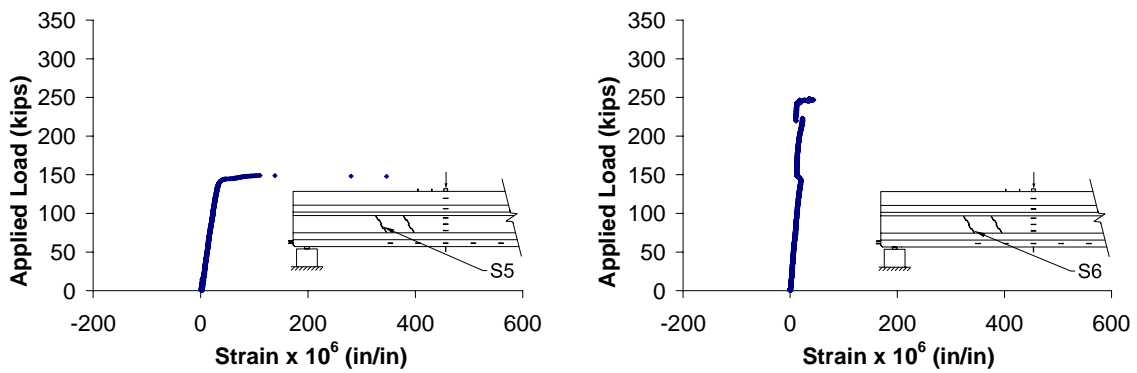


Figure 142. Web shear strain positions five and six in F1-STDF2

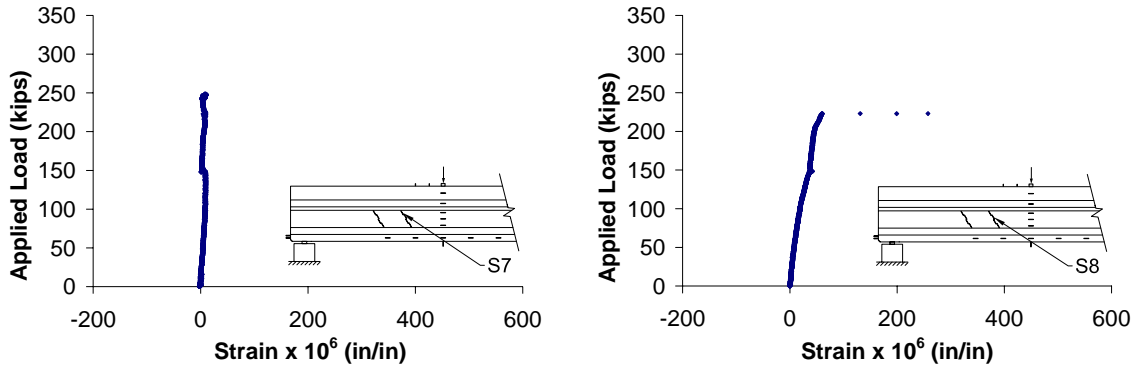


Figure 143. Web shear strain positions seven and eight in F1-STDF2

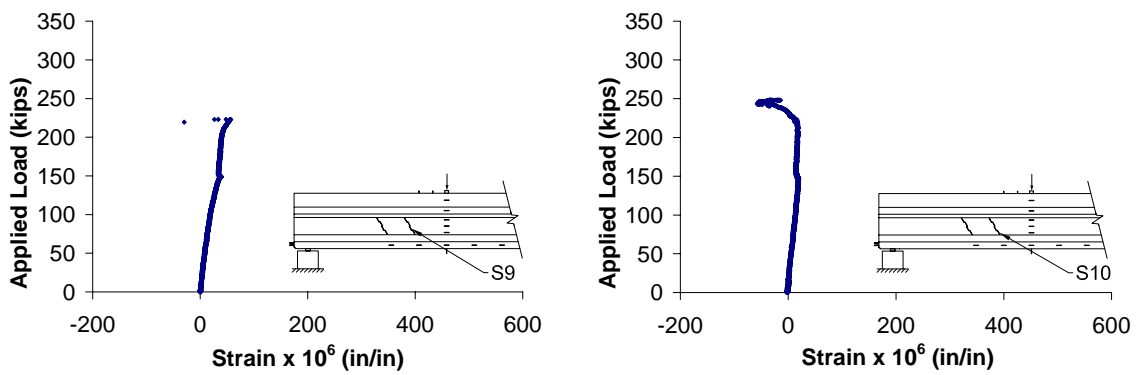


Figure 144. Web shear strain positions nine and ten in F1-STDF2

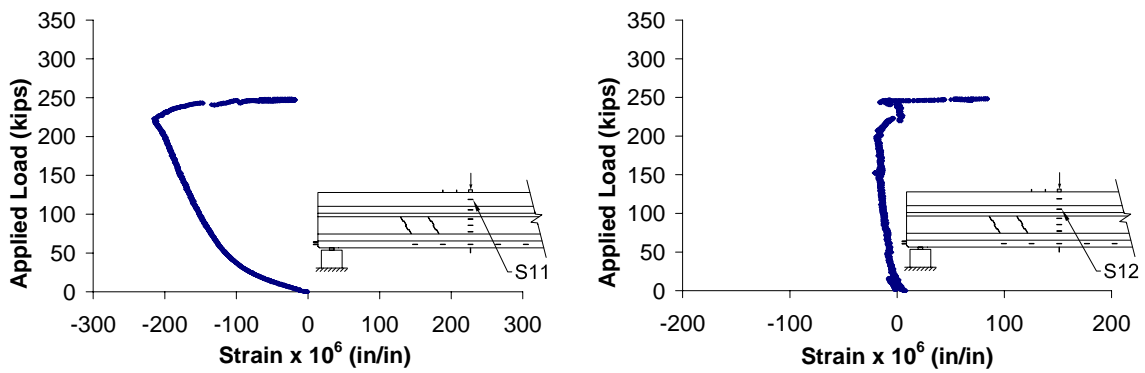


Figure 145. Flexural strain positions eleven and twelve in F1-STDF2

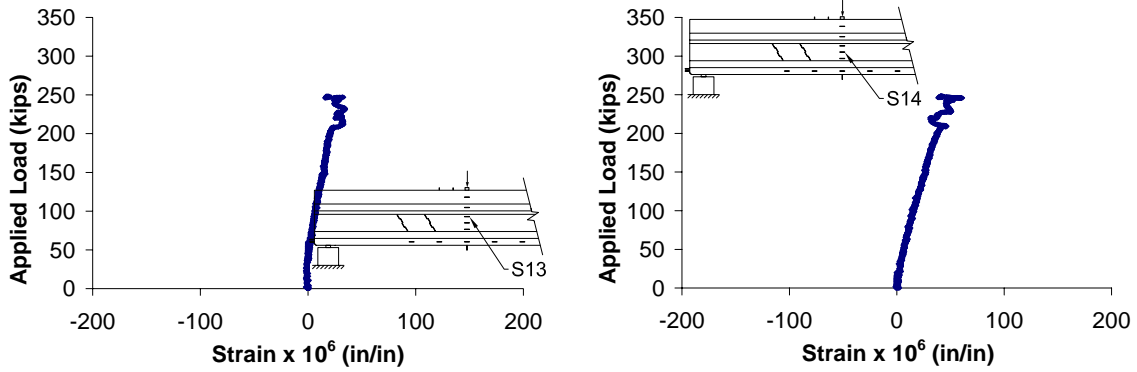


Figure 146. Flexural strain positions thirteen and fourteen in F1-STDF2

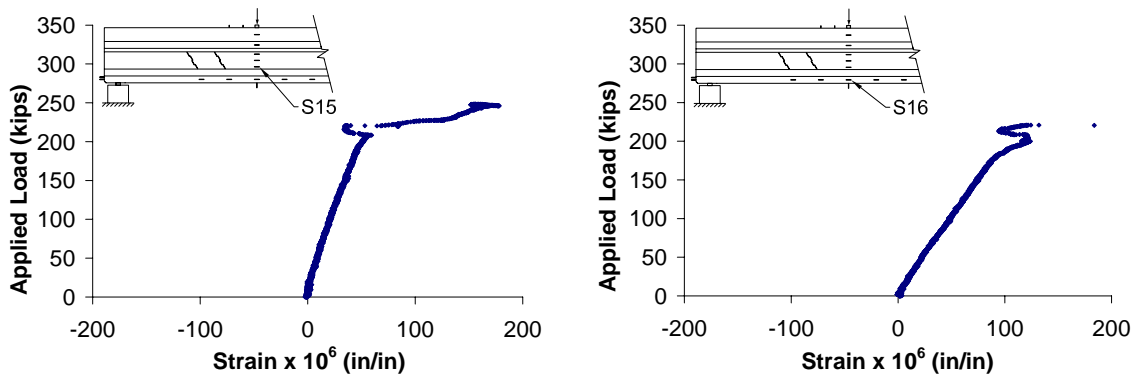


Figure 147. Flexural strain positions fifteen and sixteen in F1-STDF2

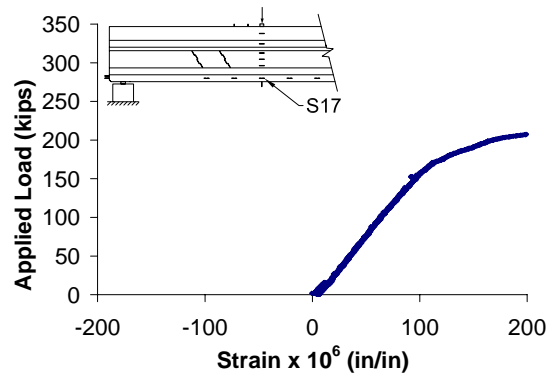


Figure 148. Flexural strain position seventeen in F1-STDF2

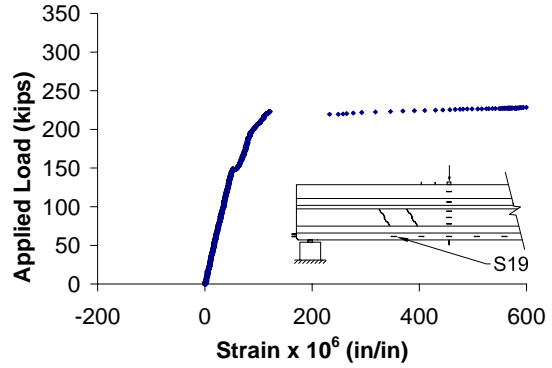
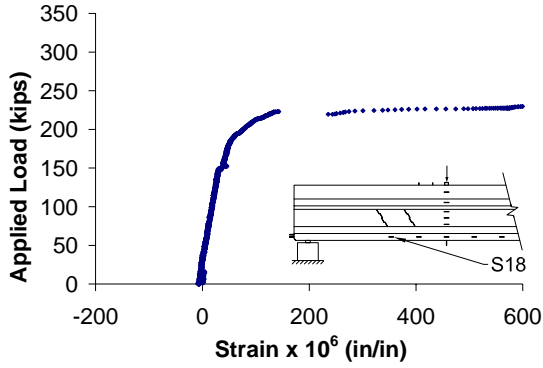


Figure 149. Strain positions eighteen and nineteen in F1-STDF2

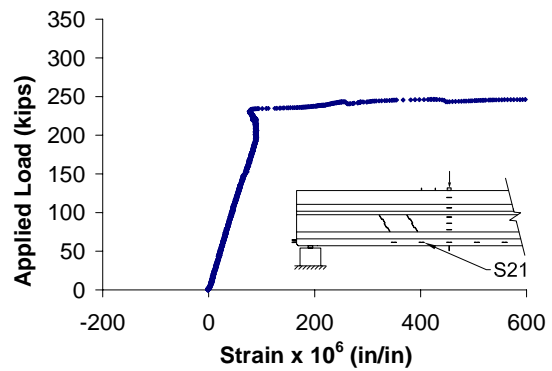
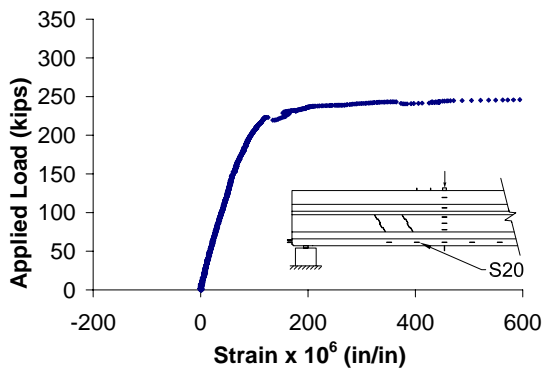


Figure 150. Strain positions 20 and 21 in F1-STDF2

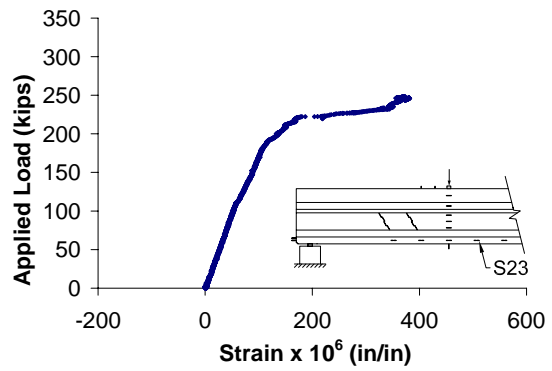
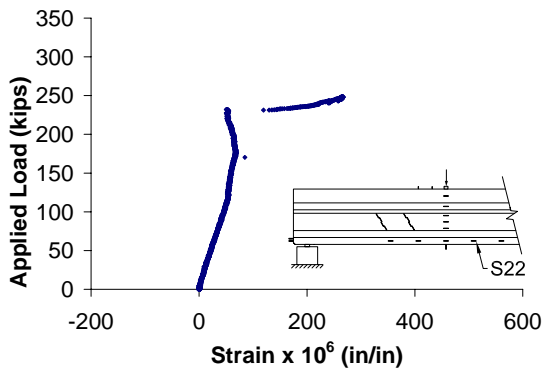


Figure 151. Strain positions 22 and 23 in F1-STDF2

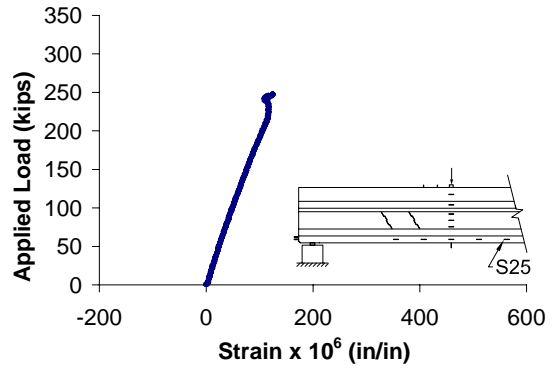
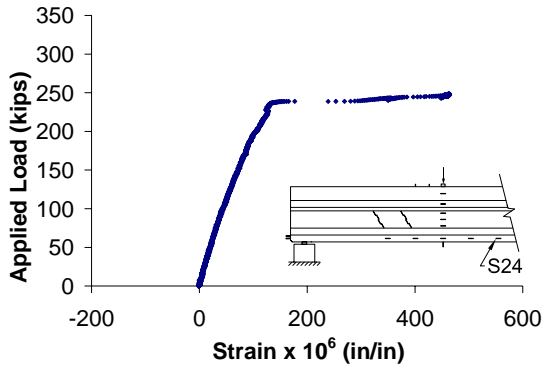


Figure 152. Strain positions 24 and 25 in F1-STDF2

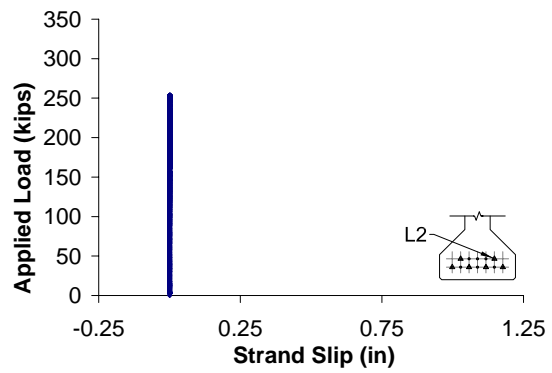
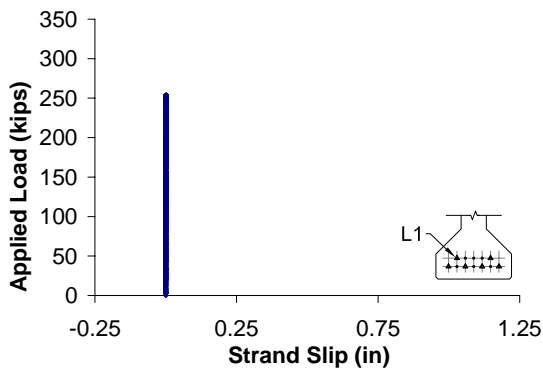


Figure 153. Strand slip for strands one and two in F2-STDF2

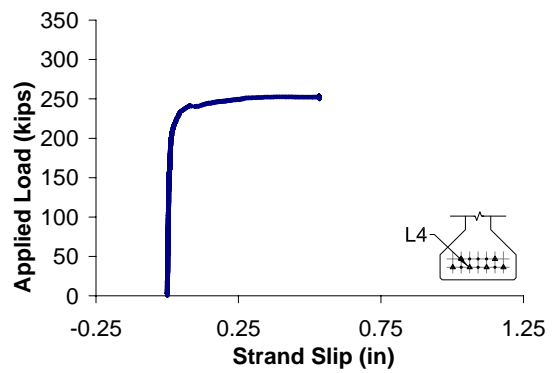
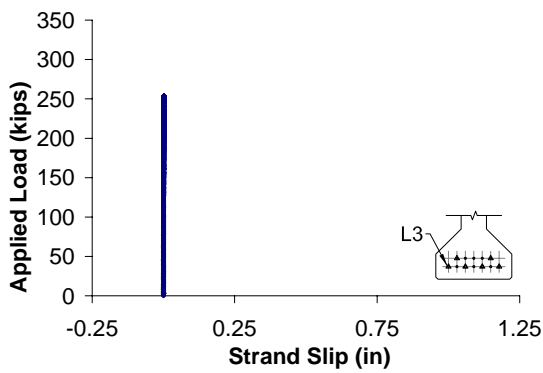


Figure 154. Strand slip for strands three and four in F2-STDF2

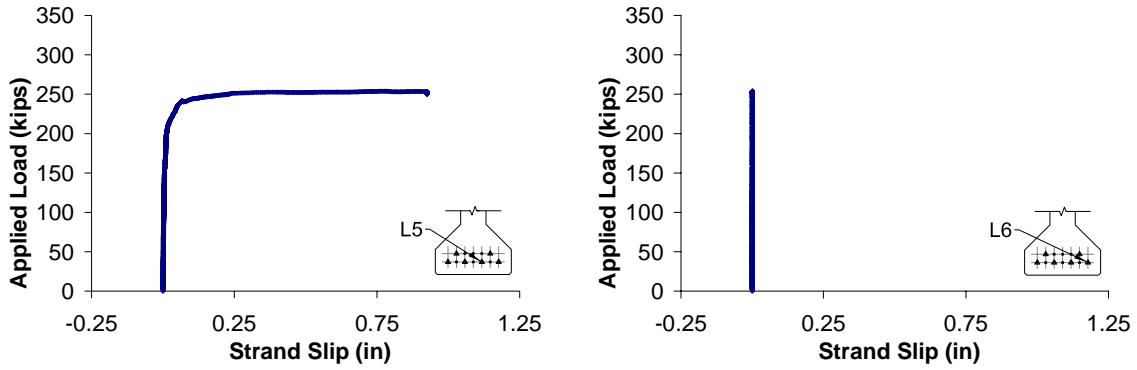


Figure 155. Strand slip for strands five and six in F2-STDF2

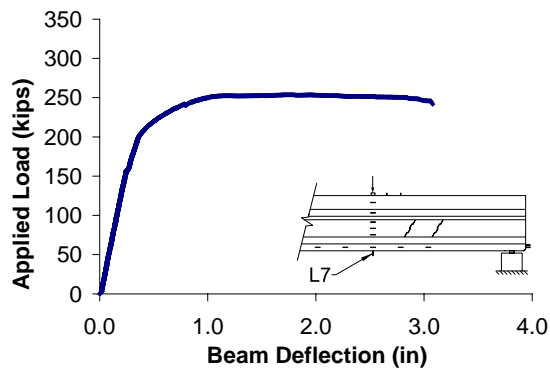


Figure 156. Beam deflection in F2-STDF2

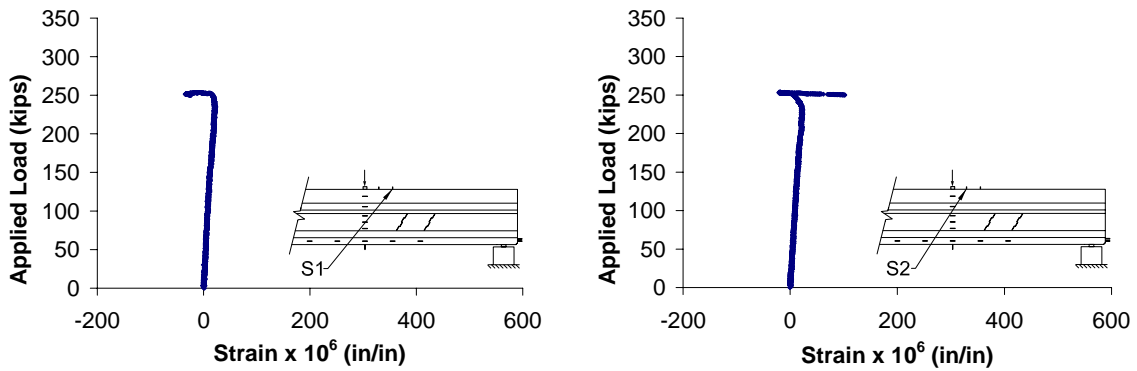


Figure 157. Top face transverse strain positions one and two in F2-STDF2

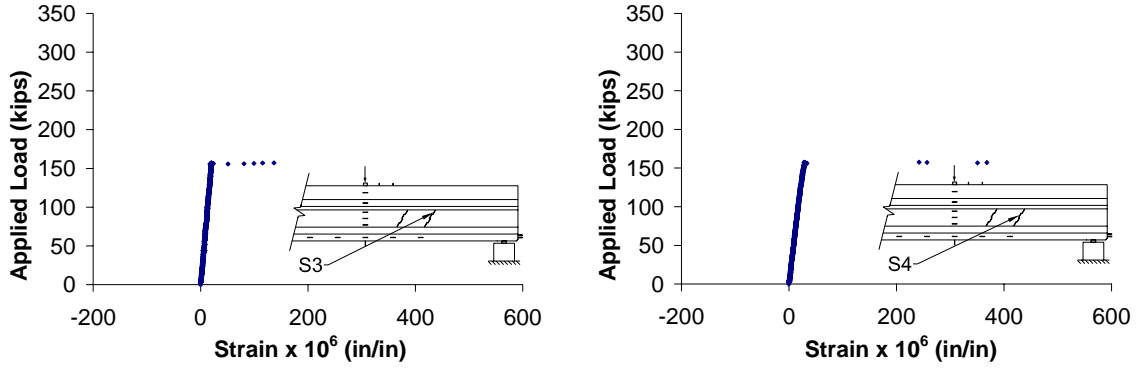


Figure 158. Web shear strain positions three and four in F2-STDF2

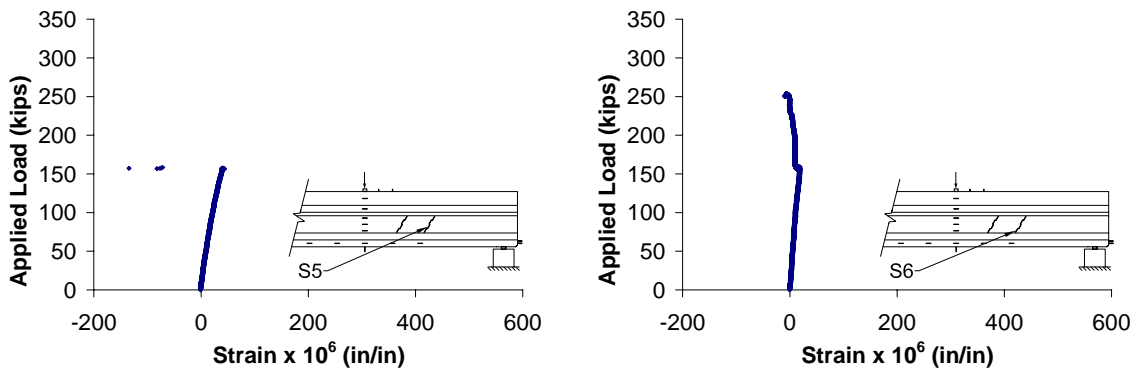


Figure 159. Web shear strain positions five and six in F2-STDF2

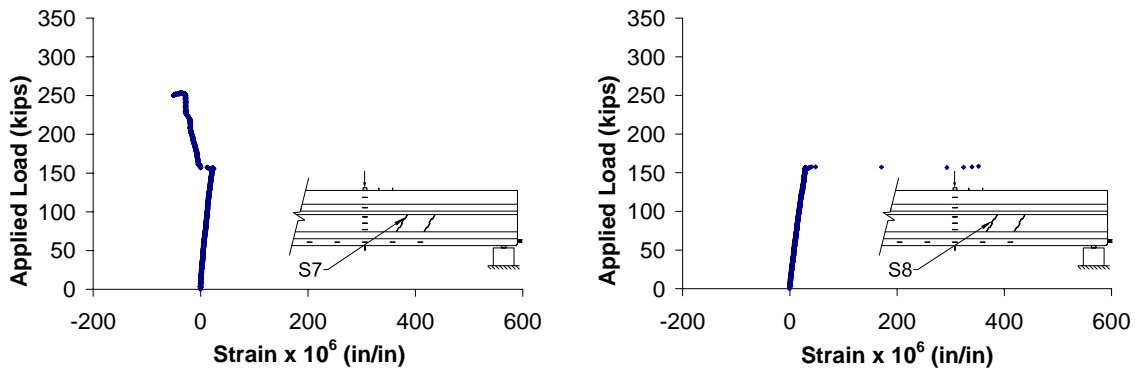


Figure 160. Web shear strain positions seven and eight in F2-STDF2

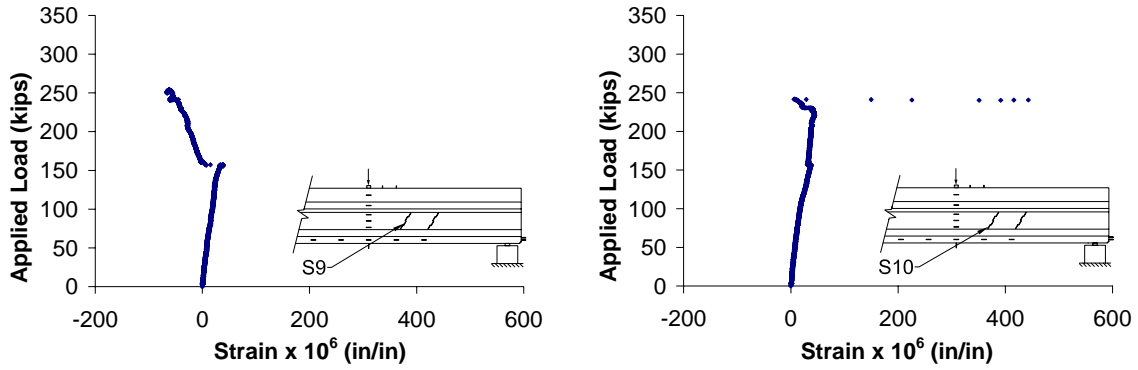


Figure 161 Web shear strain positions nine and ten in F2-STDF2

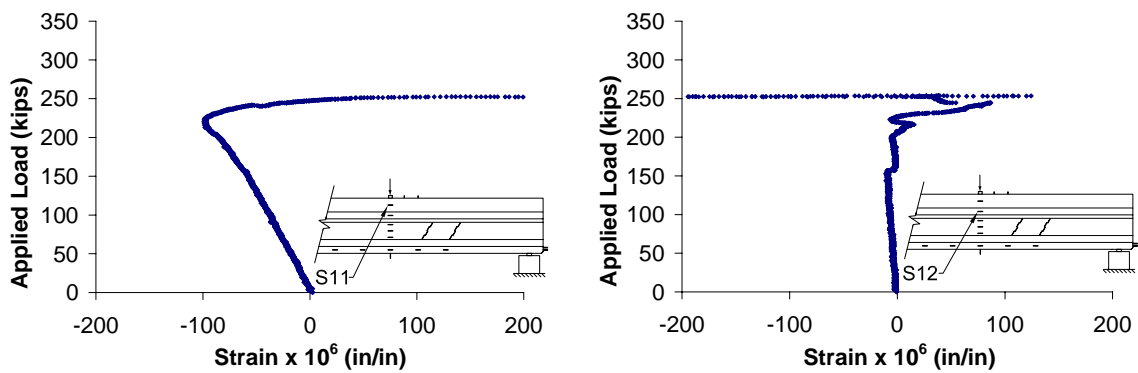


Figure 162. Flexural strain positions eleven and twelve in F2-STDF2

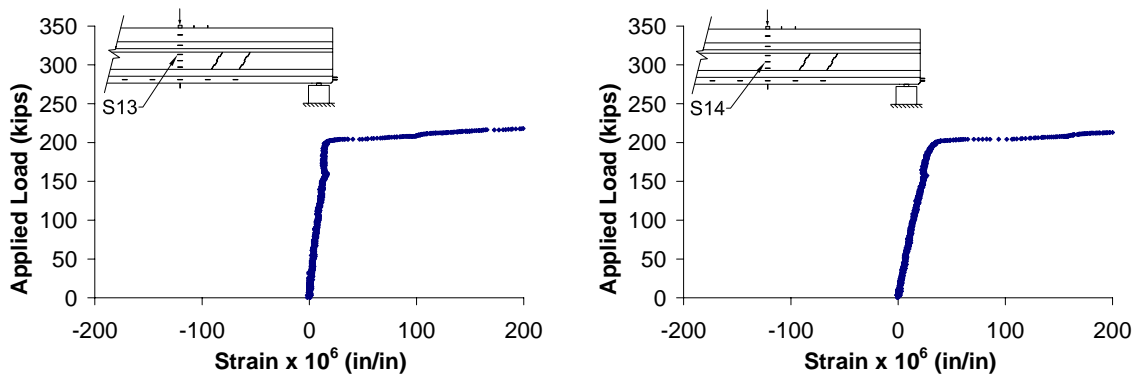


Figure 163. Flexural strain positions thirteen and fourteen in F2-STDF2

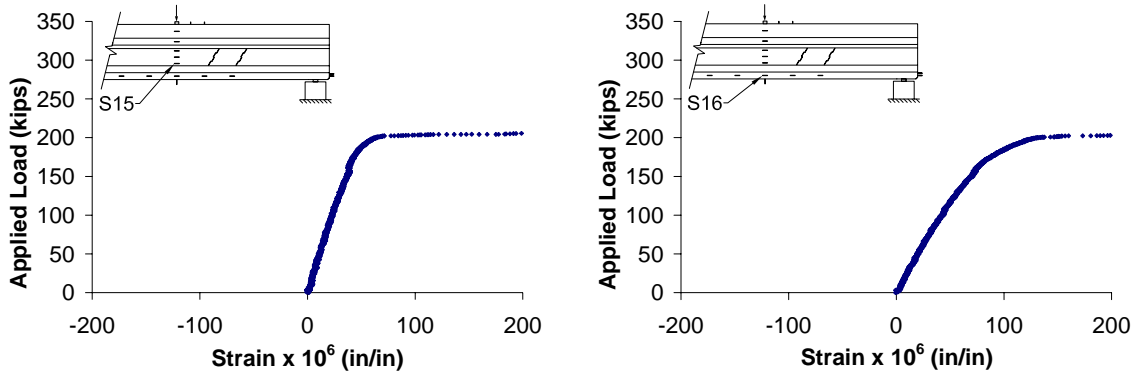


Figure 164. Flexural strain positions fifteen and sixteen in F2-STDF2

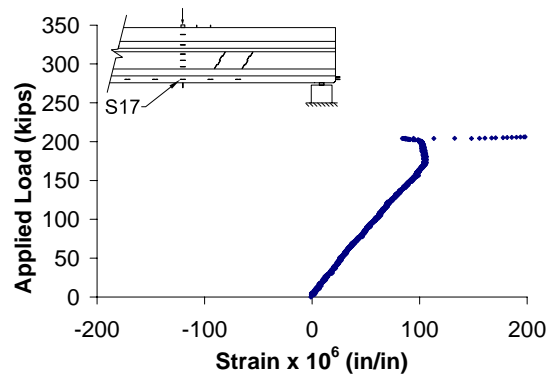


Figure 165. Flexural strain position seventeen in F2-STDF2

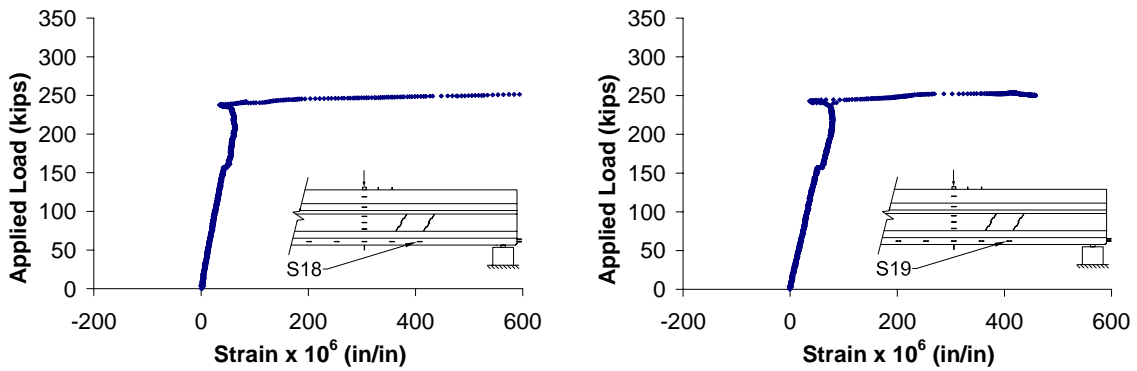


Figure 166. Strain positions eighteen and nineteen in F2-STDF2

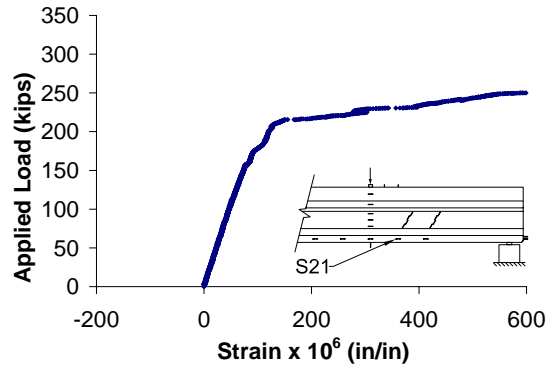
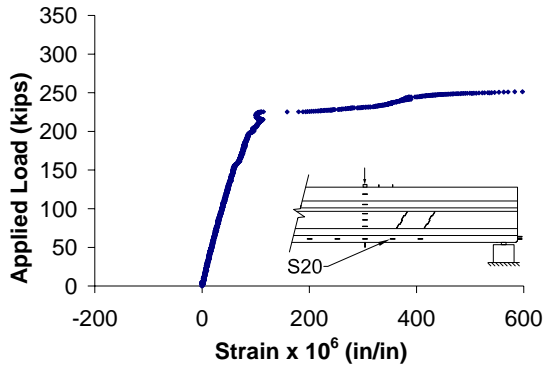


Figure 167. Strain positions 20 and 21 in F2-STDF2

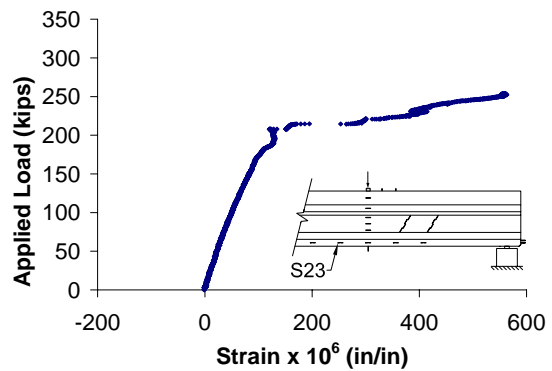
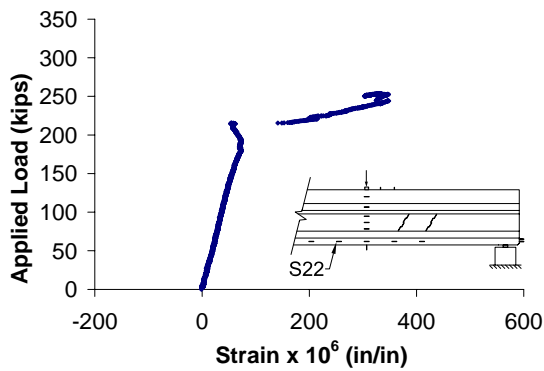


Figure 168. Strain positions 22 and 23 in F2-STDF2

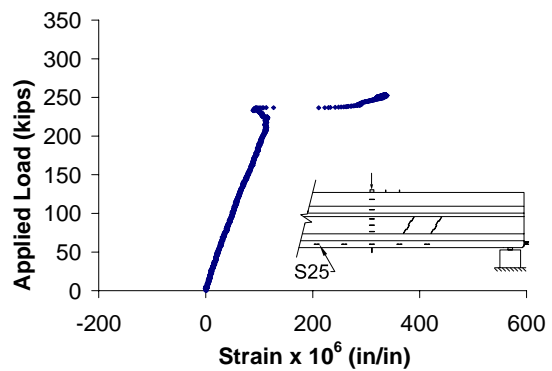
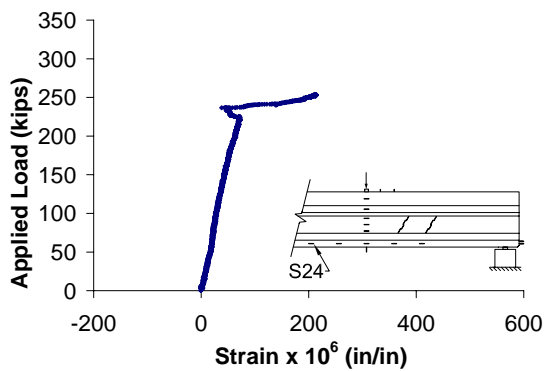


Figure 169. Strain positions 24 and 25 in F2-STDF2

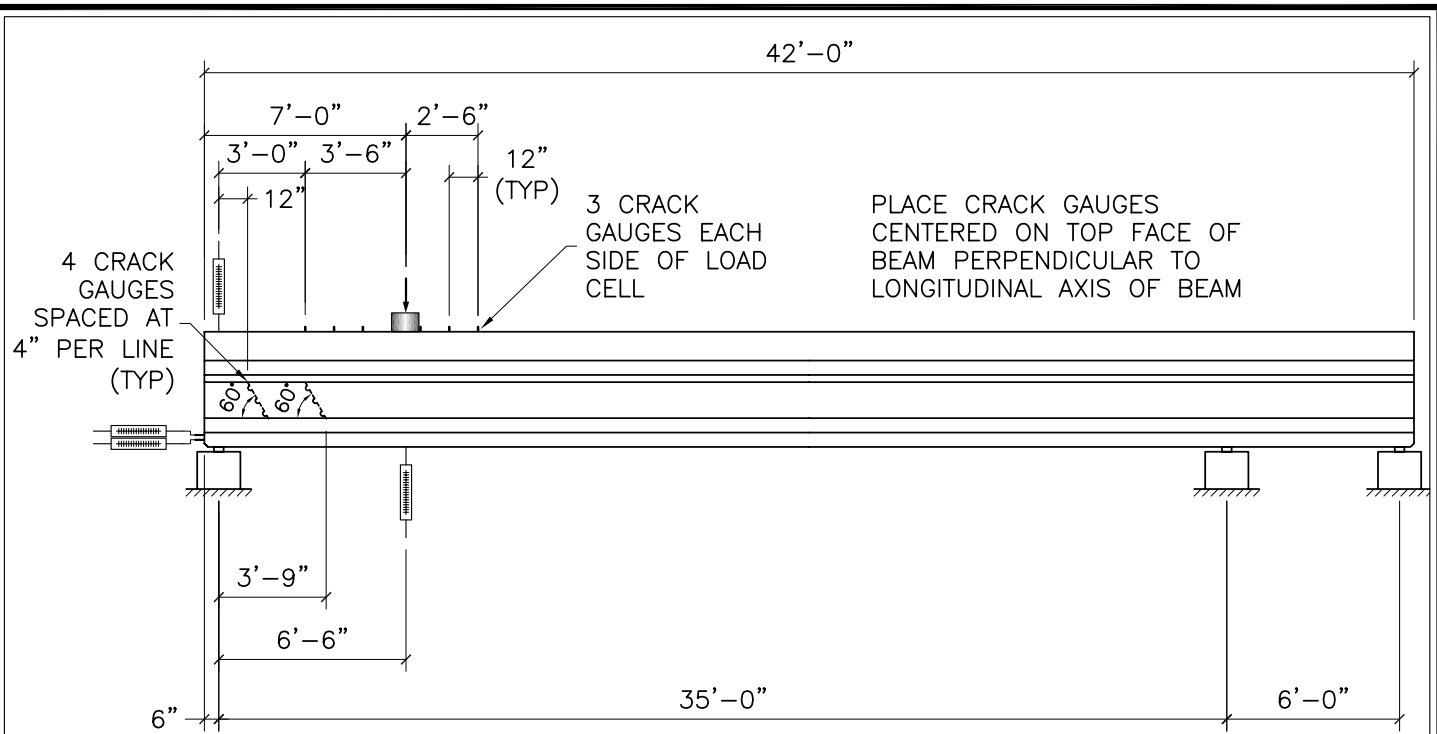
APPENDIX F - SHEAR-SLIP TEST

TEST SETUP

Two of the six AASHTO Type II beams were constructed and tested to investigate the structural behavior of SCC as compared to the control concrete in a condition of high shear with an available development length that would permit the possibility of a strand slip failure mode. Unlike the beams used for the first shear tests, the shear-slip test beams had a full standard arrangement of stirrups and a composite cap. The non-SCC composite cap was constructed on top of both beams to match an actual application of an AASHTO Type II beam. The detailed as-built figures are located in Appendix C. Single-leg number five stirrups spaced at 12 inches were used in the shear span. A short development length caused by placing the center of the support six inches from the end of the beam was used to produce the likely chance of having strand movement with the possibility of a strand slip failure mode.

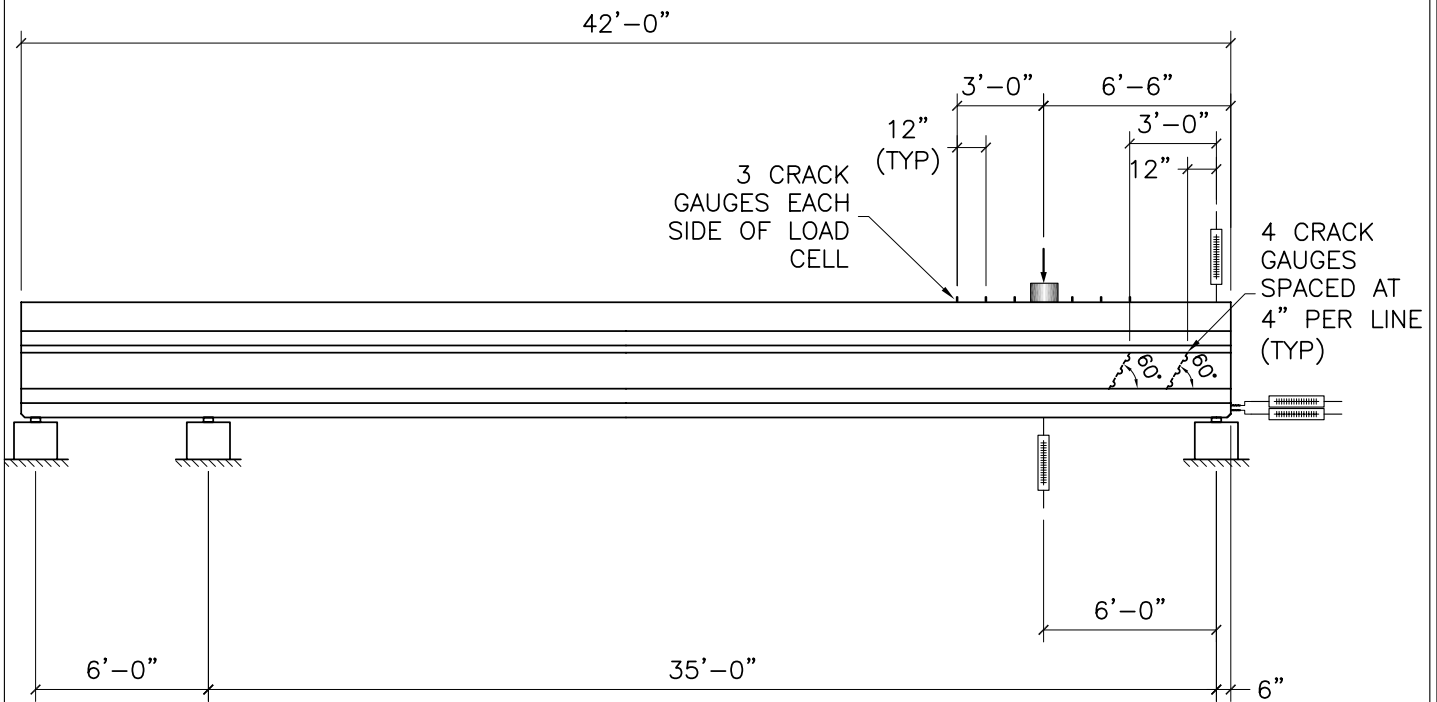
The test setup for the shear tests is shown in Figure 170. An LVDT at the point of load was used to measure beam deflection with increasing load. LVDTs were also installed on the strands to monitor strand movement. Additionally, crack gauges were installed on the vertical face of the beam web and oriented to measure tension strain due to shear. Finally, crack gauges were installed on top of the beam and oriented to measure strain in the transverse direction. The load was gradually increased as each gauge was sampled until a failure condition was reached. Each end of both beams was tested.

SCC Instrumentation 7.dwg L7 5/13/04



SINGLE BEAM - TEST 1 LAYOUT

SCALE: NTS



SINGLE BEAM - TEST 2 LAYOUT

SCALE: NTS

STRAND INSTRUMENTATION TO BE SAME AS PREVIOUS TESTS

Figure 170
Shear-Slip Test
Test Setup
AASHTO Type II Girder

Research Project 982
Self-Consolidating Concrete For
Use In FDOT Bridge Elements

Results

Table 32. Shear-slip tests web cracking strain

Gauge	SS1-SCCF2		SS1-STDF1		SS2-SCCF2		SS2-STDF1	
	Line 1 Strain ($\mu\epsilon$)	Line 2 Strain ($\mu\epsilon$)	Line 1 Strain ($\mu\epsilon$)	Line 2 Strain ($\mu\epsilon$)	Line 1 Strain ($\mu\epsilon$)	Line 2 Strain ($\mu\epsilon$)	Line 1 Strain ($\mu\epsilon$)	Line 2 Strain ($\mu\epsilon$)
1	25.9	10.0	19.8	22.5	39.8	-0.6	23.3	-8.1
2	14.2	-5.6	37.3	19.4	25.6	74.4	20.9	160.0
3	36.7	73.1	17.5	34.4	53.6	-11.9	24.5	-2.5
4	10.6	11.2	16.9	-5.6	0.6	33.8	30.6	8.8
Average	21.8	22.2	22.9	17.7	29.9	23.9	24.8	39.6

Table 33. Shear-slip tests web strain due to loads in elastic region for shear-slip tests

Gauge	SS1-SCCF2				SS1-STDF1			
	Load = 78 kips		Load = 88 kips		Load = 78 kips		Load = 88 kips	
	Line 1 Strain ($\mu\epsilon$)	Line 2 Strain ($\mu\epsilon$)	Line 1 Strain ($\mu\epsilon$)	Line 2 Strain ($\mu\epsilon$)	Line 1 Strain ($\mu\epsilon$)	Line 2 Strain ($\mu\epsilon$)	Line 1 Strain ($\mu\epsilon$)	Line 2 Strain ($\mu\epsilon$)
1	13.4	10.6	7.3	15.6	13.3	11.9	14.1	14.4
2	9.7	9.4	16.6	17.5	12.5	16.2	13.8	16.9
3	14.8	20.6	19.5	11.9	12.7	15.6	15.3	11.9
4	11.3	14.4	8.8	18.1	11.3	12.5	13.1	14.4
Average	12.3	13.8	13.0	15.8	12.4	14.0	14.1	14.4

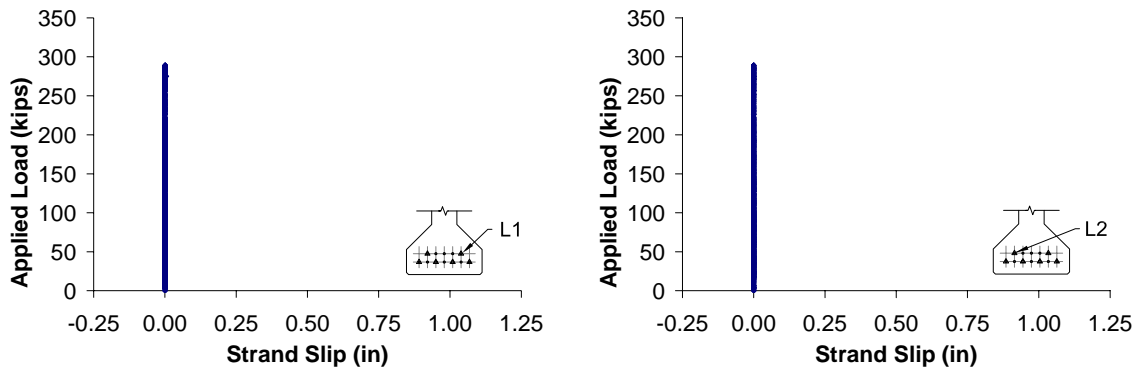


Figure 171. Strand slip for strands one and two in SS1-SCCF2

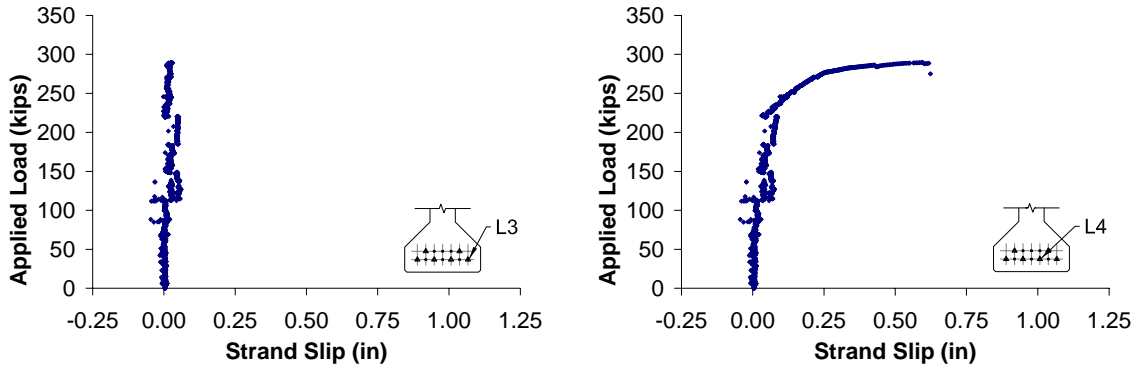


Figure 172. Strand slip for strands three and four in SS1-SCCF2

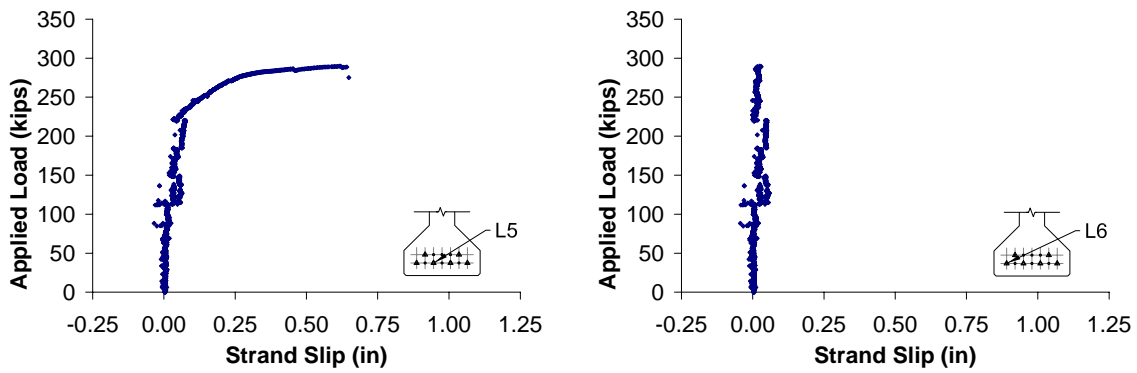


Figure 173. Strand slip for strands five and six in SS1-SCCF2

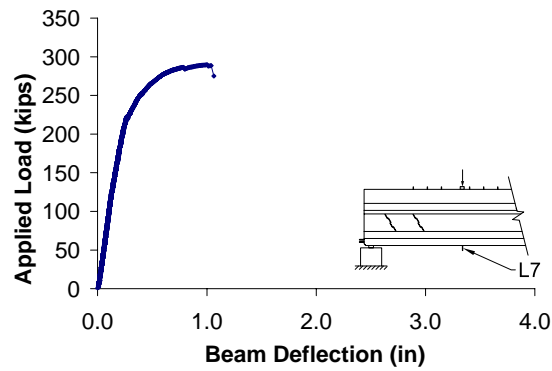


Figure 174. Beam deflection in SS1-SCCF2

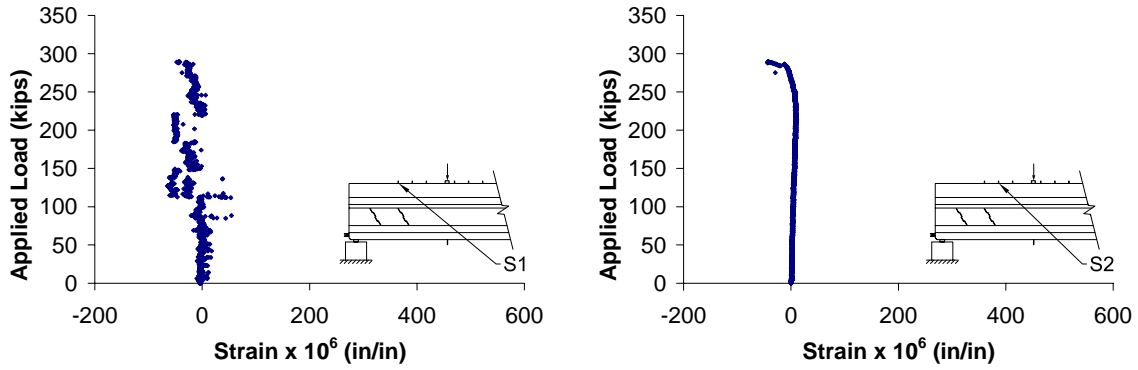


Figure 175. Top face transverse strain positions one and two in SS1-SCCF2

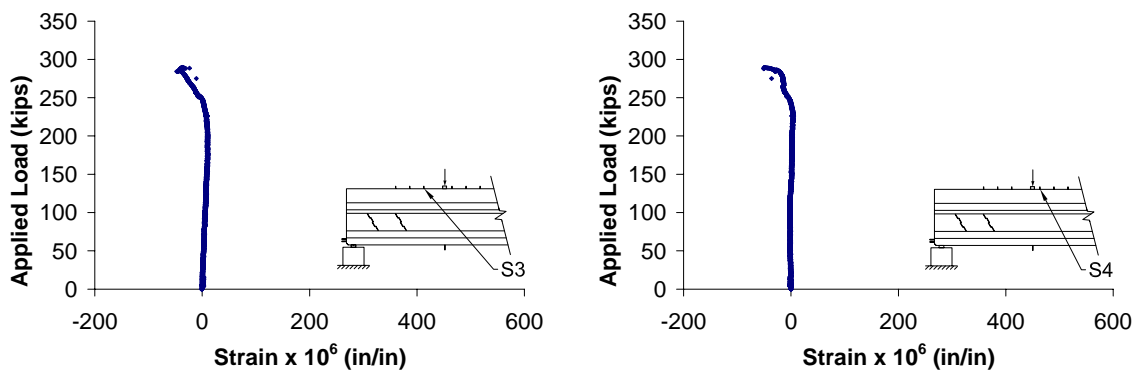


Figure 176. Top face transverse strain positions three and four in SS1-SCCF2

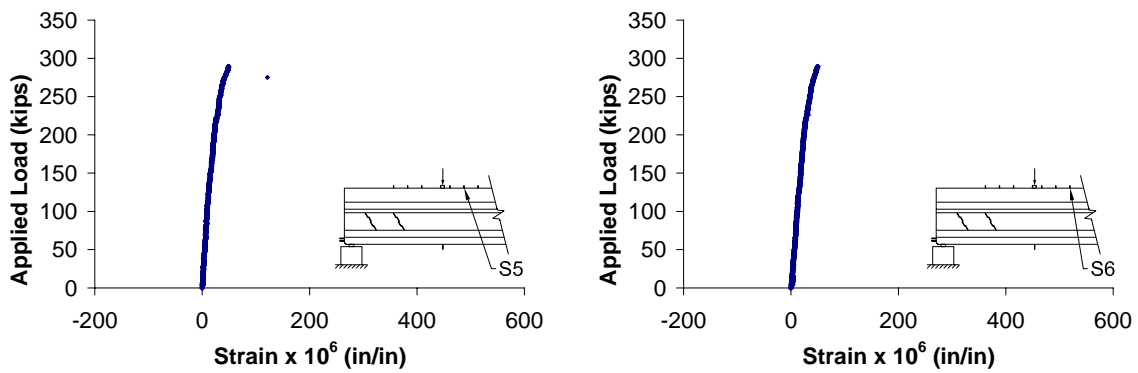


Figure 177. Top face transverse strain positions five and six in SS1-SCCF2

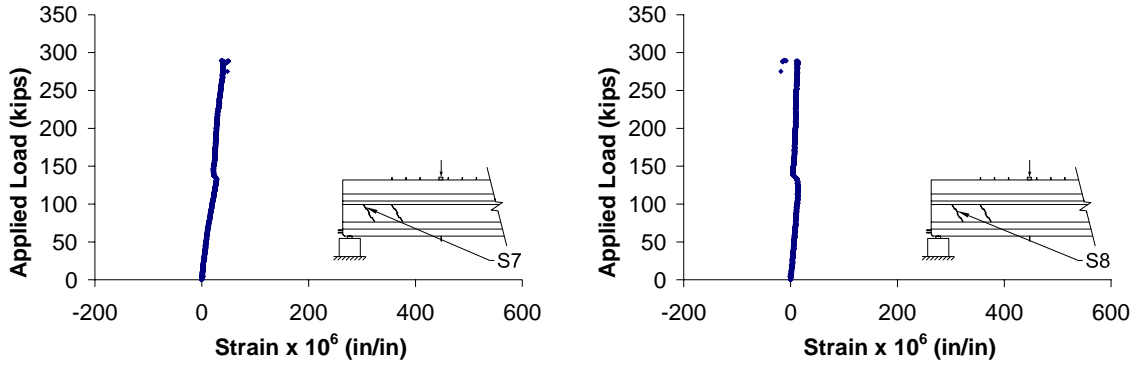


Figure 178. Web shear strain positions seven and eight in SS1-SCCF2

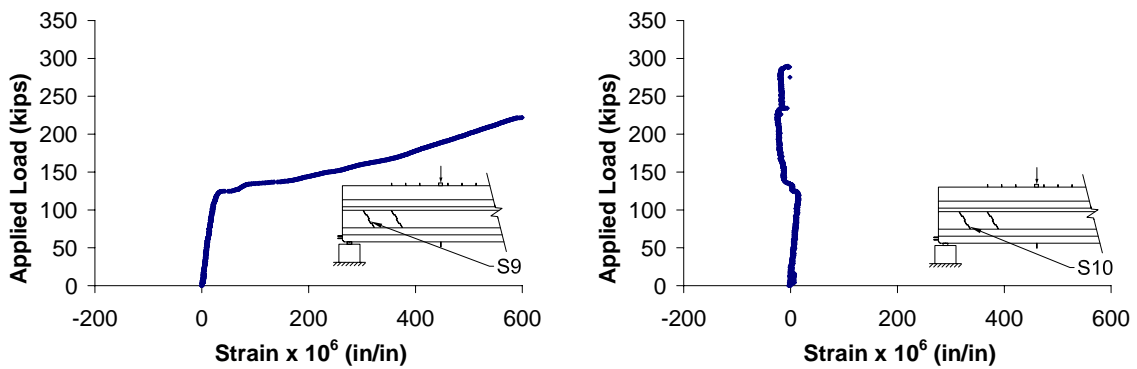


Figure 179. Web shear strain positions nine and ten in SS1-SCCF2

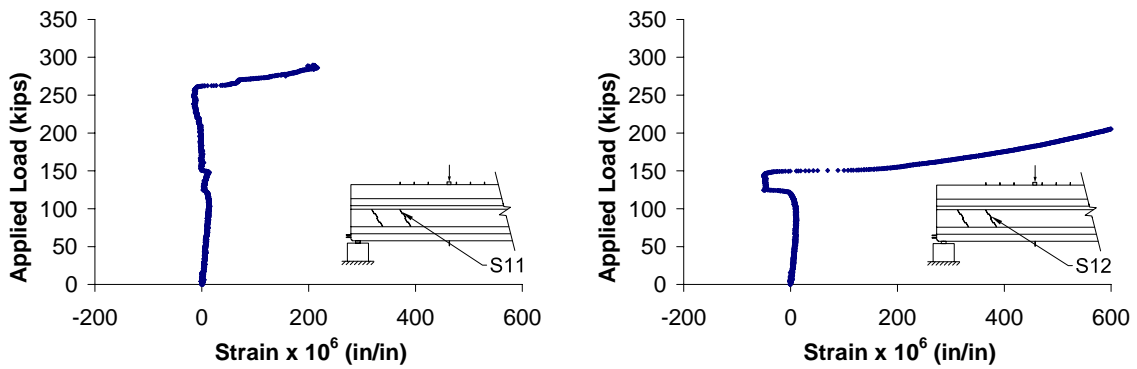


Figure 180. Web shear strain positions eleven and twelve in SS1-SCCF2

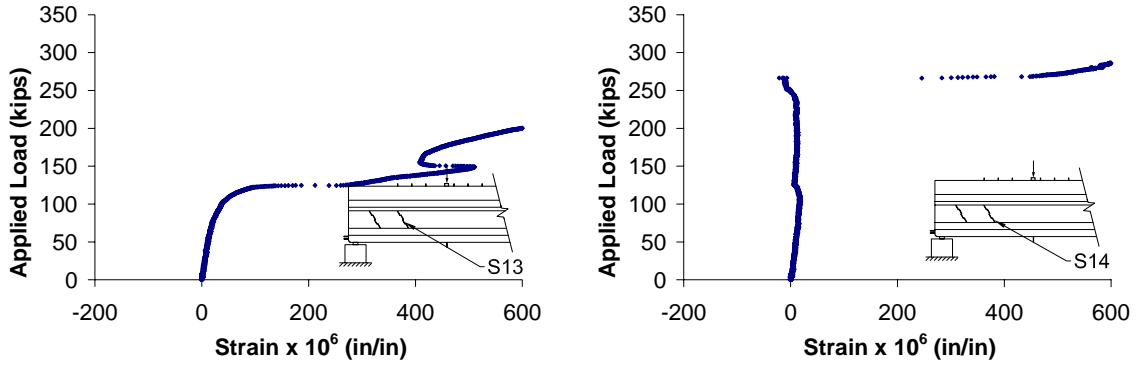


Figure 181. Web shear strain positions thirteen and fourteen in SS1-SCCF2

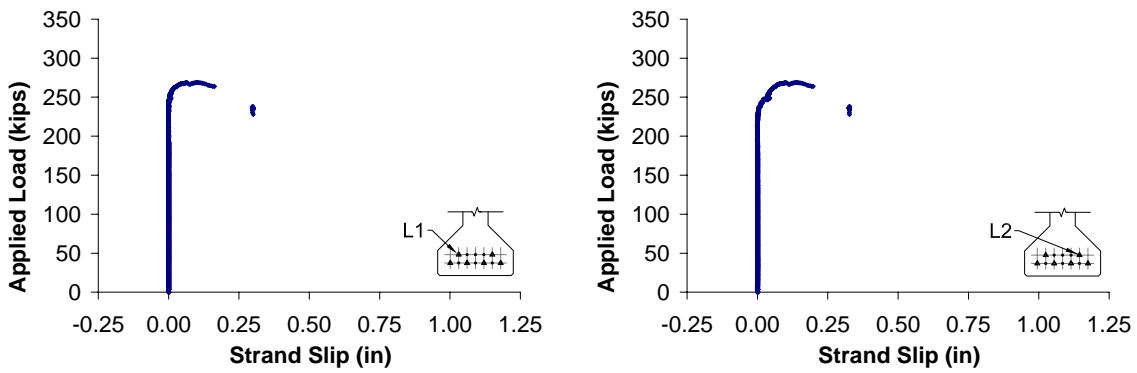


Figure 182. Strand slip for strands one and two in SS2-SCCF2

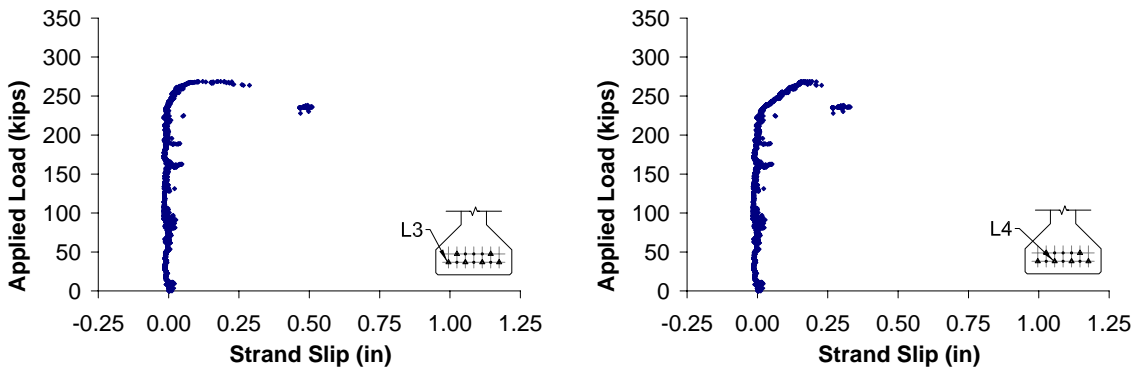


Figure 183. Strand slip for strands three and four in SS2-SCCF2

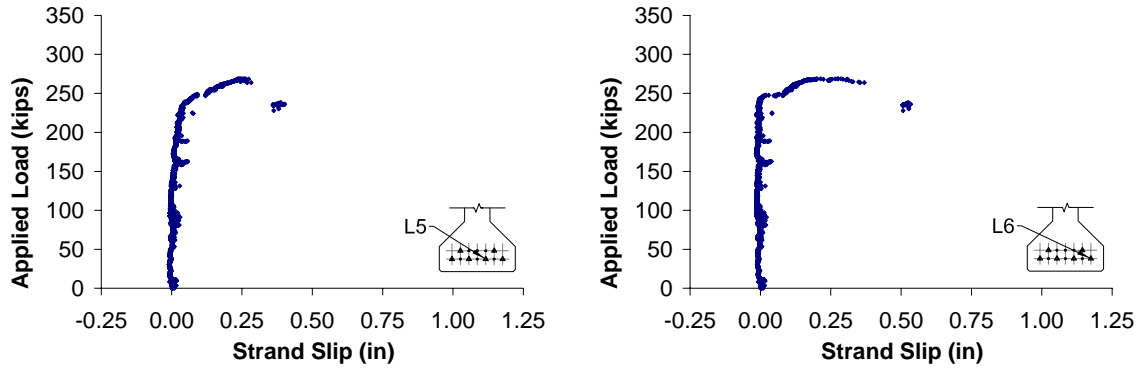


Figure 184. Strand slip for strands five and six in SS2-SCCF2

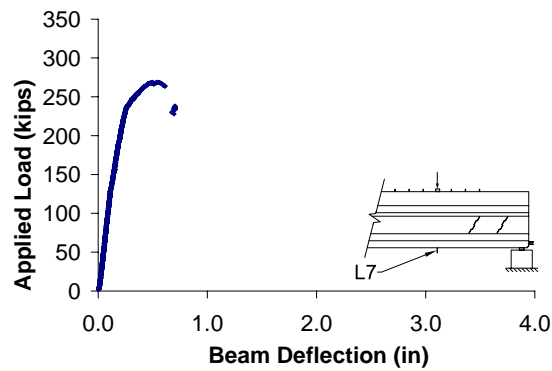


Figure 185. Beam deflection in SS2-SCCF2

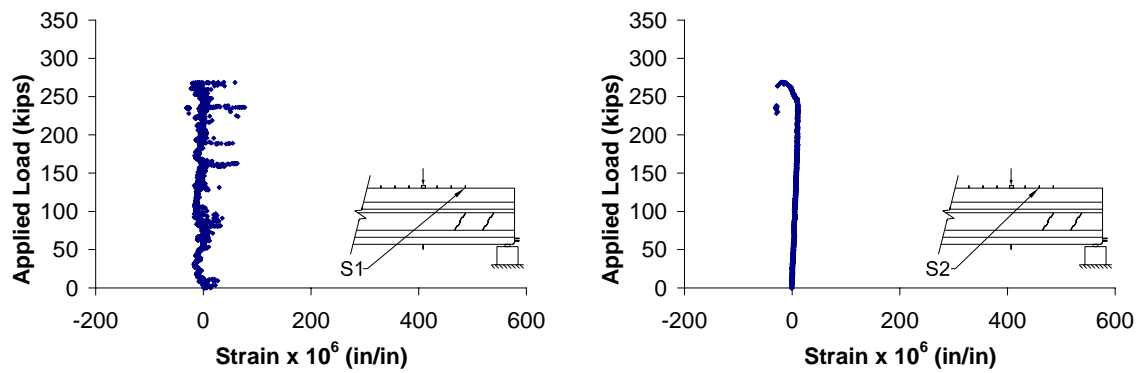


Figure 186. Top face transverse strain positions one and two in SS2-SCCF2

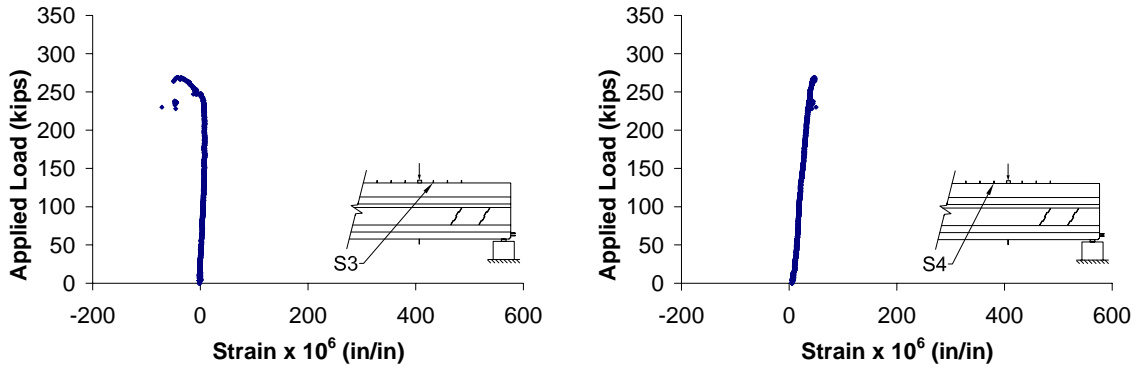


Figure 187. Top face transverse strain positions three and four in SS2-SCCF2

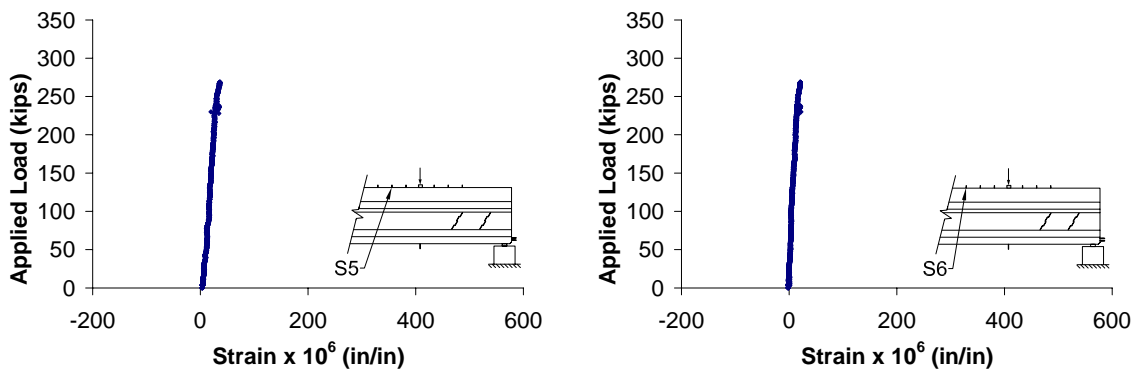


Figure 188. Top face transverse strain positions five and six in SS2-SCCF2

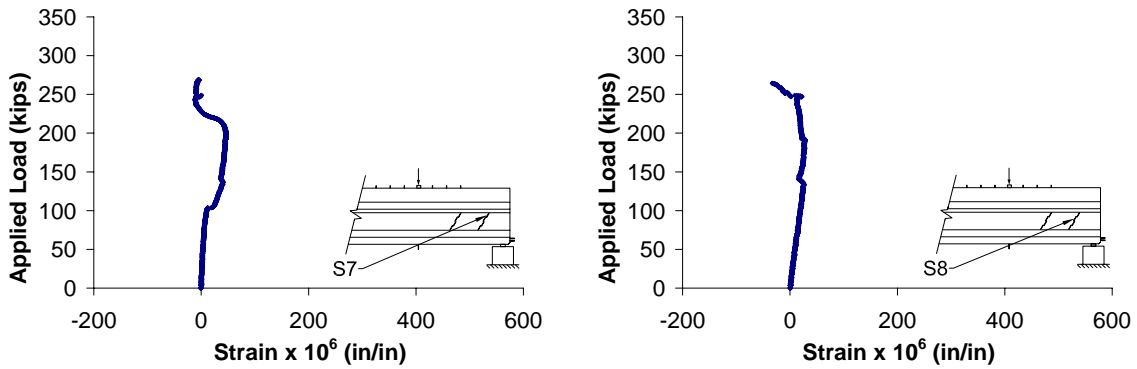


Figure 189. Web shear strain positions seven and eight in SS2-SCCF2

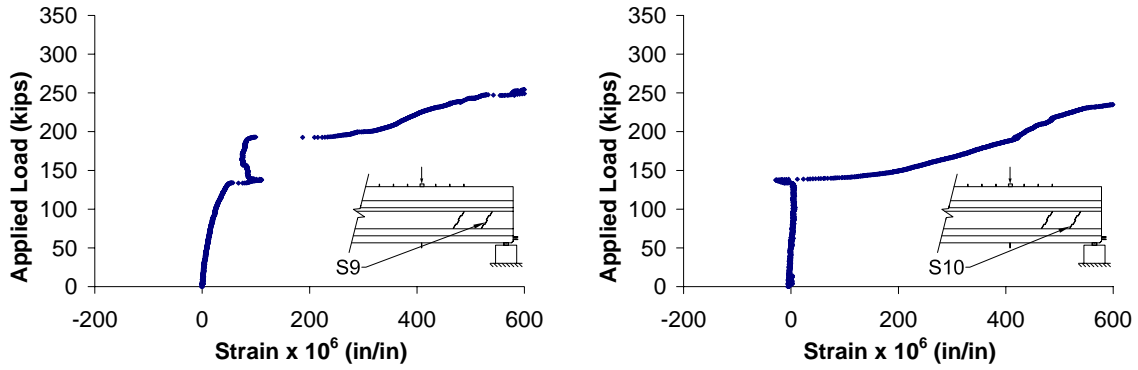


Figure 190. Web shear strain positions nine and ten in SS2-SCCF2

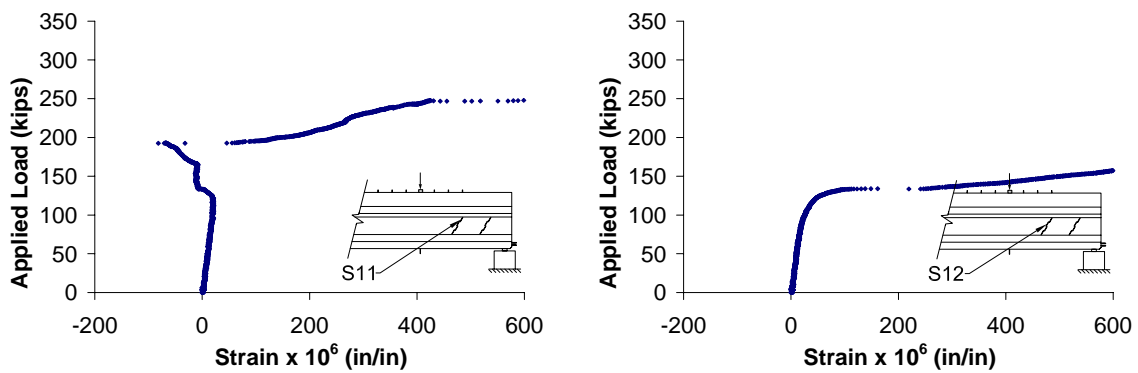


Figure 191. Web shear strain positions eleven and twelve in SS2-SCCF2

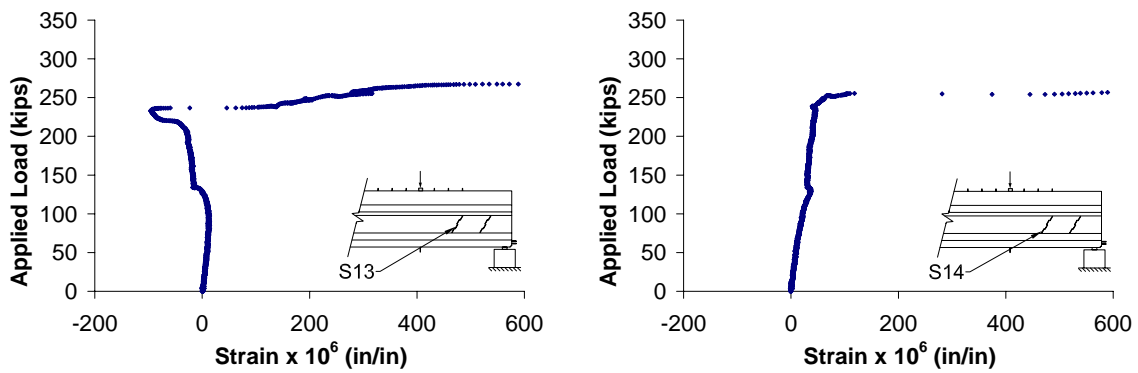


Figure 192. Web shear strain positions thirteen and fourteen in SS2-SCCF2

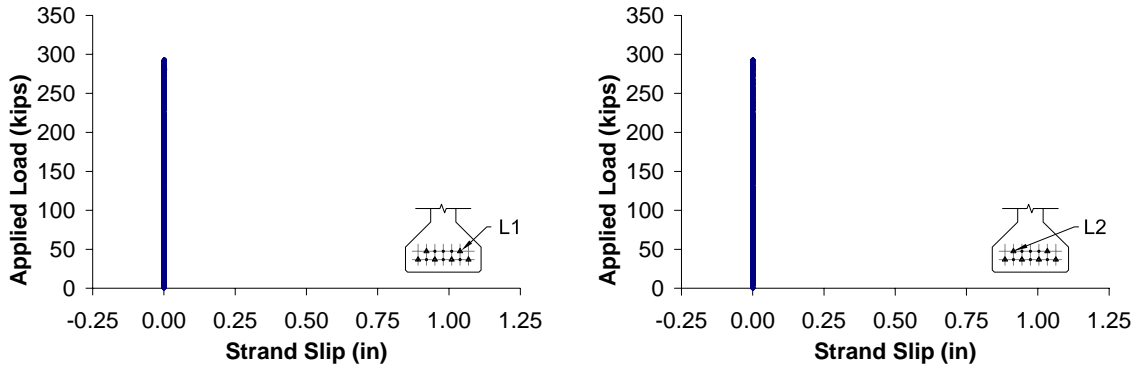


Figure 193. Strand slip for strands one and two in SS1-STDF1

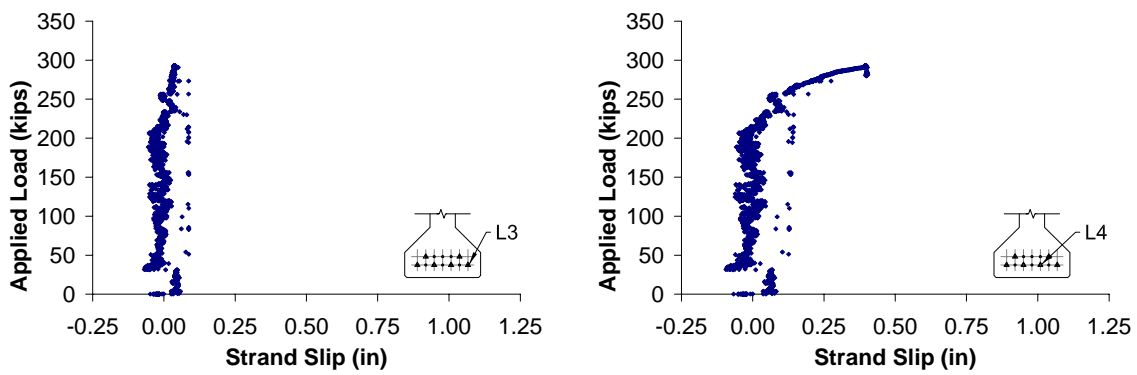


Figure 194. Strand slip for strands three and four in SS1-STDF1

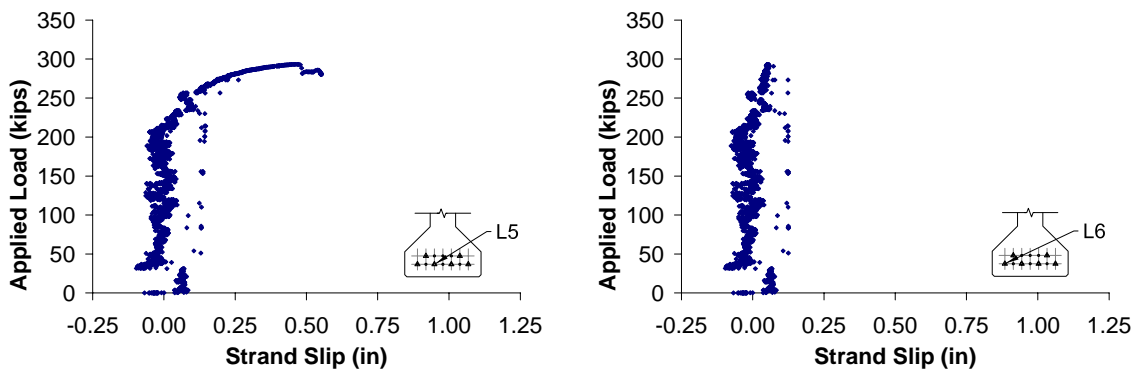


Figure 195. Strand slip for strands five and six in SS1-STDF1

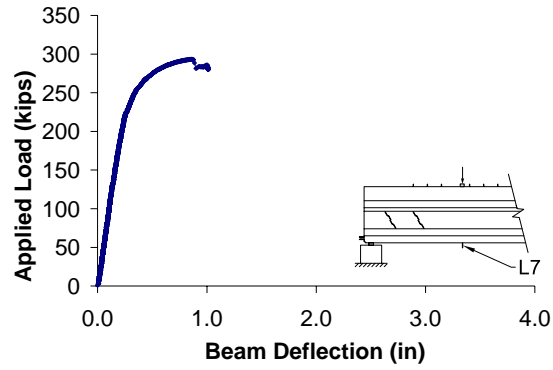


Figure 196. Beam deflection in SS1-STDF1

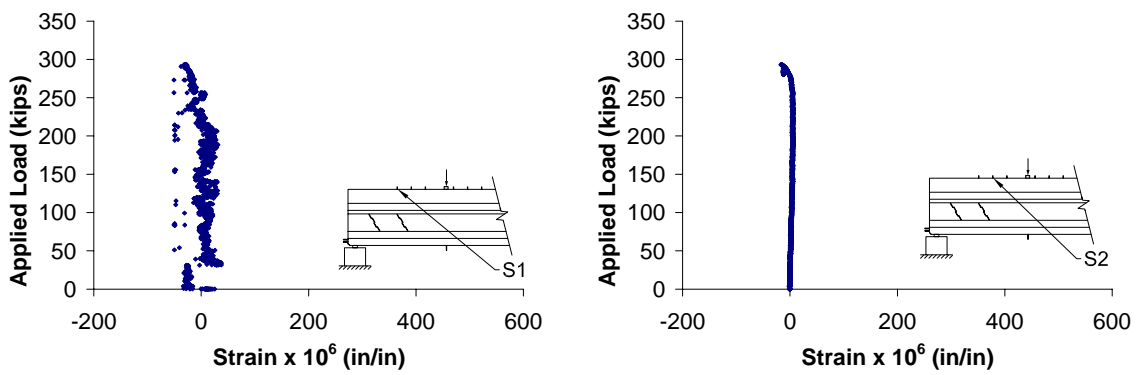


Figure 197. Top face transverse strain positions one and two in SS1-STDF1

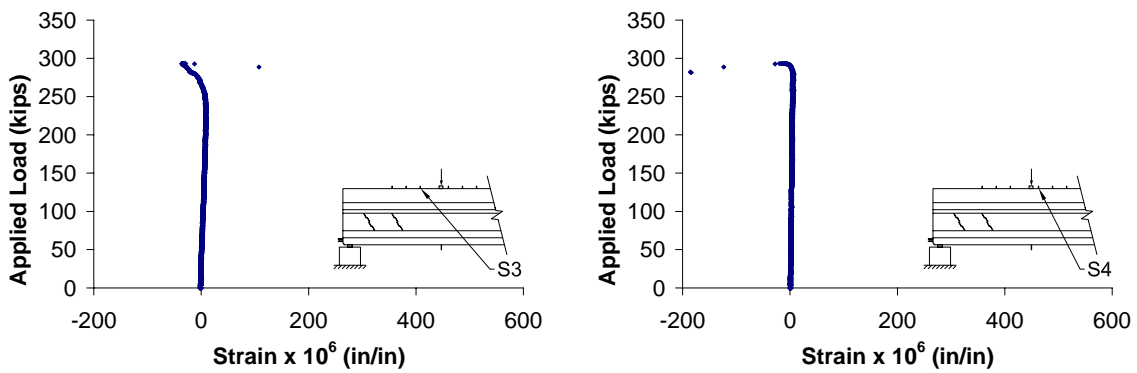


Figure 198. Top face transverse strain positions three and four in SS1-STDF1

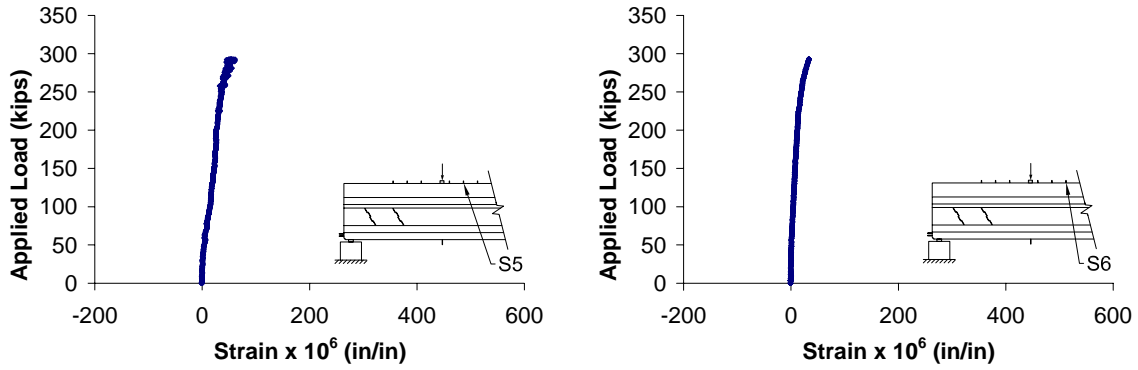


Figure 199. Top face transverse strain positions five and six in SS1-STDF1

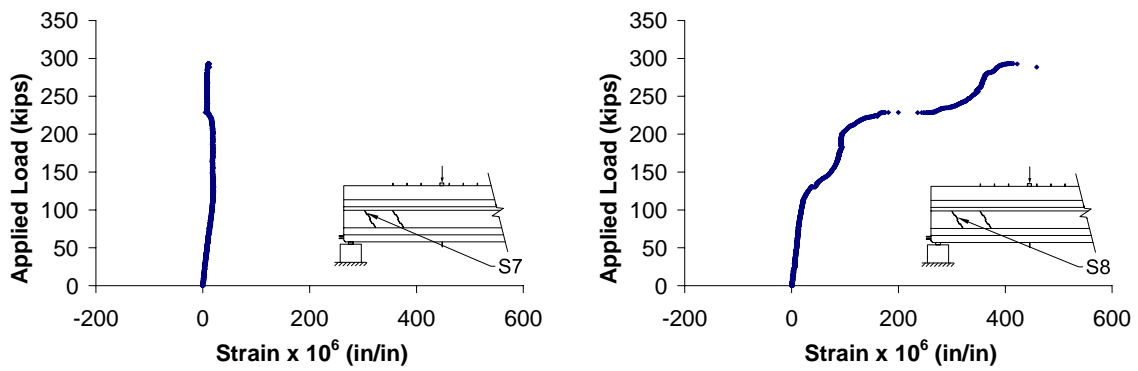


Figure 200. Web shear strain positions seven and eight in SS1-STDF1

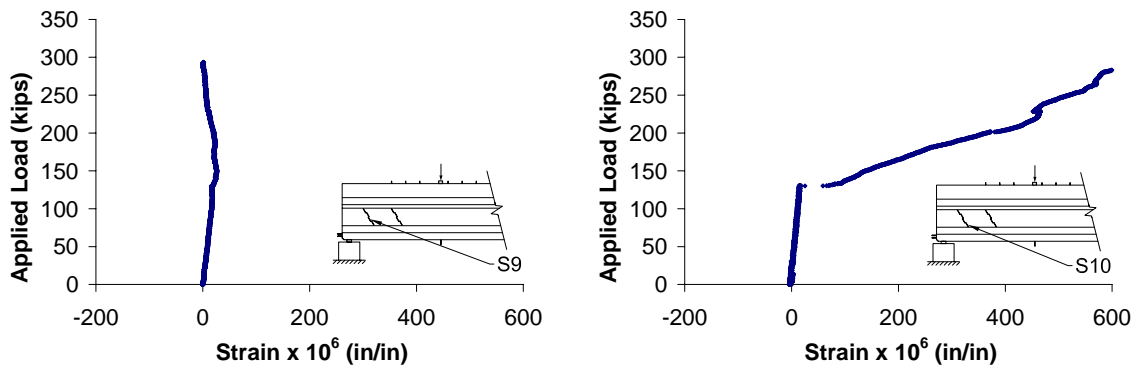


Figure 201. Web shear strain positions nine and ten in SS1-STDF1

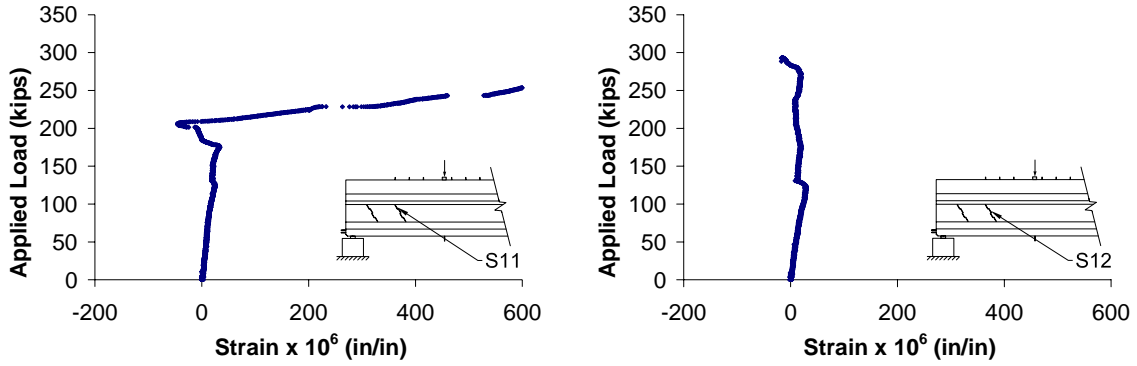


Figure 202. Web shear strain positions eleven and twelve in SS1-STDF1

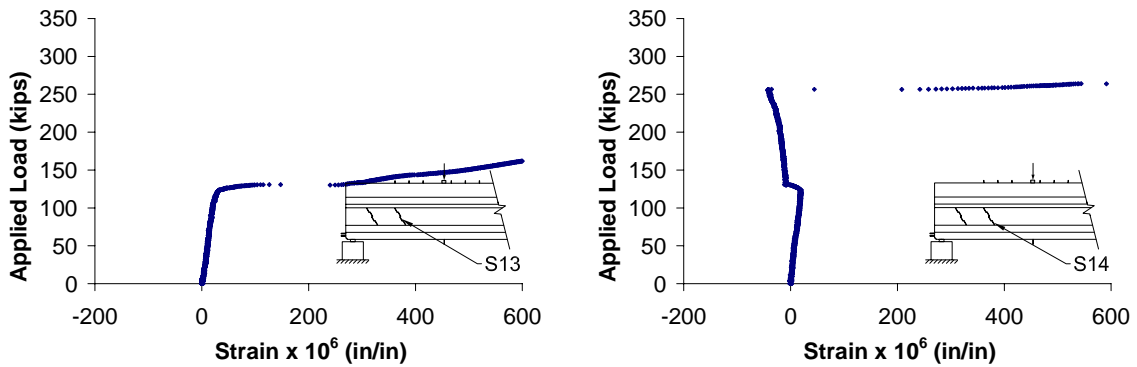


Figure 203. Web shear strain positions thirteen and fourteen in SS1-STDF1

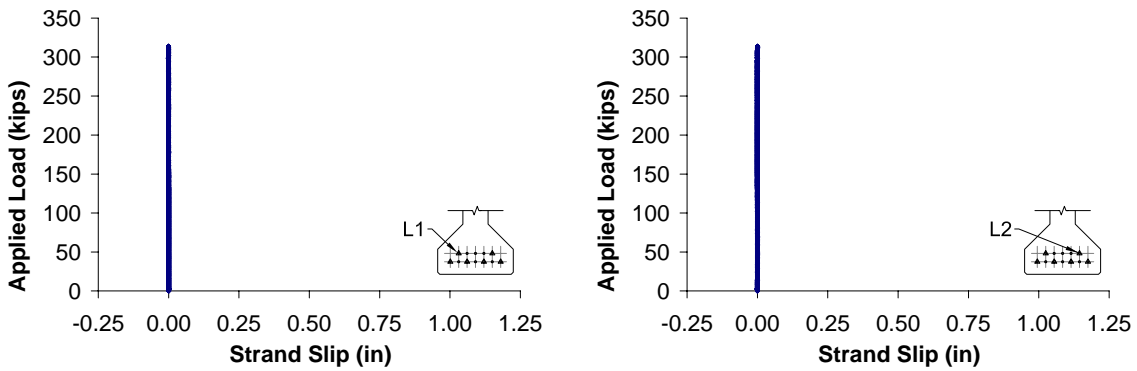


Figure 204. Strand slip for strands one and two in SS2-STDF1

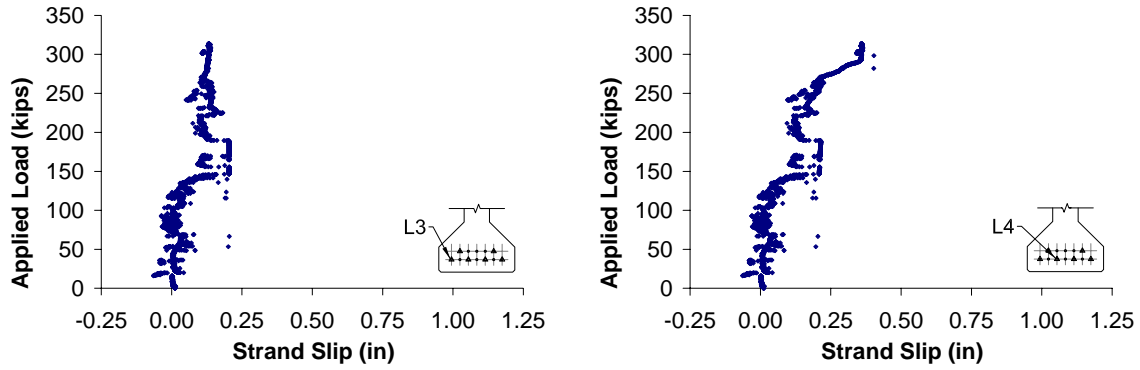


Figure 205. Strand slip for strands three and four in SS2-STDF1

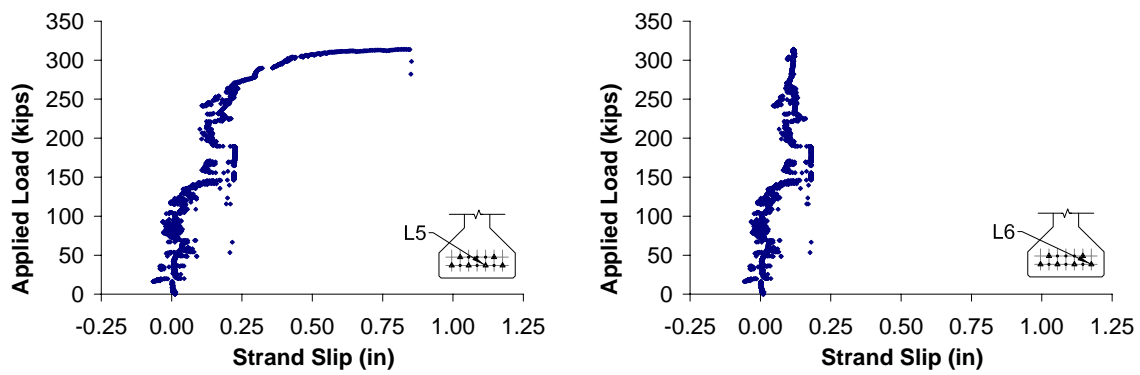


Figure 206. Strand slip for strands five and six in SS2-STDF1

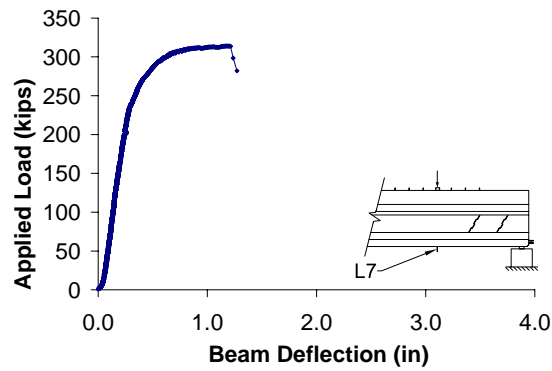


Figure 207. Beam deflection in SS2-STDF1

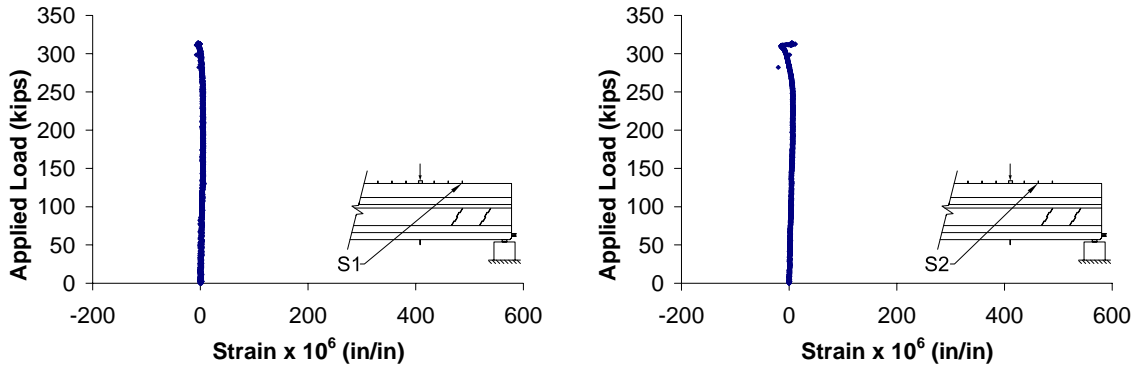


Figure 208. Top face transverse strain positions one and two in SS2-STDF1

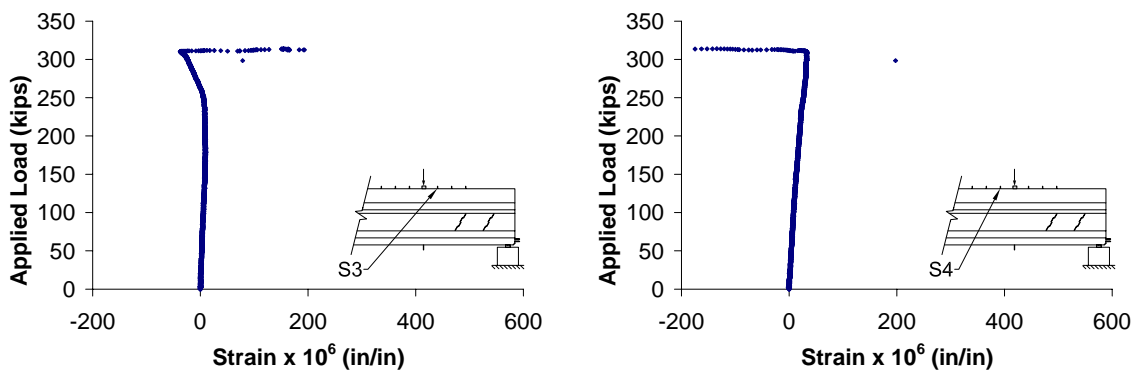


Figure 209. Top face transverse strain positions three and four in SS2-STDF1

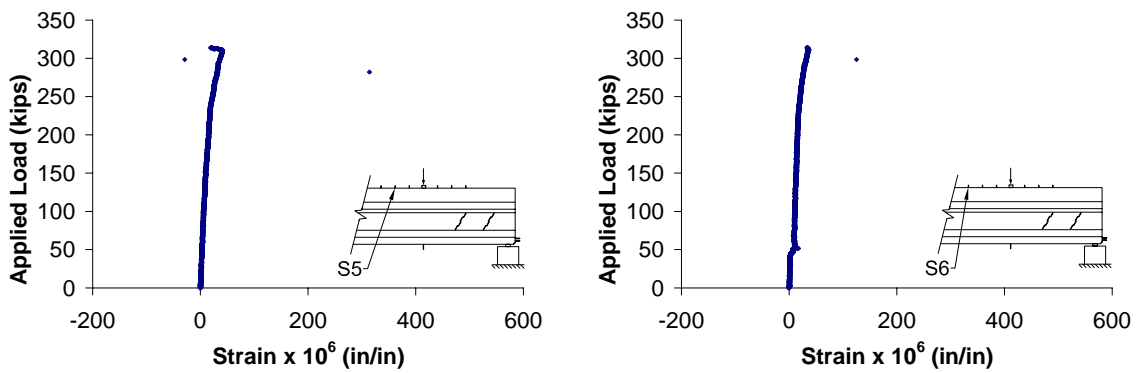


Figure 210. Top face transverse strain positions five and six in SS2-STDF1

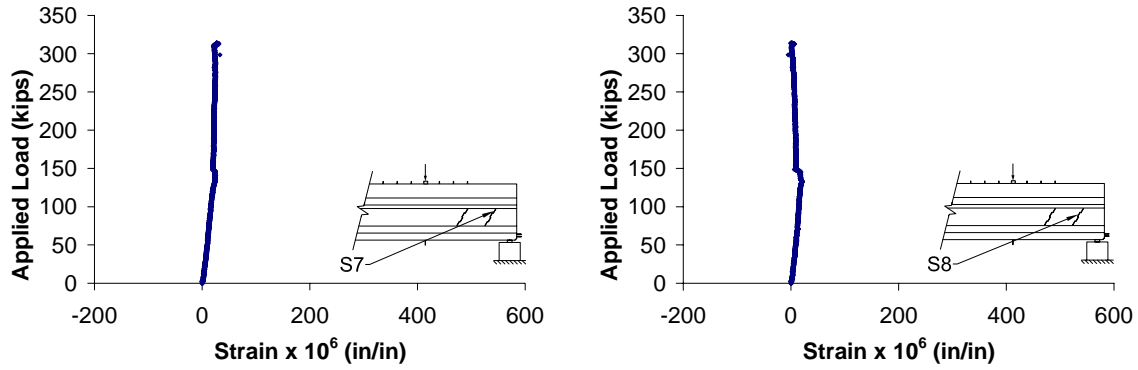


Figure 211. Web shear strain positions seven and eight in SS2-STDF1

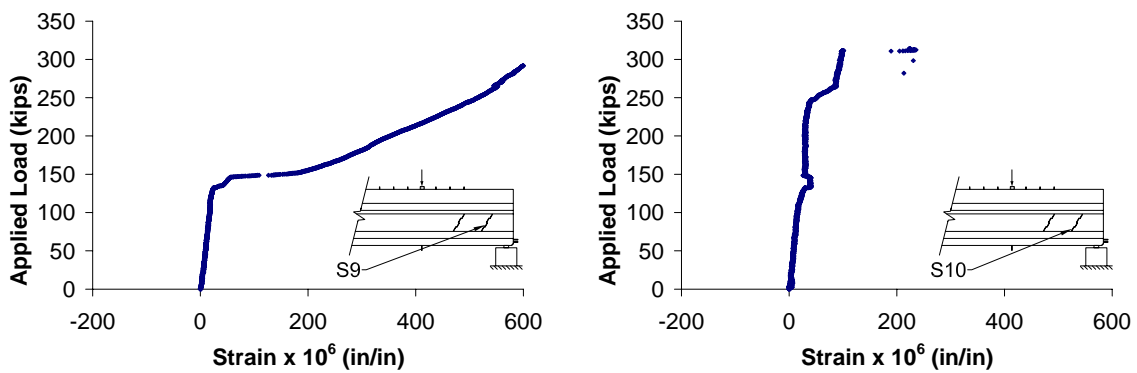


Figure 212. Web shear strain positions nine and ten in SS2-STDF1

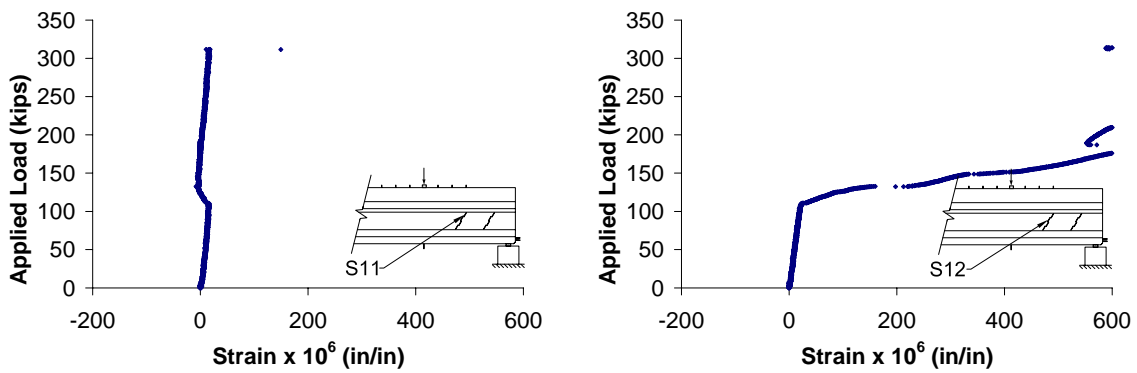


Figure 213. Web shear strain positions eleven and twelve in SS2-STDF1

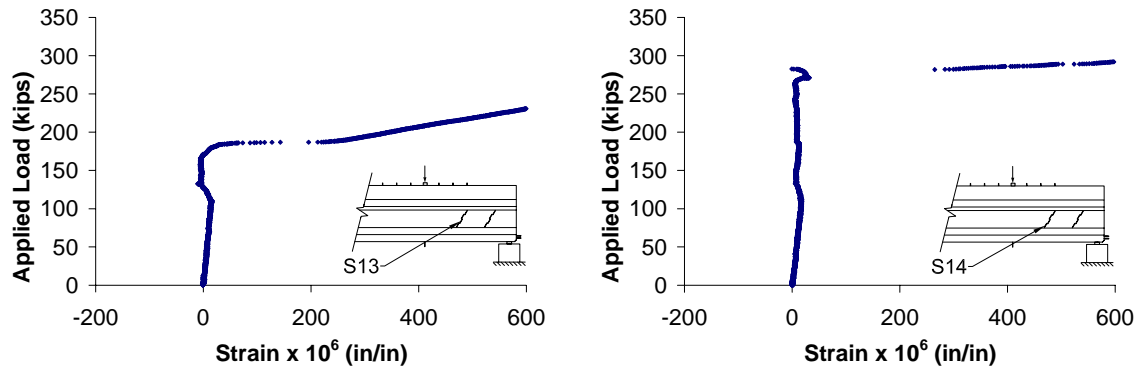


Figure 214. Web shear strain positions thirteen and fourteen in SS2-STDF1